

Janusz Sempruch
Editor

Development

in control and machinery design



Wydawnictwa Uczelniane
Akademii Techniczno-Rolniczej
w Bydgoszczy

Janusz Sempruch
Editor

Development **in control** **and machinery design**

Biblioteka Główna ATR w Bydgoszczy



000000103276



Wydawnictwa Uczelniane
Akademii Techniczno-Rolniczej
w Bydgoszczy

RECENZENCI

prof. dr hab. inż. Leopold Berkowski, prof. zw. dr hab. inż. Zygmunt Drzymała,
prof. dr hab. Krzysztof Gołoś, dr hab. inż. Jerzy Iwaszko,
dr hab. inż. Franciszek Siemieniako, dr hab. inż. Andrzej Zajac



Opracowanie redakcyjne i techniczne
mgr Dorota Ślachciak

© Copyright

Wydawnictwa Uczelniane Akademii Techniczno-Rolniczej, Bydgoszcz 2002

ISBN 83-87274-39-9

Wydawnictwa Uczelniane Akademii Techniczno-Rolniczej

Redaktor Naczelny

dr hab. inż. Janusz Prusiński, prof. nadzw. ATR

ul. Ks. A. Kordeckiego 20, 85-225 Bydgoszcz, tel. (052) 3749482, 3749426

e-mail: wydawucz@atr.bydgoszcz.pl <http://www.atr.bydgoszcz.pl/~wyd>

Wyd.I. Nakład 250 egz. Ark. aut. 8,5. Ark. druk. 7,0. Papier druk. kl. III.

Oddano do druku i druk ukończono w kwietniu 2002 r. Zamówienie nr 5/2002

Uczelniany Zakład Małej Poligrafii ATR Bydgoszcz, ul. Ks. A. Kordeckiego 20

2002 5 14 11

*The authors wish to dedicate the book to the memory of
Lech M. Kamiński, Assoc. Prof.*

CONTENTS

Preface	7
Fatigue plane stress state modelling	9
<i>Artur Cichański, Janusz Sempruch</i>	
Integrity of designing machines or the environment?	17
<i>Józef Flizikowski</i>	
Empirical determining of movement parameters for the pneumatic servo-motor	25
<i>Mieczysław Gawda</i>	
Computer aided kinematics analysis of 3D mechanisms	31
<i>Tomasz Kuźmierowski, Franciszek Siemieniako</i>	
Computer-aided multiple-disc-shredding research	41
<i>Marek Macko</i>	
Calculations of fatigue life according to Polish Register of Ships for selected research results	47
<i>Adam Mazurkiewicz</i>	
Jet flow visualisation for an axi-symmetric nozzle	55
<i>Kazimierz Peszyński, Zdeněk Trávníček</i>	
Physical models of the unit loads stream sorting process	65
<i>Tomasz Piątkowski, Janusz Sempruch</i>	
Some aspects of constructions dimensioning with fracture mechanics	71
<i>Eugeniusz Ranatowski</i>	
FEM in calculation of the stress and deformation of welding constructions	87
<i>Andrzej Skibicki</i>	
CT anemometric velocity profile investigation behind the axi-symmetric nozzle	95
<i>Sylwester Wawrzyniak</i>	
Complex milling of plate-like elements	101
<i>Ryszard Wocianiec, Jarosław Zdrojewski, Dariusz Skibicki</i>	
Plate-like elements machining programming in CAD environment	107
<i>Ryszard Wocianiec, Jarosław Zdrojewski, Dariusz Skibicki</i>	

PREFACE

To start with, a brief explanation of the reasons for which the book is published.

In 1996 the Faculty of Mechanical Engineering of the University of Technology and Agriculture in Bydgoszcz created the Department of Control and Machinery Design. Not to go deep into its organisational structure, one shall bear in mind that it was a common interest in creating state-of-the-art computer labs to enhance modelling of geometrical features, dynamic constructional-element behaviours, control system and automation simulations and numerical enhancement of engineering calculations which was one of the main reasons for teaming up the two, previously independent, academic groups. The creation has brought about not only the academic and organisational but also scientific integration. By incorporating those related to the Department of Control and Machinery Design, outstanding colleagues of the Faculty of Mechanical Engineering, and thanks to the highly appreciated co-operation with colleagues from other foreign and domestic scientific centres, a representative group was created which, over the last five annual seminars, have been discussing advances in control and design. In my opinion, it was indispensable to document it all in a collection of monographs reflecting selected topics covered. The selection offered is not randomly sampled; it has been my intention, as its editor, to make it representative of the scientific interests of a group of people who attend the annual meetings.

A few words on the contents. The book covers, by putting together the collection of monographs, selected issues of machine and device design and their constructional elements in its broader sense. Design and construction are taken up originally against the environment we function in as creators and recipients of both machines and the natural environment. The enhancement of the design and construction engineering is represented by papers which cover the basic issues, e.g. constructions dimensioning with fracture mechanics, complex fatigue plane stress state modelling as well as those which focus on applications, e.g. finite elements method or defining fatigue life following the regulations of the Polish Register of Ships. The reader interested in CAD tools is offered papers on computer simulation and computer-aided research. Here one will find ideas on power fluidics, constructional issues related to developing axisymmetric nozzle without mechanical movable parts in experiments (to define airflow velocity spread) which, in my opinion, constitute an interesting part of the book.

Last but not least, about the people around the book. As it is seen from the authors' affiliation, seven different scientific groups from three Polish schools of higher education and the Czech Academy of Sciences are represented. The debate of the seminars has gathered a much wider group of scientists from the University of Sheffield, State Academy of Refrigeration in Odessa, Polytechnic of Białystok,

Polytechnic of Koszalin, Polytechnic of Warsaw, Polytechnic of Gdańsk, Czech Academy of Sciences and, obviously, from the University of Technology and Agriculture in Bydgoszcz. Their participation in numerous discussions made it possible to make the monographs of the desired high standard. I wish to express my gratitude to the staff of the Publishers of the University of Technology and Agriculture for their patience and professionalism and to the reviewers for their effort and kindness and to the Dean of the Faculty of Mechanical Engineering of the University of Technology and Agriculture for financing the present publication.

Following the considerations I made editing the present volume, the next volumes are to follow which would reflect **development in control and design engineering** observed by my colleagues and myself. We wish to express our gratitude to the readers of the present volume for their interest and we hope to meet you with the next collection of monographs. I wish the authors of respective parts of the book further research papers which would be equally successful.

Janusz Sempruch

Artur Cichański
Janusz Sempruch

University of Technology and Agriculture
Faculty of Mechanical Engineering
Department of Control and Machinery Design

FATIGUE PLANE STRESS STATE MODELLING

Summary. The work aims at formulating a method of determining biaxial fatigue properties. The present method assumes that the tests are carried out in uniaxial loading conditions. The tests used flat test bars made of material in its virgin state and after plastic prestrain. A model was proposed combining fatigue stress amplitude with initial yield stresses determined for different states of the material; the parameters incorporate both stresses determined for the material in its virgin state, cycle model number and plastic strain accepted for the initial yield stress definition. Modelling offers characteristics of the material in the form of a curve which lies in the space of fatigue plane stress.

Key words: biaxial fatigue, plasticity, modelling, test methods

1. INTRODUCTION

Fatigue properties tests are carried out on fatigue machine in conditions depending on the test method accepted. Uniaxial fatigue test methods are formulated explicitly. The stands for tests in uniaxial loading conditions are widely available. Biaxial fatigue tests are carried out with different methods. Methods considered to be standard assumed the occurrence of biaxial fatigue stress state as a result of two cyclic loading. In these conditions the tests are performed with tubular specimens, thin-walled specimens or cruciform specimens. The methods considered non-standard there include test methods in uniaxial cyclic loading conditions when biaxial stress state results from the specimen geometry. In these conditions the tests are carried out with the use of specimens in the shape of revolving discs [3], cantilever and elliptical plate [5] and rhombic plate [7] ones. There are also specimens whose geometrical form was developed by the author [4].

The present formulation, developed by the author, of the biaxial fatigue properties determination method has been offered. The method assumed the use of specimens with controlled anisotropy of plastic properties tested in uniaxial cyclic loading condition [2] and used flat test bars made of material in the shape of prestrained steel sheet. The interpretation of the test results is considerably affected by the description of the material plastic prestrain on the fatigue strength effect which has been presently determined with a model combining allowable stress amplitude with initial yield stress.

2. TEST METHOD

The testing method accepted is based on the one proposed by Szczepiński [6] for determining yield surface changes. The material in the shape of plates is plastically

prestrained in a specially constructed grip (Fig. 1). During the plastic prestrain the value of ϵ_{pl} – plastic strain in the central part of the plate is controlled. Flat test bars are cut out from the plate at different angle α in relation to the plastic loading direction.

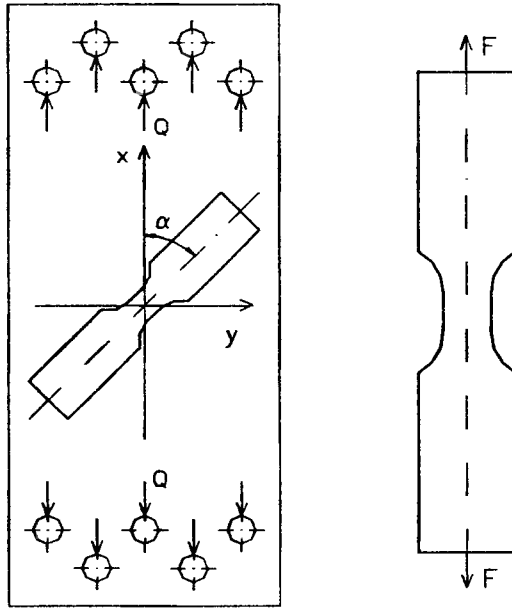


Fig. 1. Material prestrain method

FEM and strain gauges allow obtaining the area of the plate from which specimens with repeatable properties [1] were established. The geometric shape of the specimen that does not buckle during fatigue tests was also established experimentally [1]. Specimens made of prestrained material are used for fatigue and plastic property tests on uniaxial fatigue machine.

3. DESCRIPTION OF PLASTIC PROPERTIES

The isotropy of the material plastic properties in its virgin state [1] was assumed. The review of the literature available allowed to make an assumption that the plastic surface is described by the Hubert–Mises–Hencke's (H–M–H) condition with kinematics hardening [6]. The plasticity condition H–M–H for plane stress defined by nominal stresses for the virgin material is shown by Equation 1.

$$\sigma_x^2 + \sigma_y^2 - \sigma_x \sigma_y + 3\tau_{xy}^2 = \sigma_{pl}^2 \quad (1)$$

where:

- σ_x, σ_y – normal stress,
- τ_{xy} – shear stress,
- σ_{pl} – initial yield stress.

The graphic presentation of Equation 1 is an ellipsoid lying within the stress space described by a coordinate system $0\sigma_x\sigma_y\tau_{xy}$. One of the ellipsoid axes overlaps with the $0\tau_{xy}$ axis and the two other ones are bisectors of the angles between the $0\sigma_x$ and $0\sigma_y$ axes.

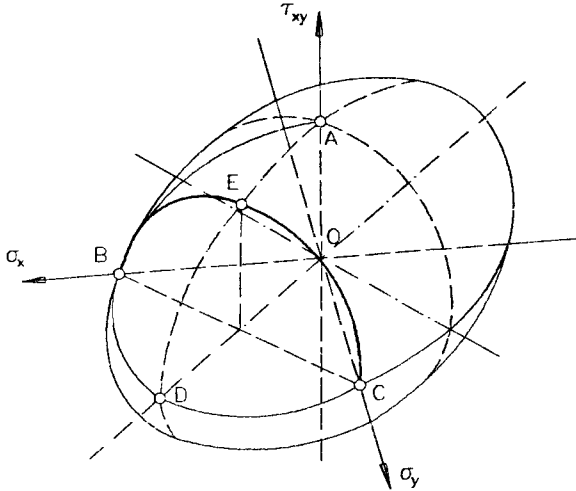


Fig. 2. Huber–Mises–Hencke's ellipsoid

Out of the ellipses created by cutting the H–M–H ellipsoid with the planes describing stress states, which arise in different specimens during tests, the *BEC* ellipse has been distinguished by cutting the H–M–H ellipsoid with the plane described by Equation 2.

$$\sigma_x + \sigma_y = \sigma_{pl} \quad (2)$$

The analysis of the Mohr's circle made for the stress state described by Equations 1 and 2 suggests that one of the main stresses must equal zero, which indicates that the points of the *BEC* ellipse correspond with the initial yield stresses determined in the uniaxial loading conditions. Coordinates of the points creating the *BEC* ellipse, in the stress space, are determined with these initial yield stresses and appropriate transforming dependencies.

The assumed shape of the *BEC* ellipse observed in the *D0* direction, in the arrangement offered in Fig. 2, for the virgin material is presented in Fig. 3 with lines with circles-like markers.

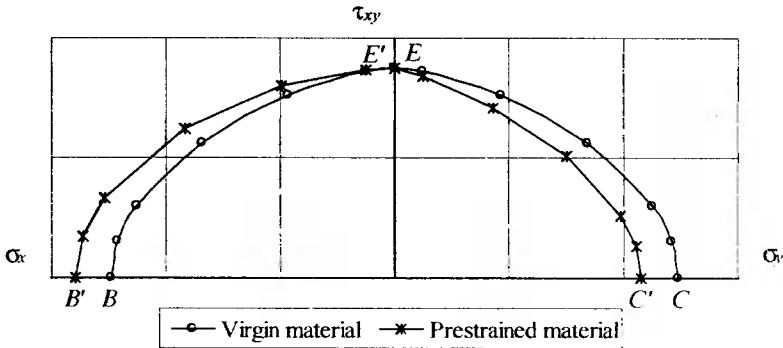


Fig. 3. BEC and $B'E'C'$ ellipses view in the $D0$ direction (assumption)

Provoking plastic strains in the material will cause, according to the kinematic hardening rule, a shift of the plasticity surface in the direction in which the plastic strains have arisen, which is represented by the shift of the H-M-H ellipsoid and the displacement of the BEC ellipse. A new ellipse, for the prestrained material in the direction σ_x marked as $B'E'C'$, is presented in Fig. 3 with a line with star-like markers. Giving the structure of material its preferential orientation results from the plastic prestrain. As it has been assumed, this preferential orientation will be described by the α angle measured in relation to the direction of plastic loading. An increase in the initial yield stress values occurs in the $\alpha = 0^\circ$ direction (point B' in Fig. 3). A decrease in the initial yield stress values occurs in the $\alpha = 90^\circ$ direction (point C' in Fig. 3). The plastic strain used in the definition of initial yield stresses affects the shape and magnitude of BEC and $B'E'C'$ ellipses.

4. FATIGUE PROPERTIES DESCRIPTION

The isotropy of the material fatigue properties in its virgin state [1] has been assumed. The material fatigue limit is assumed to be proportional to yield point [1] and the plastic prestrain to be the cause of a decrease in the fatigue strength [6]. To describe fatigue properties, three characteristic directions $\alpha = 0^\circ$, 45° and 90° have been chosen.

The assumed isotropy of mechanical properties shows that the same value of initial yield stress is characteristic of the virgin material for all α directions, like the fatigue properties which should be invariable along with the α direction. Lines having similar parameters should describe Wöhler's lines, which represent them, for three characteristic directions (Fig. 4).

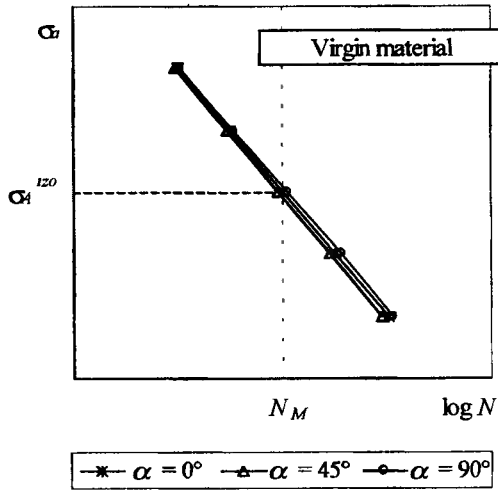


Fig. 4. Assumed Wöhler's lines for the virgin material

For prestrained material both plastic and fatigue properties change along with the α angle. According to the accepted assumption the increase in the initial yield stresses is connected with a decrease in fatigue strength. The decrease in fatigue strength should be expected in the direction in which plastic stresses increased, namely for $\alpha = 0^\circ$, while the increase in fatigue strength should be expected in the direction in which plastic stresses decreased, namely for $\alpha = 90^\circ$.

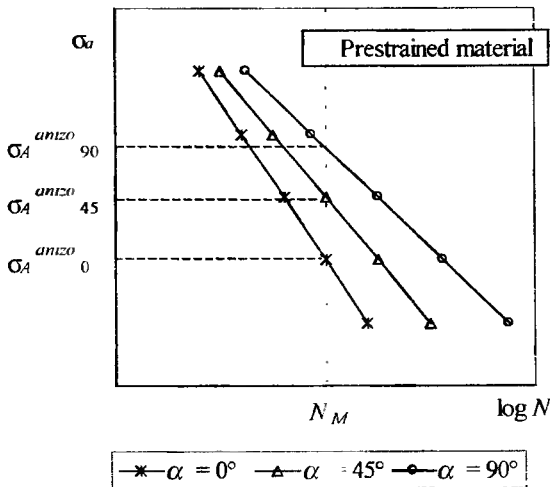


Fig. 5. Assumed Wöhler's lines for prestrained material

The above has been presented in Fig. 5 with a hypothetical position of Wöhler's line for characteristic angles $\alpha = 0^\circ$, 45° and 90° .

5. ALLOWABLE STRESS AMPLITUDE IN MODEL APPROACH

The accepted assumption about fatigue strength proportionality to initial yield stresses for the virgin material is expressed by Equation 3.

$$\text{def.} \quad \sigma_A = a \cdot \sigma_{pl} \quad (3)$$

$$a = \frac{\sigma_A^{izo}}{\sigma_{pl}^{izo}} \quad (4)$$

where:

- σ_A – allowable stress amplitude,
- a – scaling coefficient of the model,
- σ_A^{izo} – allowable stress amplitude for virgin material,
- σ_{pl}^{izo} – initial yield stress for virgin material.

When the stress state crosses the plastic ellipse BEC line which lies in the $0\sigma_x\sigma_y\tau_{xy}$ space, the virgin material will gain plasticity and turn in prestrained material. The plastic ellipse BEC is determined by σ_{pl} which are also the base values of Equation 3, the relationship can be presented as a fatigue ellipse bec within the $0\sigma_{xa}\sigma_{ya}\tau_{xya}$ stress space (Fig. 6). Crossing the fatigue bec ellipse line by stress amplitude for the virgin material will result in the occurrence of fatigue damage.

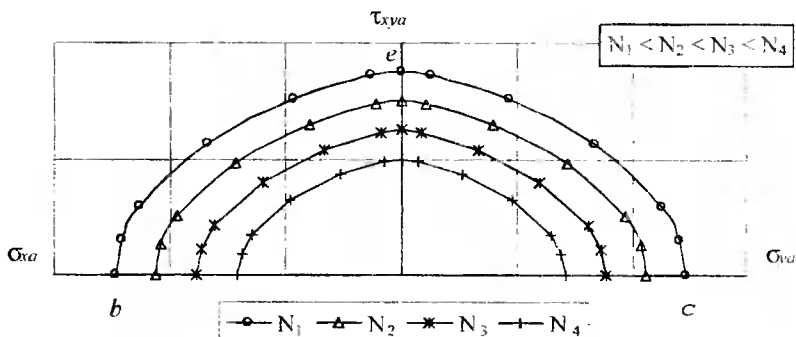


Fig. 6. Assumed bec ellipses; view into the $D0$ direction

As described earlier, provoking stresses with values exceeding the yield point in a given direction causes an increase in yield point in this direction. Its representation in Fig. 3 is a shift of the ellipse $B'E'C'$ in the σ_x direction. The $b'e'c'$ ellipse connected with it by Equation 3 also moves in the σ_x direction (Fig. 7). Since the plastic prestrain decreases the fatigue strength, which is not seen from Fig. 7, a model approach of the allowable amplitude σ_M has been introduced.

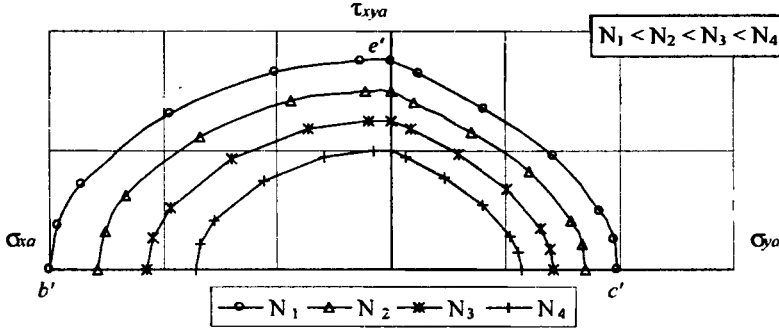


Fig. 7. Assumed $b'e'c'$ ellipses; view in the $D0$ direction

Stresses σ_M described by Equation 5 consist of a base part, σ_{Mb} described by Equation 6, which does not depend on the α direction, and of modifying part - σ_{M0} described by Equation 7, which change along with the α direction.

$$\sigma_M = \sigma_{Mb} + \sigma_{M0} \tag{5}$$

$$\sigma_{Mb} = \sigma_A^{izo} \tag{6}$$

$$\sigma_{M0} = \frac{1}{a} (\sigma_A^{izo} - \sigma_A^{anizo}) \tag{7}$$

where:

- σ_A^{izo} – allowable stress amplitude for virgin material,
- σ_A^{anizo} – allowable stress amplitude for prestrained material,
- σ_M – allowable stress amplitude in model approach,
- σ_{Mb} – model base stresses,
- σ_{M0} – model-modifying stresses.

Values of σ_A^{izo} are determined for the accepted life N based on Wohler's line for the virgin material (Fig. 4). Values of σ_A^{anizo} are determined for the accepted life N from the Wohler's line of proper α direction for prestrained material (Fig. 5). For the virgin material, $\sigma_A^{anizo} = \sigma_A^{izo}$ is accepted and so $\sigma_{M0} = 0$ and, finally, $\sigma_M = \sigma_A^{izo}$. The values σ_M obtained by transforming dependencies lead to determination of bec (Fig. 6) and $b'e'c'$ (Fig. 7) ellipses which depend on the number of N cycles accepted. In the model presented, there has been distinguished a model number of cycles accepted and marked as N_M . For N_M the value σ_M determined with fatigue test results is compared with σ_A determined by rescaling the test results of plastic properties. Symbolically, it is described by $\sigma_M = \sigma_A$ equation. For this case Equation 3 may be interpreted as a dependency between plastic BEC ellipse and fatigue bec ellipse for the virgin material and dependency between $B'E'C'$ and $b'e'c'$ for the prestrained material.

6. CONCLUSIONS

The model combining fatigue stress amplitudes with initial yield stresses has been formulated and called a model approach to allowable stress amplitude. There has been proposed an experimental method of determining the indicated fatigue and plastic properties.

An apparent parameter of the presented model is the relation of the allowable fatigue stress amplitude to initial yield stresses determined for the virgin material. Non-apparent parameters of the model are the model number of cycle and the plastic strain value accepted for the initial yield stress definition.

Using the model suggested and the material with modified plastic properties, in uniaxial loading conditions one can carry out the fatigue tests whose results could be presented in the form of a curve lying in the $0\sigma_{xa}\sigma_{ya}\tau_{xya}$ plane stress space.

REFERENCES

- [1] Cichański A., 2000. Modelowanie płaskiego stanu naprężeń zmęczeniowych. Doctor thesis. Mechanical Faculty, The Bydgoszcz University of Technology and Agriculture, Poland.
- [2] Cichański A., Sempruch J., 1999. Uniaxial fatigue test of anisotropy material as a model of biaxial fatigue. Proc.VII Inter. Fatigue Congress, Fatigue '99, Beijing-China, 977-982.
- [3] Findley W.N., Mathur P.N., Szczepanski E., Temel A.O., 1961. Energy versus stress theories for combined stress – a fatigue experiment using a rotating disk. Trans. ASME. J. Basic Engng. D, 83 (2), 10-14.
- [4] Sawert W., 1943. Verhalten der Baustähle bei wechselnder mehrachsiger Beanspruchung. Z. Ver. Deut. Ing. 87 (39/40), 609-615.
- [5] Schewchuk J., Zamrik S.Y., Marin J., 1968. Low-cycle fatigue of 7075-T651 aluminum alloy in biaxial bending. Experimental Mechanics 8 (11), 504-512.
- [6] Szczepiński W., 1984. Metody doświadczalne mechaniki ciała stałego. PWN Warszawa, 43-86.
- [7] Zamrik S.Y., Ledger D.J., Date C., 1997. Fatigue characteristics of thin titanium plates due to biaxial stress cycling. Proc. 5th Inter. Conf. Biaxial/Multiaxial Fatigue & Fracture, Opole-Cracow, II, 167-187.

Józef Flizikowski

University of Technology and Agriculture

Faculty of Mechanical Engineering

Department of Food Machines and Environment Protection

INTEGRALITY OF DESIGNING MACHINES OR THE ENVIRONMENT?

Summary. The paper presents the applicability of environmental methods development to the analysis of machines exploitation in the environment and offers potentials, actively controlled: machines operation in the environment as well as the environment for machines described by reliability, that is by the function incorporating its active and passive value, quality, namely the distance of practical effects from the pattern of theoretical possibilities.

Key words: machine designing, machine environment

1. INTRODUCTION

A dynamic and 'uncontrolled' development of machines exploitation in the environment made it necessary to provide a new approach to machine designing and technological mega systems as the environmental processors of energy and matter (processor - machine/person who processes; computer - device which processes information (Oxford Dictionary) in order to rationalize natural resources [1-15].

The value of the existing machine construction and exploitation should be appreciated, however it is also necessary to arrange and supplement some of the information to cover specific environmental problems, including the development of a new model and criteria of environmental significance of energy processors (including matter); supplementing designing, calculation bases, survey of applicability, adequacy of a well-known and intentionally modernized environmental theories of energy processors; technical systems operation efficiency systematization; work recognition and description, energy and ecology outlays; specification of system movement characteristics, suggestions and experimental verification of new techniques of calculation monitoring temporary loading of energy systems and cooperation.

Machine construction and exploitation are said to require combining the machine theory and environmental issues and to shape the nature of environment bearing in mind the imperfection of machines.

2. METHODOLOGY

The environmental and functional potential of operation, energy and renovation

The functional potential of technical system represents its external operating capacity [5]:

- human potential $P^L(t)$,
- technical potential $P^T(t)$,
- energy and material potential $P^E(t)$,
- controlling potential $P^S(t)$.

Operating potential function:

$$P_d(t) = \Phi \left[P^L(t), P^T(t), P^E(t), P^S(t) \right] \quad (1)$$

and especially:

$$P_d(t) = \pi_d(t) \cdot M_d(t) \cdot \varepsilon \quad (2)$$

Operating (energy) potential equation over the period $[t_0, T]$:

$$P_d(T) = P_d(t_0) - \int_{t_0}^T p_d^E(t) dt - \int_{t_0}^T p_d^S(t) dt + \int_{t_0}^T p_d^O(t) dt \quad (3)$$

where:

$P_d(t_0)$ - initial operating potential,

$p_d^E(t)$ - density of effectively used stream of potential,

$p_d^S(t)$ - density of lost stream of potential,

$p_d^O(t)$ - density of recovered (or obtained from the environment) stream of potential.

Each machine operation potential in the environment as well as the machine environment is described by reliability, namely by the function taking into account its active and passive value, quality, being the distance of practical effects from the pattern of theoretical capacities.

Reliability of controlling potential

The following are indicators describing the controlling potential: the description is limited to controlling potential exclusively, as the basic concept tool of designer's activity) [5,6,7]:

- possible volume of controlling information, S^S .
- volume of information used actively, usefully $M^S(t)$.
- theoretical possibilities and decision-informative needs. ε^S .
- temporary course of real executive possibilities, $\pi^S(t)$.

Theoretical information possibilities assume the value equal to one, if:

- information ensures realization of the process in the autonomous, reliable, solid and integral mode ($\varepsilon_a^S = 1$),
- controlling system automatically eliminates negative after-effects of processing. ($\varepsilon_c^S = 1$),
- controlling system is adopted for self-diagnosing and operating in the defined, efficient tolerance zone ($\varepsilon_{d-d}^S = 1$),

$$\varepsilon^E = \varepsilon_a^S \cdot \varepsilon_c^S \cdot \varepsilon_{d-d}^S \Rightarrow 1 \quad (4)$$

The modelling performed aiming at objectivisation of operating efficiency measurements and renewal of technical systems together with their environment (surrounding) allow for certain practical observations and conclusions:

1. Environment-friendly energy reliability, operating, renewal and processing involve a system and its surroundings can be addressed with the analysis of the factors describing the environment, human, technical, energy-material and controlling potential.
2. The risk of unfavourable effects of the operation and reaching the working target is measured with the reliability index and the index of needs of creative work, and renovation, recovery and restoration of potentials play a tremendous innovative and strategic role in designing environmental energy processes.

For the co-generation in Poland, the initial potential [15] has been used: in cannelite – 1.201.825 TJ – 66.8 %; in brown coal – 528.673 TJ – 29.4 %; in other media – 67.700 TJ – 3.8 %; a total of 1.798.208 TJ – 100.0 %.

Conventional coal processors

According to the criteria indices of the power model accepted – operating potentials, well-known, used and non-used power processors can be evaluated. An exemplary evaluation of a conventional coal processor (power station) is shown in Table 1, and willow-sewage processor in Table 2.

Table 1. Environmental consistency of the coal processor designed in Poland [7]*

No	Variables, indices	People	Technique	Energy-matter	Controlling	For environment	Total/ index of potential processor consistency
1.	Initial potential	1	3	0	3	6	13/30
2.	Recovered potential	1	3	1	1	1	7/30
3.	Environment protection	1	1	3	3	3	11/30
4.	Environment development	1	1	3	3	3	11/30
5.	Regeneration, environment renovation	6	3	1	3	1	14/30
6.	Aim, consistency of form with the need	3	3	1	3	1	11/30
7.	Consequences of the aim, after-effects	3	3	1	1	1	9/30
8.	Accessibility	3	6	6	3	6	24/30
9.	Efficiency	1	1	1	3	1	7/30
10.	Investment costs	3	1	1	3	1	9/30
11.	Exploitation costs	1	3	3	1	1	9/30
12.	Entropy	6	3	3	0	1	13/30
	Index of environmental consistency	30/72	31/72	24/72	27/72	26/72	0.38333

* Mark: 0 – critical, 1 – unsatisfactory, 3 – satisfactory, 6 – excellent

Table 2. Environmental consistency of willow energy processor in Poland [7]*

No	Variables, indices	People	Technique	Energy-matter	Controlling	For environment	Total/ index of potential processor consistency
1.	Initial potential	6	6	6	1	6	25/30
2.	Recovered potential	6	6	6	1	6	25/30
3.	Environment protection	3	6	3	3	3	18/30
4.	Environment development	3	1	3	3	6	16/30
5.	Regeneration, environment renovation	6	6	6	3	6	27/30
6.	Aim, consistency of form with the need	6	3	3	6	6	24/30
7.	Consequences of the aim, after-effects	6	3	6	3	6	24/30
8.	Accessibility	3	6	1	3	3	16/30
9.	Efficiency	3	6	3	6	3	21/30
10.	Investment costs	6	3	6	6	6	27/30
11.	Exploitation costs	6	6	1	3	6	22/30
12.	Entropy	6	6	6	3	6	27/30
	Index of environmental consistency	60/72	58/72	50/72	41/72	63/72	0.75555

* Mark: 0 – critical, 1 – unsatisfactory, 3 – satisfactory, 6 – excellent

- period of insolation over vegetation reaches 40–45 %,
- highly changeable rainfall in space and in time; mean values reaching 500–700 mm.

Foreign sources of late 1998 report on no intention of the leading world coal producers to reduce production. China with its 1369 million tons plans to reach 2100 million tons in 2010, and the USA, respectively, from 882 to 1002 million, Russia from 326 to 381 million tons, the RSA from 205 to 326 million tons, the other big producers from 669 to reach 1121 million tons. Poland is the only big producer which plans a reduction from 136 to 112 million tons [4].

Is it justified by designing criteria of energy processors? It seems that Polish power engineering based on coal will require some further application. Many conventional attitudes also show whether the world coal markets will change or not.

Wastewater processor with photosynthesis

Herbal energy processors use wastewater and sludge. Power-generating forests making use of quickly growing species of willows and alders [9,11,12] must be considered first, especially willows being very useful in biomass production and the Polish climate are advantageous:

- growing period with its mean daily temperature exceeding 5 °C, in Poland 210–215 days,
- a total of respective heat within 1600–1750 days.

Today power plantations produce, as reported from Sweden, about 15–18 tons of dry matter of willow wood from one hectare annually. Once the leaf and root matter is added, extra 4–7 tons of biomass is obtained. The annual production exceeding 12 tons of wood per ha is considered cost-effective.

The following can be regarded disadvantageous: the necessity to ensure a big area, of preliminary mechanical wastewater treatment, a close relationship between the treatment and air temperature variations, periodical increase in the volume of ammonia nitrogen in the wastewater treated, periodical hydrogen sulfide smell due to oxygen-free conditions in deposits.

Table 3. Environmental energy processors ranking up to 2020 in Poland [7]

Potentials ranking	Energy processor	Index of potentials consistency	Efficiency %	Efficiency ranking
1	Wastewater willows	0.75555	70.00	4
2	Oilseed crops	0.73611	60.00	5
3	Corn straw	0.69444	80.00	1
4	Flowing rivers	0.68611	80.00	2
5	Wind	0.66944	43.33	11
6	Sunrays	0.66385	53.33	8
7	Hydrogen	0.59444	80.00	3
8	Magnetohydrodynamics	0.57222	43.33	12
9	Farm biogas	0.54166	60.00	6
10	Heat pumps	0.49722	53.33	9
11	The Baltic Sea	0.49166	60.00	7
12	Fuel cell	0.49166	50.00	10
13	Coal	0.38333	23.33	14
14	Nuclear energy	0.36111	36.66	13

The wastewater treatment is not the main objective of the plantation activity; it is wood production to generate energy. Logging starts usually after two years of cultivation.

Generally harvesting takes place in winter. However wastewater irrigating requires removing maximum amounts of biogens from the ecosystem. Purple willow stems include usually 0.6–0.8 % of N in dry matter, which corresponds to 80–120 kg·ha⁻¹ of N. Harvesting, when accompanied by leaf collection, and assuming that half of the total leaf biomass is obtained, it is possible to remove an additional of 50–60 kg of N per ha from the ecosystem. Similarly phosphorus and potassium are obtained. Harvesting takes place every 3–5 years depending on the current plantation productivity. The production should proceed rather undisturbed for at least 20–30 years, while logging 5–8 times at least.

Heating value of dry willow wood amounts to 4.5 MWh·t⁻¹ (heavy fractions of crude oil (11 MWh·t⁻¹), light heating fuel (12 MWh·t⁻¹), and bituminous coal (7–8 MWh·t⁻¹).

Willow wood dried up to 25 % of water content shows the heating value corresponding to 18 MJ·kg⁻¹, which is two times lower than that of bituminous coal. The content of ash in willow wood amounts to about 1 %, i.e. a few dozen less than in bituminous coal. The relationship between the weight and volume: 1 ton of dry wood mass corresponds to the volume of 2.7 m³ of solid wood or 6.7 m³ of chips. For the third year of growth, wood production ranges from an annual of 12–15 tons of dry mass per hectare, of leaves and roots – 2–4, and 2–3 t/dry mass per ha. The biomass obtained from plantations ranges to 4.32 t, which corresponds to 28.81 m³ of chips.

3. CONCLUSIONS

Designing a form of energy carriers processing, we address a specific field of machine designing, technical mega systems, energy processors. However, the willow plantation itself is both a necessary supplement of the energy processor and the natural environment. Is it a machine and an environment?

The answer is simple: it is the environment, surroundings and neighbourhood of willow energy processor operating. However the answer to the question whether the windmill is a machine or an environment is available only with the processor definition. If it converts one type of energy into another – then it is a processor, a machine, technical mega system in the environment. So designing a windmill do we design environment? Or, maybe, do we design a windmill while designing an environment?

Avoiding the answer, we may say that willow energy production is economically and environmentally justifiable (Tables 2 and 3). Economy-wise, the following should be considered: energy generation from biomass as limited by the farm, reducing the farm wastewater removal costs and even additional income from harmless wastewater from households, low investment costs and low exploitation costs. However, oxygen production by plants with a combined reduction of CO₂ from the air is very environment-friendly, except for wastewater detoxification. At the same time due to H₂S emission and other odorous compounds, except for plantation location far from buildings, a construction of a green filter surrounding the plant is necessary; the plants are to isolate the plant, enhance the landscape and produce oxygen.

In general macrophytes treatment plant construction is economically and environmentally justifiable.

Last but not least

Presenting all the major environmental power processors as part of integral solutions of designing machines and environment (Table 3) offers universal conclusions. A designer most often searches for a suggestion: which processor is the best, most profitable, simplest, etc. and uses the criteria and construction arguments, time parameters and co-ordinates of the place of application and makes a subjective ranking (Table 3) up till 2020 in Poland.

Considering the environmentally conditioned working potentials, the municipal or specially composed wastewater-treated willow power processor comes first on the list. However, when efficiency is targeted, the maximum of 80 % is available from cereal straw, flowing rivers and hydrogen which come first.

The decision on the machine, environment, processor designing is taken by many people, including the designer.

REFERENCES

- [1] Buraczewski G., Bartoszek B., 1990. Biogaz - wytwarzanie i wykorzystanie. PWN Warszawa.
- [2] Buraczewski G., 1990. Ustalenie optymalnych parametrów technologii fermentacji metanowej gnojowicy. SGGW Warszawa.
- [3] Cieśliński J., Mikielwicz J., 1996. Niekonwencjonalne źródła energii. Wyd. P.G., Gdańsk.

- [4] ENERGIA, 1996-1999. Zagadnienia energetyki niekonwencjonalnej z wybranego okresu publikacyjnego: od 1/96 do 3/99. Agencja Promocji Poszanowania Energii, Warszawa.
- [5] Flizikowski J., 1998. Projektowanie środowiskowe maszyn. Wyd. Uczeln. ATR Bydgoszcz.
- [6] Flizikowski J., 1998. Rozdrabnianie tworzyw sztucznych. Wyd. Uczeln. ATR Bydgoszcz.
- [7] Flizikowski J., Bieliński K., 2000. Projektowanie środowiskowych procesorów energii. Wyd. Uczeln. ATR Bydgoszcz.
- [8] Johansson A., 1997. Czysta technologia. WNT Warszawa.
- [9] Kikiewicz Z., Flizikowski J., 1997. Zasoby energii i drewna dla środowiska XXI wieku. VII Konf. Inżynieria Maszyn 9, Bydgoszcz, 6-21.
- [10] Niewiedział E., 1998. Aktualne zasady tworzenia taryf na moc i energię elektryczną. III OP Kurs Techniczno-Szkoleniowy. Poznań-Kiekrz.
- [11] Pahl M.H., 1994. Umwelt und Energie. Universitaet-GH, WUZ, Paderborn.
- [12] Siemiński M., 1994. Fizyka zagrożeń środowiska. PWN Warszawa.
- [13] Sutkowski T., 1998. Zasady sporządzania dokumentacji projektowej w zakresie elektroenergetyki. OW Politechniki Warszawskiej, Warszawa.
- [14] Szumanowski A., 1988. Czas energii. WKŁ Warszawa.
- [15] Tymiński J., 1997. Potencjał energetyczny odnawialnych źródeł energii i jego rozmieszczenie na terenie Polski oraz stosowane technologie. Prace IBMER, Warszawa 3/1994, 2/1997, 35-58.

Mieczysław Gawda

University of Technology and Agriculture

Faculty of Mechanical Engineering

Department of Control and Machinery Design

EMPIRICAL DETERMINING OF MOVEMENT PARAMETERS FOR THE PNEUMATIC SERVO-MOTOR

Summary: Many different structural and pneumatic factors, due to some physical phenomena, affect servo-motor movement nature. The structural factors include piston diameter, piston travel length, minimal passage diameters, minimal filling and evacuating line diameters, coefficient of the initial volume, which is harmful, and dead space. Receiving the required power feed cycle is most essential due to its precise servo-motor mouth (exhaust) throttling arrangement. The paper discusses changeable movement parameters, due to servo-motor mouth throttling arrangement, effect of supply pressure on the servo-motor movement regularity and effects of line length of power system connecting elements.

Key words: control, pneumatic cylinder, dynamic characteristics, modelling

1. INTRODUCTION

Pneumatic power systems play very important role in automatics and their main advantage is reliability and operational simplicity. The pneumatic power system theory has been developing only recently, due to a great complexity of pneumatic device processes which have not been recognised yet. Air compressibility, movement irregularity of parts dislocated by forces connected with friction, load, weight and many other factors changing with a slide movement are critical for the experiment.

The standard slide dynamism is described by a system of non-linear differential equations which cannot be solved as finite. Many simplifications and assumption have been offered: air pressure permanence in one or two servo-motor chambers, piston movement is possible only as monotonous or monotonously accelerated, thermodynamical processes can only take place in a constant temperature.

It was necessary to consider in equations all those factors to meet the computation accuracy requirements of both customers and users; changeability of load and friction forces, heat replacement with an environment and leakage of the compressed air into the atmosphere or any other lower pressure space due to leakiness.

General non-linear differential equations system is a mathematical recording of a two-sided pneumatic device dynamism with a simultaneous filling and evacuating of the working chamber.

Examining pneumatic power system, movement equations and slide dynamism equations have to be solved, including the thermodynamic process ones.

Pneumatic power systems can be divided into two major groups:

- a) power systems that operate discreetly with a possibility of a slide stop in one or a few locations,
- b) power systems that operate constantly.

Both groups have been tested by the Control and Construction Unit of the University of Technology and Agriculture in Bydgoszcz. First of all, a two-sided pneumatic servo-motor with a one-sided piston rod and a 100 mm, according to ISO 4393, standard piston travel was tested.

2. RANGE OF EXAMINATION

Pneumatic servo-motor piston movement parameters have been tested, including dislocation, speed and acceleration which depended on supply pressure, throttling intensity at the delaying chamber mouth and length of lines connecting power system elements.

Construction parameters:

- D = 40 mm servo-motor diameter,
- L = 100 mm piston travel length,
- Φ = G ¼ diameters of filling and evacuating lines.

Pneumatic parameters.

- X - dislocation,
- \dot{X} - speed,
- \ddot{X} - acceleration.

3. TEST STAND FOR SERVO-MOTOR DYNAMIC CHARACTERISTICS EXAMINATION

Fig. 1 shows a test stand for pneumatic servo-motors examination which allows to examine different types of servo-motors when combined with corresponding sensors. The test stand is made up of a movement parameters measurement system and compressed air power supply system with a pitching pressure value.

The AP 50 compressor is used to supply the measurement system with compressed air. The pneumatic two-sided piston servo-motor (5) is supplied by the precise pressure reducing valve (1), expansion tank (3) and electromagnetic distributor (4). The supply pressure value is read with the pressure-measuring instrument.

The input signal from the inductive sensor of dislocation (PtX 200) is the output signal for the extensometer MGC. The MGC is connected with a computer unit with coupling RS-232c.

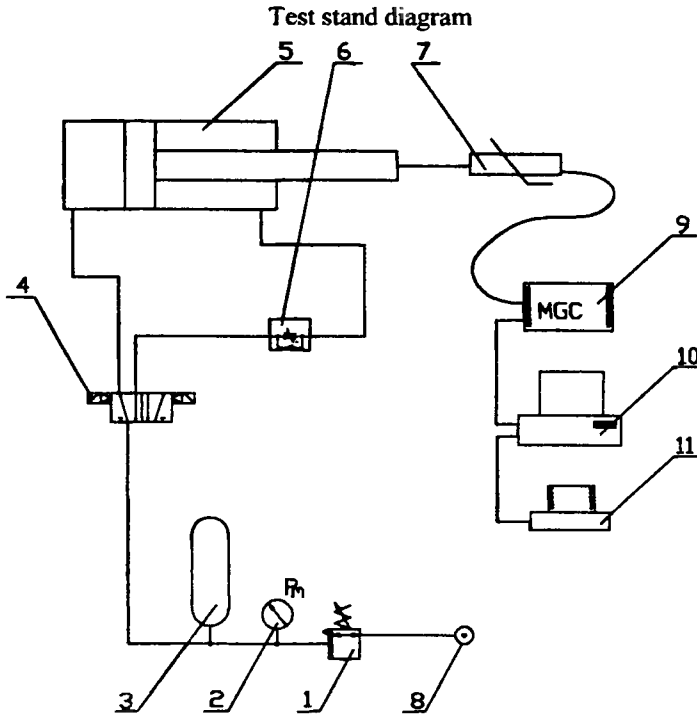


Fig. 1. Pneumatic power system diagram: 1 - precise pressure reducing valve, 2 - pressure measuring instrument, 3 - expansion tank, 4 - electromagnetic distributor, 5 - pneumatic piston servo-motor, 6 - gland seal, 7 - Ptx 200 inductive sensor, 8 - compressed air power supply source, 9 - MGC extensometer, 10 - computer, 11 - printer

The computer equipped with the main control program is an overriding unit and to record data. All the program parameters can be modified if necessary. The supply pressure was changed from 50 to 250 kPa and the pitch was 25 kPa. During the experiment a full cycle of servo-motor dislocation was recorded and the piston rod dislocation in time was measured.

4. DATA ACQUISITION

A special computer program was created to collect and record all the important data (based on documentation). The program to control the MGC extensometer (with RS-232c) has been developed with QBASIC. Fig. 2 shows the algorithm of data collecting and recording over the full cycle of a servo-motor dislocation.

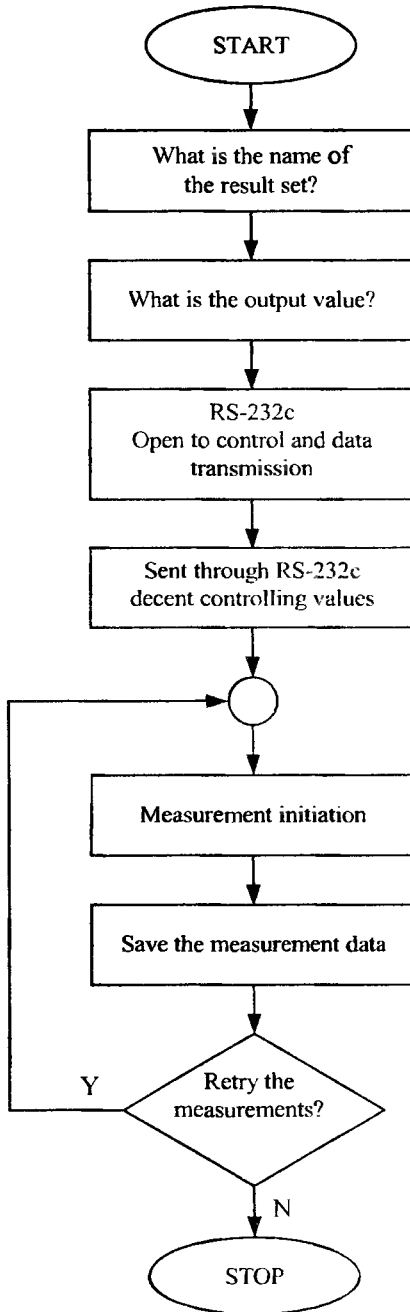


Fig. 2. Algorithm of the computer program which controls the extensometer with a coupling RS-232c used for disposition measurements

5. HYPOTHETICAL RESULTS OF THE EXPERIMENT

During the experiment the value of the supply pressure for the pneumatic servo-motor was changed from 50 to 250 kPa. With every single change, the pitch was 25 kPa. Servo-motor piston dislocation results depending on the supply pressure value are shown in Fig. 3.

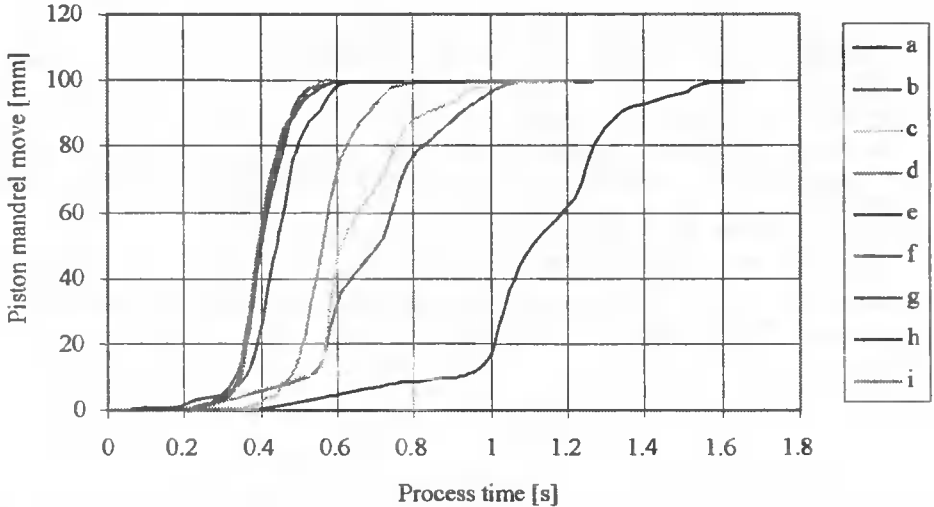


Fig. 3. Servo-motor piston rod dislocation results depending on the supply pressure: a) 50 kPa, b) 75 kPa, c) 100 kPa, d) 125 kPa, e) 150 kPa, f) 175 kPa, g) 200 kPa, h) 225 kPa, i) 250 kPa

6. CONCLUSIONS

The results of the piston rod dislocation in time were recorded with an about 1 % accuracy and are supposed to determine dynamic characteristics parameters, and to determine the dependence on the supply pressure.

Our experiments showed that test stand can be used for pneumatic servo-motor piston rod movement parameters measurements while changing pitch of various supply pressure values.

The test stand is very flexible allowing the examination of dynamic properties of various pneumatic servo-motors having been compiled with the corresponding sensors.

The analysis of some hypothetical results of the experiment show that the parameters describing T_0 (delay time) and T_z (substitute time constant) depend on the supply pressure and other factors and some further experiments should allow for defining quantitative dependencies between piston rod movement parameters, supply pressure and other parameters.

All the above suggests that the servo-motor piston rod movement parameters can be defined with a careful selection of structural servo-motor and supply and run-off pressure parameters. Some further experiment and analysis are required, including modelling, simulations and identifications whose results can help creating indices

(rates), tables and even methodology for pneumatic power systems designing with specific movement parameters.

REFERENCES

- [1] Gerc E. W., 1973. Napędy pneumatyczne. Teoria i obliczanie. WNT Warszawa.
- [2] Siedlaczek A., 2000. Podstawy obliczeń układów napędowych. Część I. Napędy i sterowanie 4.
- [3] Siedlaczek A., 2000. Podstawy obliczeń układów napędowych. Część II. Napędy i sterowanie 5.
- [4] Szenajch W., 1992. Napęd i sterowanie pneumatyczne. WNT Warszawa.
- [5] Iwaszko J., 1999. Funkcja przejścia pomiędzy parametrami C i b opisanymi w ISO 6358 a współczynnikiem wymiarowym K_v dla elementów pneumatycznych. Hydraulika i Pneumatyka 4.
- [6] Szydelski Z., 1999. Sterowanie ciśnieniowe. Hydraulika i Pneumatyka 4.
- [7] Gawda M., 1998. Przetworniki wielkości fizycznych. Praca dyplomowa. ATR Bydgoszcz.
- [8] Kaźmierczak M., 1999. Wieloobwodowe pneumatyczne układy napędowe – modelowanie i symulacja. Praca Dyplomowa. Politechnika Białostocka.

Tomasz Kuźmierowski
Franciszek Siemieniako
Polytechnic of Białystok
Faculty of Mechanical Engineering
Department of Mechatronic

COMPUTER AIDED KINEMATICS ANALYSIS OF 3D MECHANISMS

Summary: This article presents methodology of computer aided analysis of 3D kinematics mechanisms as well as the application of principles and functions for the computer analysis of 3D mechanisms.

Key words: kinematics, 3D mechanism, computer aided

1. ANALYTICAL ANALYSIS METHOD

The kinematics analysis of 3D mechanisms is offered by the authors in the form of TMM lectures and labs:

- a) defining coordinates of points in different systems,
- b) transforming coordinates of the kinematics IV and V classes pairs,
- c) transforming coordinates of 3D mechanisms,
- d) defining positions, velocity and acceleration for the definite points in mechanisms,
- e) kinematics analysis of twin-limbs mechanisms (motion parameters and working space),
- f) computer-aided kinematics analysis of 3D mechanisms.

Defining the motion parameters is realized in the following sequence:

- a) Introducing systems of coordinates in individual kinematics pairs

The relationships between respective axis and links are as follows: all z_i axes coincide with geometric axis of the ties. It is assumed that x_{i-1} axis lies on the common perpendicular to axis of rotative (rotated) pairs of the $i-1$ and i link. Axis z_i lies on rotated pair axis that joins links $i-1$ with i , y_i axis supplements the right-twirl rectangular system of coordinated, the same applies to the remaining pairs of kinematics chain. Besides for every link and every rotated union you can state the value of four parameters defining their position and orientation and referred to as the Denavit-Hartenberg parameters, defined as a_i – length i -link, measured along x_i axis, α_i – twirl angle of i -link, d_i – displacement of i -link along z_i axis, θ_i – configuration angle of i -rotated union.

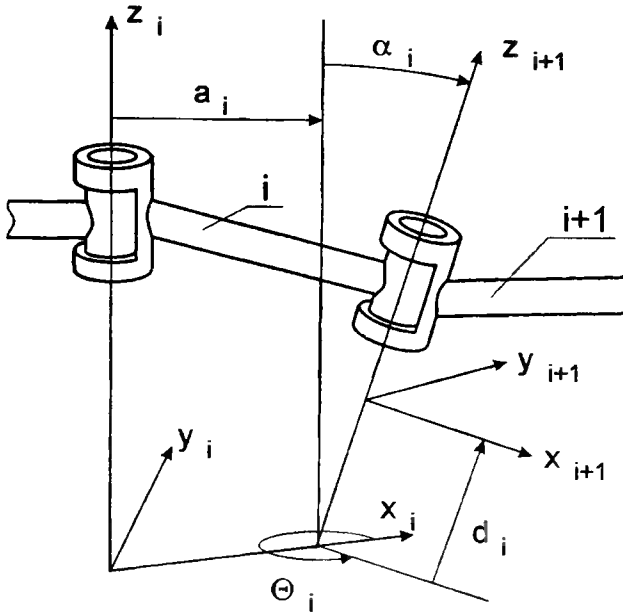


Fig. 1. Denavit-Hartenberg configuration parameters

b) Defining Denavit-Hartenberg parameters (constant and variable)

Four parameters define a relative position of two adjacent systems; three of which are always constant and one is variable. The kind of variable parameter depends on the type of kinematics pair (in rotated pair it is angle θ_i , and in displaced pair – length d_i). Two adjacent systems i and $i-1$ may be transformed by transporting i system to $i-1$ system with two rotations and two displacements, yet that transformation shows a different sequence in different kinematics pair. Each of the elementary movement corresponds to transformation matrix A_i , while the product of their matrixes makes ${}^{i-1}T_i$ – transformation matrix from $i-1$ system to i system.

c) Defining transformation matrix system of coordinates x_p, y_p, z_p to system x_0, y_0, z_0

General form of transformation matrix is, as follows:

$${}^0_pT = \begin{bmatrix} {}^0_pR & {}^0_pD \\ 0 & 0 & 0 & 1 \end{bmatrix} \quad (1)$$

where :

- 0_pR – rotation matrix of P system to 0 system (3 x 3 dimension),
- 0_pD – translation vector of P system to 0 system (3 x 1 dimension).

d) Motion parameters

Position of optional point lying, for example, on the last element of the manipulator in the global system of coordinates related to immovable base (0 system) can be calculated as follows:

$${}^0_{r=0}P_T \cdot P_T \quad (2)$$

where :

- ${}^0_{r=0}P_T$ – position vector of P point in 0 system,
- P_T – position vector of P point in the system of last element (P) of manipulator,
- ${}^0_P T$ – transformation matrix from P system to 0 system,
- ${}^0_P T = {}^0_1 T \cdot {}^1_2 T \cdot \dots \cdot {}^{P-1}_P T$,
- ${}^0_1 T, {}^1_2 T, \dots, {}^{P-1}_P T$ – transformation matrixes of indirect systems of kinematics chain.

Coordinates of vector ${}^0_{r=0}P_T$ of P point are examined as complicated functions of adequate Denavit-Hartenberg configuration parameters that are changeable in time. Velocity vector v_P of P point is derivative of time of ${}^0_{r=0}P_T$ vector. First derivatives of coordinates of the position vector of time equal coordinates of velocity vector v_P and the second derivatives equal coordinates of acceleration vector p_P , which can be expressed as:

$$v_P = d({}^0_{r=0}P_T)/dt \quad (3)$$

$$p_P = d(v_P)/dt = d^2({}^0_{r=0}P_T)/dt^2 \quad (4)$$

2. ALGORITHM OF COMPUTER ANALYSIS OF 3D MECHANISMS

The application developed for the analysis of and determining 3D mechanisms motion parameters is to enhance matrix transformations; defining the position, velocity and acceleration of the optional point.

The position and orientation of the grip system (P point) against the base system (0) is defined by 0 system translation and rotation until the position of both systems (0 and P) coincide. During transformation the 0 system takes successive positions which coincide with systems of coordinates of successive kinematics pairs of manipulator (translation and rotation pair).

Fig. 2 presents a diagram of the calculation series. First 0 system is defined as linked with the base of manipulator and then, having defined the manipulator number and kind of kinematics pairs, the respective systems of coordinates are described. Individual transformations are given by defining the transformation or rotation axis and the value of this transformation. That stage does not require giving an exact numerical value of translation or rotation but only the symbol it is represented by.

Once data is entered, the first calculations are made and 0 system-to-P system transformation matrix ${}^0_P T$ is obtained. Then formulas are derived, including position, velocity and acceleration of P point in the base system. Now numerical values of variable parameters can be entered to obtain numerical values of r , v and p .

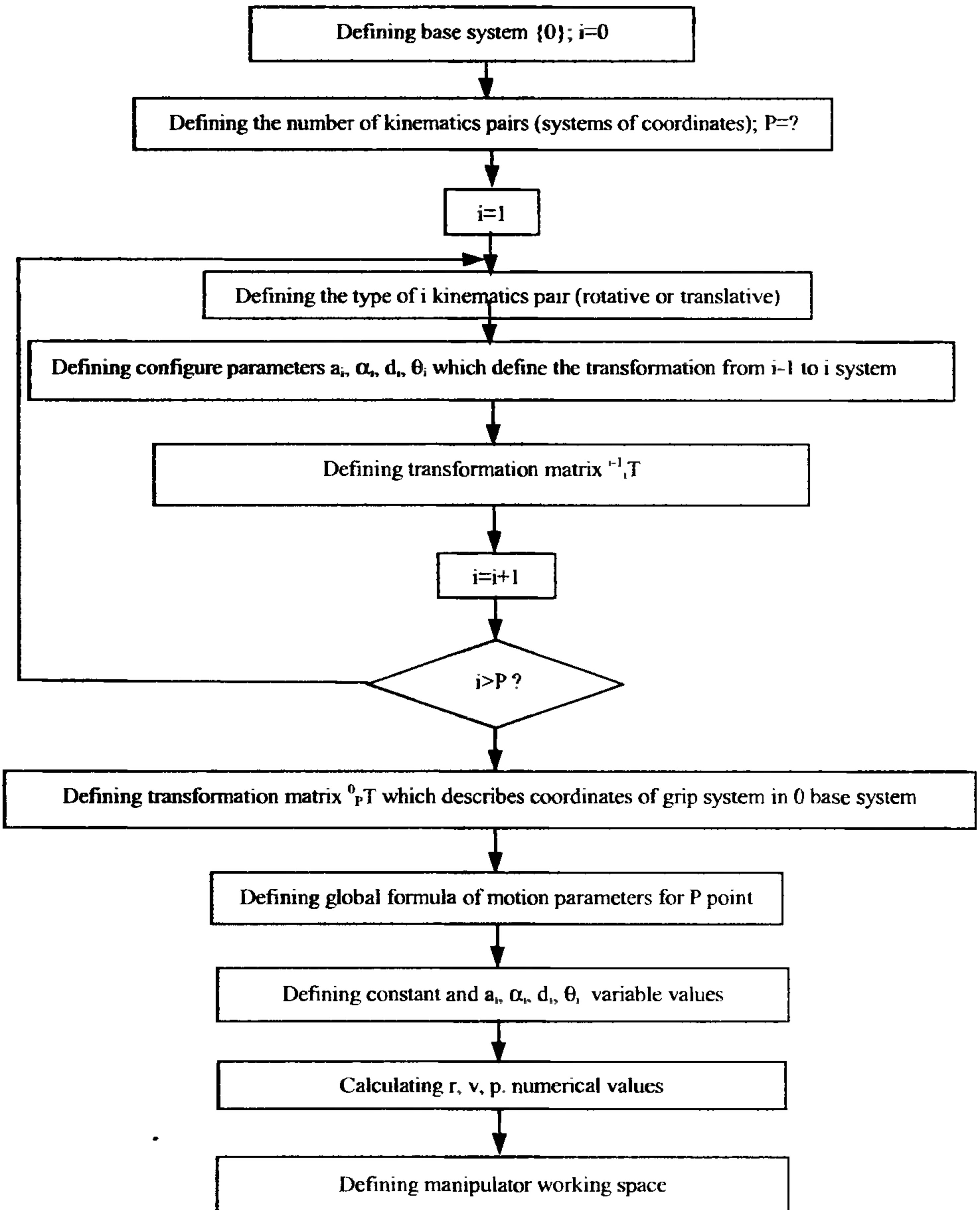


Fig. 2. 3D mechanism analysis algorithm

A major advantage of the application is a possibility of defining the formulas of motion parameters and transformation matrix as well as of manipulator working space. The present research uses the application to analyse twin links mechanisms of rotative and translative pairs in four combinations: RR, TT, TR and RT. An expanded version of the application can serve the analysis of mechanisms with multiple links.

3. DESCRIPTION OF THE APPLICATION

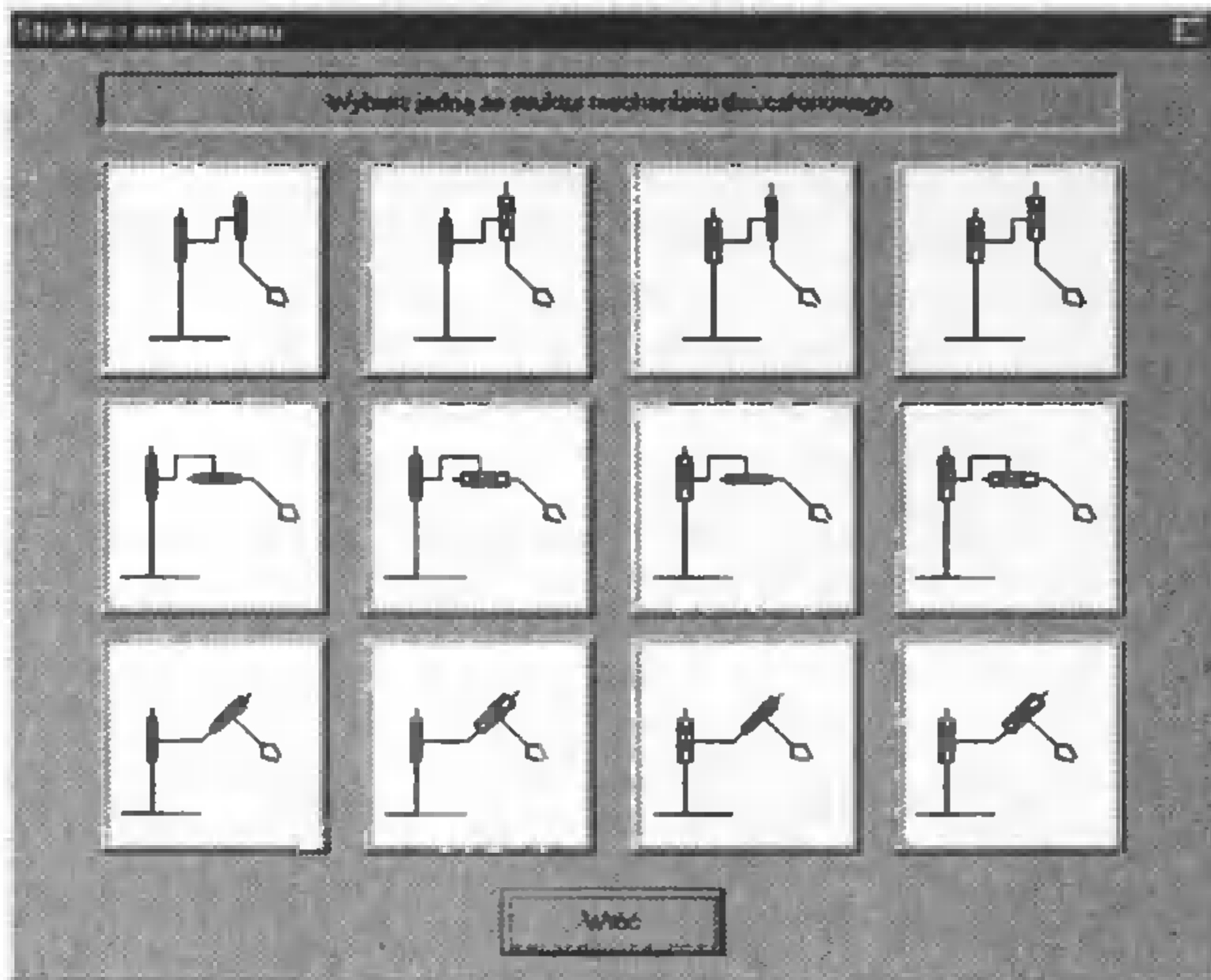


Fig. 3. Mechanism structure selection

To work with the application a new structure must be created. Press the button *Nowy mechanizm* and go to select the structure window; select one of the twelve twin links structures (Fig. 3) [4]. Next the window opens to define geometric parameters of the mechanism (Fig. 4), following the diagram markings. Denavit-Hartenberg parameters define the location of the system of coordinates of kinematics pairs. Press the button *Oblicz* and following the first calculations, transformatic matrix is given. Elements of this matrix are represented by formulas. To make it short, the following symbols are introduced: $st - \sin \theta$, $ct - \cos \theta$. The next window presents formulas of motion parameters defined for a selected mechanism (Fig. 5).

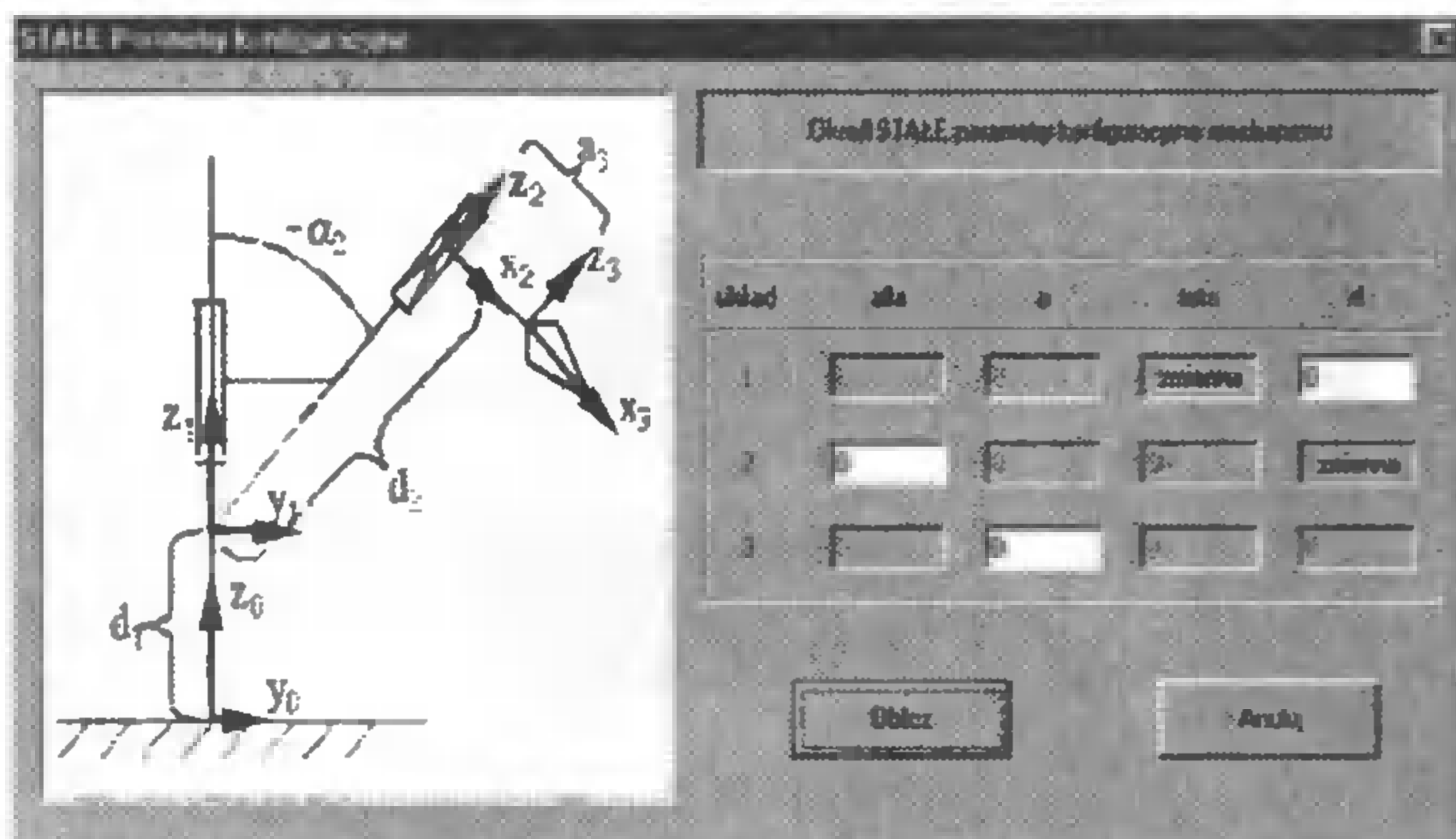


Fig. 4. Defining constant mechanism parameters

Wzory na parametry ruchu mechanizmu

Wzory na parametry ruchu mechanizmu o podanych parametrach
x, y, z – współrzędne punktu P w układzie kartezjańskim (3)

Przewidywana

$x = X_0(-0.866\sin t) + Y_0(-\cos t) + Z_0(0.5\sin t) + (-51.96\sin t - 0.5\sin t^2)$

$y = Y_0(0.866\cos t) + Y_0(-\sin t) + Z_0(-0.5\cos t) + (51.96\cos t - 0.5\cos t^2)$

$z = Z_0(0.5) + Z_0(1.866) + (10 + 0.866t^2)$

Prędkość

$\dot{x} = X_0(-0.866\cos t) + Y_0(\sin t) + Z_0(0.5\cos t) + (-51.96\cos t - 0.5\cos t^2) + 0.5\sin t^2$

$\dot{y} = Y_0(-0.866\sin t) + Y_0(-\cos t) + Z_0(-0.5\sin t) + (-51.96\sin t - 0.5\sin t^2) + 0.5\cos t^2$

$\dot{z} = 1.732t$

Przyspieszenie

$\ddot{x} = X_0(0.866\sin t) - 0.866\cos t + Y_0(\cos t) + Y_0(-\sin t) + Z_0(-0.5\sin t) + 0.5\sin t^2 + (-51.96\sin t)$

$\ddot{y} = Y_0(0.866\cos t) - 0.866\sin t + Y_0(-\sin t) + Y_0(-\cos t) + Z_0(-0.5\cos t) + 0.5\cos t^2 + (-51.96\cos t)$

$\ddot{z} = 1.732$

Wyznacz wartości liczbowe

Koniec

Fig. 5. Motion parameters formula

To define numerical values of these parameters, press the button *Wyznacz wartości liczbowe* and in the next window define coordinates of P point in grip system. In the next window the option *Punktowe – wartości chwilowe* gives Denavit-Hartenberg parameters. For the momentary values, the velocity and acceleration of P point assume momentary value as derivatives of constants with time are null. After the next calculations, numerical values of motion parameters are given.



Fig. 6. Working space of mechanism

After pressing *Ok*, return to the general window. It is possible now to change any parameter and see how it has affected the results of the calculations. We can change geometrical dimensions, configuration parameters or coordinates of P point. The kind and number of changes are optional. Now press the button *Przelicz na nowo* to obtain new formulas and numerical values of transformation matrix and motion parameters by pressing the right buttons in the general window (Fig. 7). It is possible to have a look at and print the calculations report, including all the data of a given mechanism; constant and variable configuration parameters, data for numerical values calculations, formulas derived and numerical values calculated of transformation matrix and motion parameters.

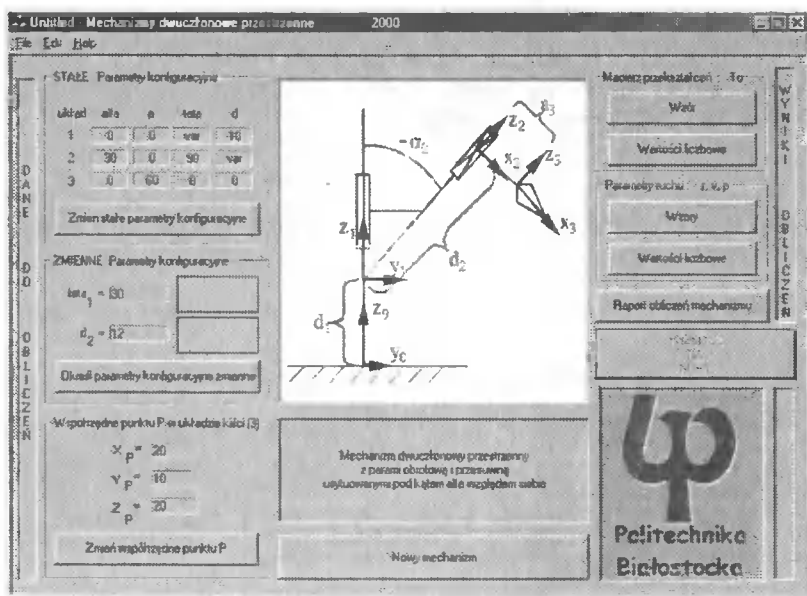


Fig. 7. Window for defining 3D mechanisms motion parameters

4. SAMPLE MECHANISMS ANALYSIS RESULTS

4.1. Twin links mechanism with two rotative pairs

Twelve such mechanism structures found in literature are available from Miller [4] and the present paper offers an analysis of two structures.

A diagram is shown in Fig. 8. The structure variable parameters include θ_1 and θ_2 , while constant parameters incorporate the following dimensions: α_2 , y_p , a_2 , d_1 , d_2 .

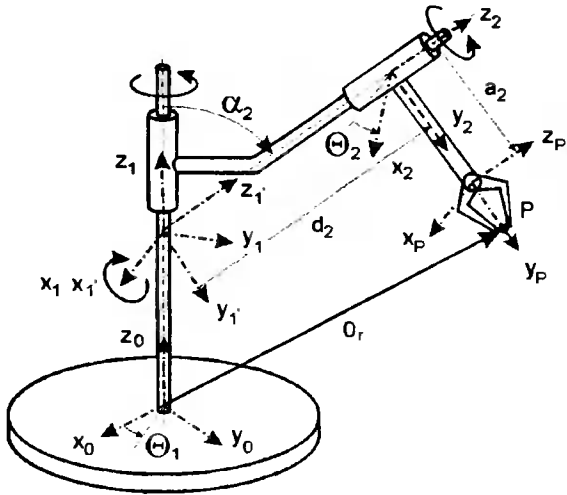


Fig. 8. 00 mechanism diagram

Following (1) and (2), transformation matrix for this mechanism takes the form of:

$${}^0_P T = {}^0_1 T \cdot {}^1_2 T \cdot {}^2_P T \quad (5)$$

$${}^0_1 T = \begin{bmatrix} c\theta_1 & -s\theta_1 & 0 & 0 \\ s\theta_1 & c\theta_1 & 0 & 0 \\ 0 & 0 & 1 & d_1 \\ 0 & 0 & 0 & 1 \end{bmatrix} \quad (6)$$

$${}^1_2 T = \begin{bmatrix} c\theta_2 & -s\theta_2 & 0 & 0 \\ c\alpha_2 s\theta_2 & c\alpha_2 c\theta_2 & -s\alpha_2 & -d_2 s\alpha_2 \\ s\alpha_2 s\theta_2 & s\alpha_2 c\theta_2 & c\alpha_2 & d_2 c\alpha_2 \\ 0 & 0 & 0 & 1 \end{bmatrix} \quad (7)$$

$${}^2_P T = \begin{bmatrix} 1 & 0 & 0 & 0 \\ 0 & 1 & 0 & a_2 \\ 0 & 0 & 1 & 0 \\ 0 & 0 & 0 & 1 \end{bmatrix} \quad (8)$$

$${}^0_P T =$$

$$\begin{bmatrix} c\theta_1 c\theta_2 - c\alpha_2 s\theta_1 s\theta_2 & -c\theta_1 s\theta_2 - c\alpha_2 s\theta_1 c\theta_2 & s\alpha_2 s\theta_1 & -a_2(c\theta_1 s\theta_2 + c\alpha_2 s\theta_1 c\theta_2) + d_2 s\alpha_2 s\theta_1 \\ s\theta_1 c\theta_2 + c\alpha_2 c\theta_1 s\theta_2 & -s\theta_1 s\theta_2 + c\alpha_2 c\theta_1 c\theta_2 & -s\alpha_2 c\theta_1 & -a_2(s\theta_1 s\theta_2 - c\alpha_2 c\theta_1 c\theta_2) - d_2 s\alpha_2 c\theta_1 \\ s\alpha_2 s\theta_2 & s\alpha_2 c\theta_2 & c\alpha_2 & a_2 c\alpha_2 c\theta_2 + d_1 + d_2 c\alpha_2 \\ 0 & 0 & 0 & 1 \end{bmatrix} \quad (9)$$

Based on (1) and matrix structures 0_1T , 1_2T , ${}^2_P T$, the following formulas of position, velocity and acceleration of P point in 0 system are given, where the variables are θ_1 , θ_2 .

$${}^0\mathbf{r} = {}^0_P T \cdot P\mathbf{r} = \begin{bmatrix} -(y_p + a_2)(c\theta_1 s\theta_2 + c\alpha_2 s\theta_1 c\theta_2) + d_2 s\alpha_2 s\theta_1 \\ -(y_p + a_2)(s\theta_1 s\theta_2 + c\alpha_2 c\theta_1 c\theta_2) - d_2 s\alpha_2 c\theta_1 \\ (y_p + a_2)s\alpha_2 c\theta_2 + d_1 + d_2 c\alpha_2 \end{bmatrix} \quad (10)$$

$${}^0\mathbf{v} = d/dt({}^0\mathbf{r}) =$$

$$\begin{bmatrix} -(y_p + a_2)(-s\theta_1 \dot{\theta}_1 s\theta_2 + c\theta_1 c\theta_2 \dot{\theta}_2 + c\alpha_2 c\theta_1 \dot{\theta}_1 c\theta_2 - c\alpha_2 s\theta_1 s\theta_2 \dot{\theta}_2 + d_2 s\alpha_2 c\theta_1 \dot{\theta}_1) \\ -(y_p + a_2)(c\theta_1 \dot{\theta}_1 s\theta_2 + s\theta_1 c\theta_2 \dot{\theta}_2 - c\alpha_2 s\theta_1 \dot{\theta}_1 c\theta_2 - c\alpha_2 c\theta_1 s\theta_2 c\dot{\theta}_2) - d_2 s\alpha_2 s\theta_1 \dot{\theta}_1 \\ -(y_p + a_2)s\alpha_2 s\theta_2 \dot{\theta}_2 \end{bmatrix} \quad (11)$$

$${}^0\mathbf{p} = d/dt({}^0\mathbf{v}) =$$

$$\begin{bmatrix} -(y_p + a_2)[-c\theta_1 \dot{\theta}_1^2 s\theta_2 - s\theta_1 \ddot{\theta}_1 s\theta_2 - 2s\theta_1 \dot{\theta}_1 c\theta_2 \dot{\theta}_2 - c\theta_1 s\theta_2 \dot{\theta}_2^2 + c\theta_1 c\theta_2 \ddot{\theta}_2 - \\ -c\alpha_2 (s\theta_1 \dot{\theta}_1^2 c\theta_2 + c\theta_1 \ddot{\theta}_1 c\theta_2 - 2c\theta_1 \dot{\theta}_1 s\theta_2 \dot{\theta}_2 - s\theta_1 c\theta_2 \dot{\theta}_2^2 - s\theta_1 s\theta_2 \ddot{\theta}_2)] - d_2 c\alpha_2 (-s\theta_1 \dot{\theta}_1^2 + c\theta_1 \ddot{\theta}_1) \\ -(y_p + a_2)[-s\theta_1 \dot{\theta}_1^2 s\theta_2 + c\theta_1 \ddot{\theta}_1 s\theta_2 + 2c\theta_1 \dot{\theta}_1 c\theta_2 \dot{\theta}_2 - s\theta_1 s\theta_2 \dot{\theta}_2^2 + s\theta_1 c\theta_2 \ddot{\theta}_2 + \\ + c\alpha_2 (c\theta_1 \dot{\theta}_1^2 c\theta_2 + s\theta_1 \ddot{\theta}_1 c\theta_2 - 2s\theta_1 \dot{\theta}_1 s\theta_2 \dot{\theta}_2 + c\theta_1 c\theta_2 \dot{\theta}_2^2 + c\theta_1 s\theta_2 \ddot{\theta}_2)] + d_2 c\alpha_2 (c\theta_1 \dot{\theta}_1^2 + s\theta_1 \ddot{\theta}_1) \\ -(y_p + a_2)s\alpha_2 (c\theta_2 \dot{\theta}_2^2 + s\theta_2 \ddot{\theta}_2) \end{bmatrix} \quad (12)$$

The three formulas make it possible to define the value of ${}^0\mathbf{r}$, ${}^0\mathbf{v}$, ${}^0\mathbf{p}$ in an optional position of the mechanism for definite functions $\theta_1(t)$, $\theta_2(t)$. For example $\theta_1 = 45^\circ$, $\theta_2 = 60^\circ$ and geometric dimensions $\alpha_2 = 30^\circ$, $y_p = 1$, $d_1 = 10$, $d_2 = 8$, $a_2 = 5$, vector ${}^0\mathbf{r}$ is obtained.

$${}^0\mathbf{r} = \begin{bmatrix} 2.6824 \\ 8.3384 \\ 18.428 \end{bmatrix} \quad (13)$$

5. SUMMARY

In the opinion of the authors, the application presented is of a considerable practical applicability as it makes it possible to:

- define motion parameters without difficult matrix calculations,
- carry out kinematics analysis for 3D mechanisms with a wide range of changes of their configuration parameters,
- follow successive calculations stages.

Additionally, the application facilitates teaching students a complex 3D-mechanisms kinematics analysis, considerably.

REFERENCES

- [1] Craig J.J., 1993. Wprowadzenie do robotyki. Mechanika i sterowanie. WNT Warszawa.
- [2] Lansdown J.J., 1992. Grafika komputerowa. WNT Warszawa.
- [3] Knapczyk I., Lebediew P.A., 1991. Teoria mechanizmów przestrzennych i manipulatorów. WNT Warszawa.
- [4] Miller S., 1989. Teoria maszyn i mechanizmów – Analiza układów mechanicznych. Wyd. Politechniki Wrocławskiej, Wrocław.
- [5] Wawrzecki J., 1994. Teoria maszyn i mechanizmów. Wyd. Politechniki Łódzkiej. Łódź.

Marek Macko

University of Bydgoszcz

Institute of Technics

Department of Mathematics, Technics and Natural Science

COMPUTER-AIDED MULTIPLE-DISC-SHREDDING RESEARCH

Summary. Shredding is one of the important stages in plastic technology. A variety of materials, part shape and product quality justify a search for constructional solutions for the energy-saving multiple disc shredder. State of the art technology makes it possible to continue computer aided research of shredding as well as to simulate machine investigation.

Key words: quasi-cutting, multiple-disc shredder, CAD

1. INTRODUCTION

A search for energy-saving production processes justifies investigating a new enhanced construction - alternative milling design [6,10] which was taken up by the Department of Mechanics of the Bydgoszcz University of Technology and Agriculture and by the Institute of Technics of the Bydgoszcz University.

The multiple-disc mills patented by Flizikowski and Bieliński [1,2] cut on hole edges in discs or drums rotating with different speed or being in a position of relative movement; it is based upon both the tool cutting edge number and the edge geometry, which can be deterministic or random. According to this classification, milling processes are featured by the tools with deterministic geometry. Each cutting edge is of a precisely defined size, radius, rake and clearance angles, and nose radius. The present study investigates a plastic-pipe-refuse multiple-disc shredder. The available literature on multiple disc shredders construction and investigation does not cover the effect of construction on the plastic pipe refuse milling.

The research included computer-aided conceptual, simulated under strain-machine conditions and as a physical experiment with multiple disc shredder. The initial research covered a range of material properties and geometric features, while the main research - the relation between quasi-cutting element velocity, the angle of blade edges of holes, gaps between discs as well as the area of holes and of pipe profile and energy efficiency [3,7].

2. METHODOLOGY

The aim of the present research was an evaluation of mathematical model, including input, exit variables and their coefficients and an experimental results comparison. According to the machine design model developed by Flizikowski and Polański, the procedures included, as follows (Fig. 1):

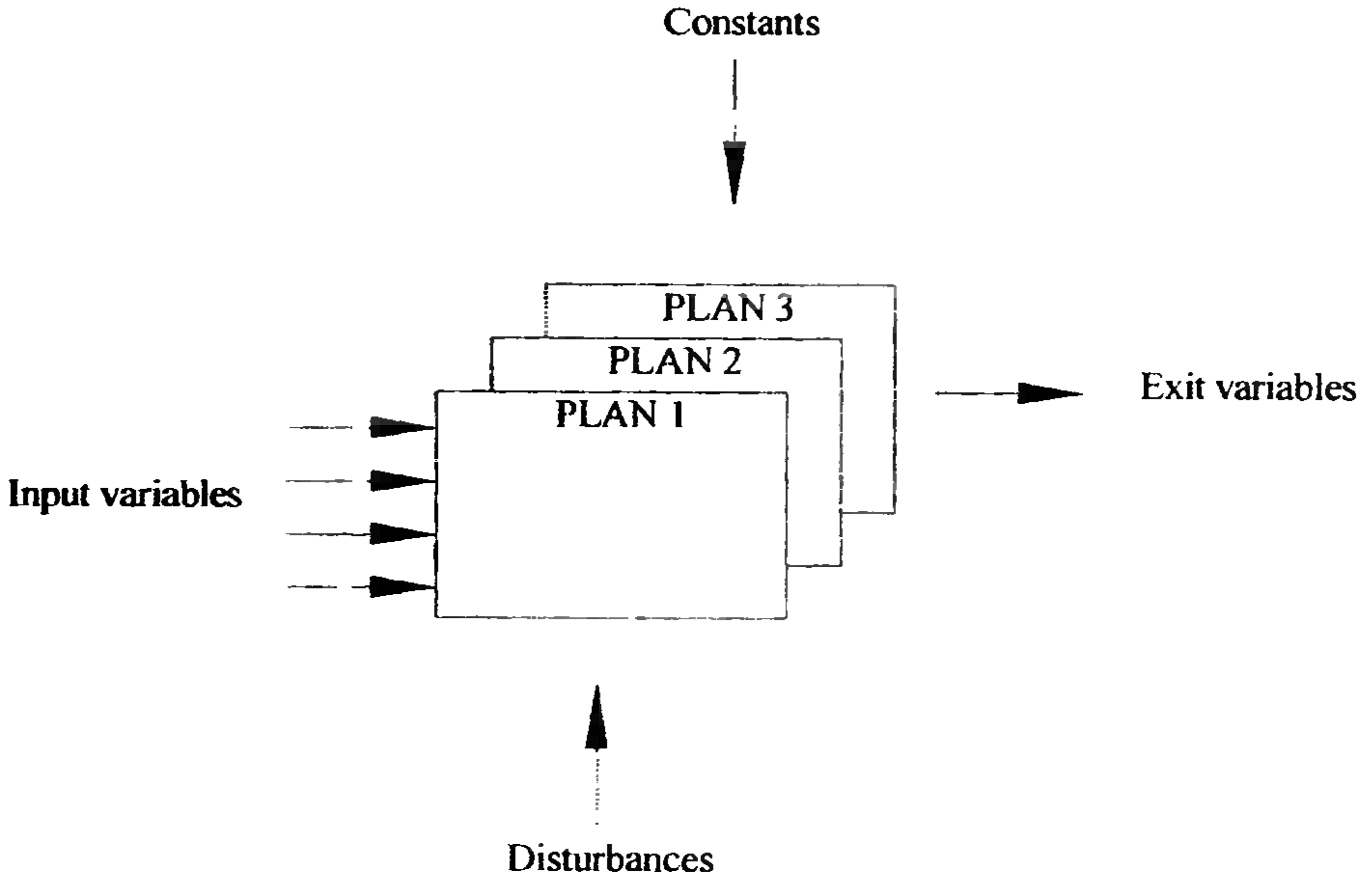


Fig. 1. General machine design research model developed by Flizikowski [11] and Polański [12]. Plan 1. Conceptual analysis; Plan 2. Machine strength investigation; Plan 3. Relations between multiple-disc shredder useful characteristics and constructional features

Cadex:Esdet based on object variables, including the velocity of quasi-cutting elements, hole blade edge angle, gaps between discs as well as the area of holes and of pipe profile and energy efficiency enabled us to select the optimum plan (Fig. 2).

The conceptual analysis (plan 1) based on constructional criteria helps to define the geometric and dynamic features of the functional system of the shredder. The computer notation of the solution has been represented as a 2D (Auto CAD) and 3D standard (Solid Works), Fig. 3.

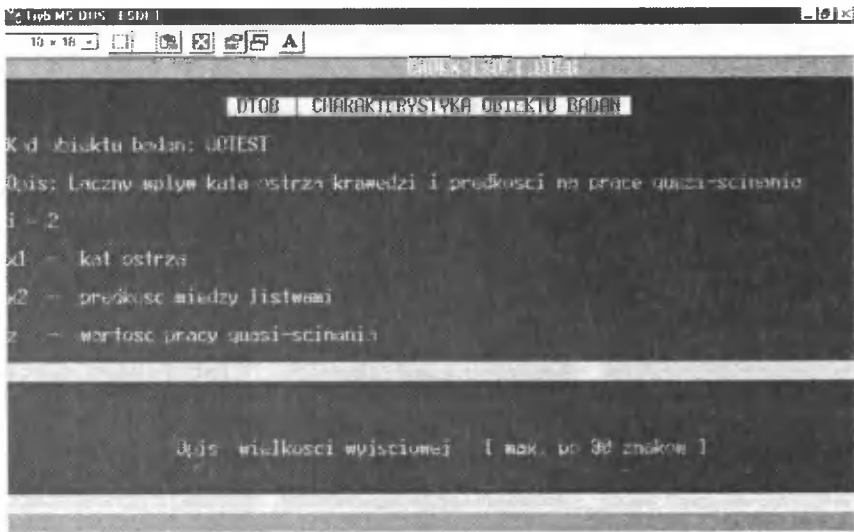


Fig. 2. Cadex:Esdet screen – recording of input variables

At the same time the features of plates and discs with holes are modernised with Excel calculations [7]. The geometric relations are created by the simulation of transient section area and strength with Test-4-TPTS (C++) [3,4]. The variations selected make it possible to develop an initial functional system design (Table 1, Fig. 4).

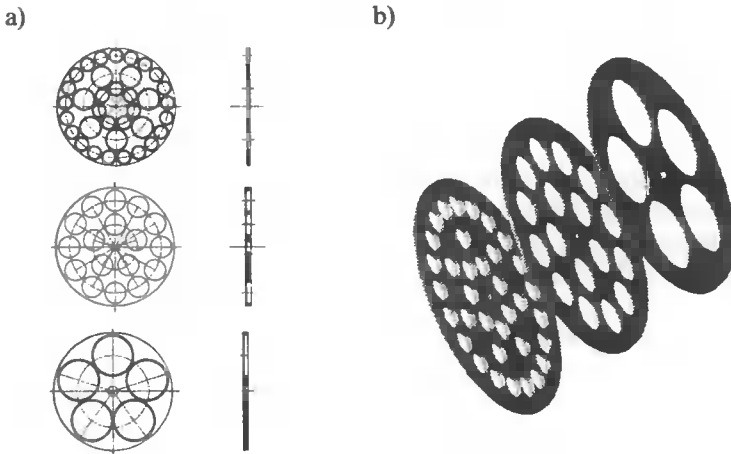


Fig. 3. View of discs with holes to quasi-cut material
a) Auto-CAD notation, b) Solid-Works notation

Table 1. Arrangement of selected features for simulated section area investigation

IDEA	First variant	Second variant	Third variant
Number of discs	3	5	7
Number of rows in the disc	2	2	2
Number of holes in the first disc	5	9	9
SOLUTION	Fig. 4a	Fig. 4b	Fig. 4c (preferred)

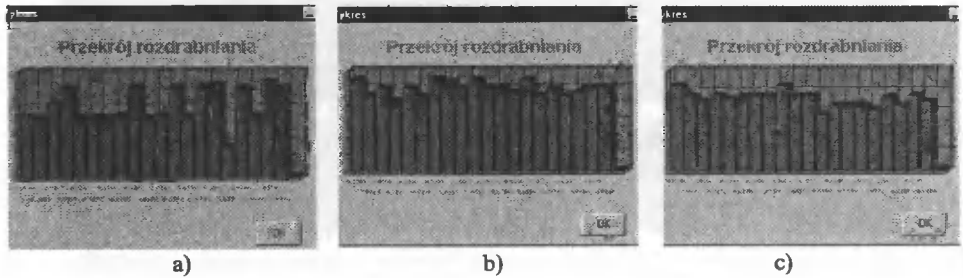


Fig. 4. Transient section area bar chart for selected multiple disc shredder variants; a) first variant (Table 1), b) second variant (Table 1), c) – third variant (Table 1)

In the experiments, based on the plate device PRR-5QS and Instron 8501 (plan 2) with the experimental stand, an attempt has been made to describe loads, strain, deformation and displacement of cut material in multiple-edge space [3,5,7]. Transient values of strength, moment and velocity were measured by transducers and converted by PSI-GAD-III system (described in [3,9]) (plan 3). Dynamic and kinematics analysis used Dynamic Designer Motion.

3. RESULTS

The present results confirm the dependence between constructional features and useful characteristics. Plan 2 distinguishes quasi-cutting functions for various materials, for different sample material lengths, for various sample shapes and arrangement in device, for different speed between slats, for variable blade angle of disc hole β edge (Fig. 5).

The results obtained were verified statistically; the calculation of the function object and multiple 4th degree non-linear regression $P = f(\Delta l)$ with Excel and Cadex:Esdet (1-5 Equations). The results helped to increase or decrease the value of the milling coefficient.

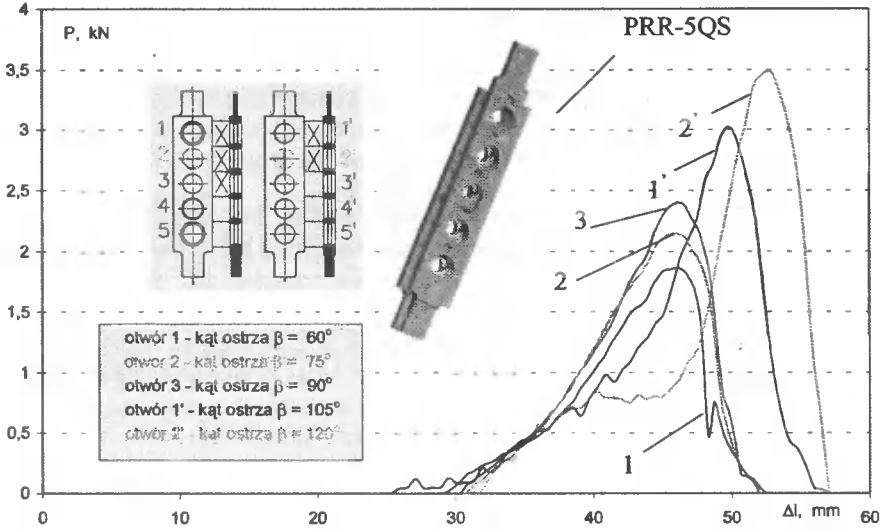


Fig. 5. Power curves for P quasi-cut as a function of slats dislocation Δl for different values of blade angle β . Material: PE-LD-pipe, outer diameter $D_z = 20$ mm, pipe thickness $g = 2$ mm. Speed between slats $v_r = 2$ mm s⁻¹

$$\beta = 60^\circ:$$

$$P = -5E-05\Delta l^4 + 0,0058\Delta l^3 - 0,2548\Delta l^2 + 4,8103\Delta l - 26,105 \quad (1)$$

$$R^2 = 0,8824$$

$$\beta = 75^\circ:$$

$$P = -3E-05 \Delta l^4 + 0,0036 \Delta l^3 - 0,173 \Delta l^2 + 3,6626\Delta l - 20,887 \quad (2)$$

$$R^2 = 0,9006$$

$$\beta = 90^\circ:$$

$$P = -2E-05 \Delta l^4 + 0,0033 \Delta l^3 - 0,1687 \Delta l^2 + 3,8256\Delta l - 22,465 \quad (3)$$

$$R^2 = 0,912$$

$$\beta = 105^\circ:$$

$$P = -2E-05 \Delta l^4 + 0,0023 \Delta l^3 - 0,1272 \Delta l^2 + 3,1637\Delta l - 20,444 \quad (4)$$

$$R^2 = 0,9071$$

$$\beta = 120^\circ:$$

$$P = -2E-05 \Delta l^4 + 0,0026 \Delta l^3 - 0,1428 \Delta l^2 + 3,4036\Delta l - 21,893 \quad (5)$$

$$R^2 = 0,9069$$

4. CONCLUSIONS

The present paper suggests the application of computer solutions for designing and researching multiple-disc-system constructional features.

The multiple-disc shredder modelling preferred and milling indicator characteristics make it possible to design milling constructions for specific cut material properties, machining parameters and milling conditions [3,7,8,9].

The present results and computer-aided research of multiple disc shredding confirm the total effect of different quantities and factors on shredder characteristics and show that an effective solution is available if we consider the relationships among construction elements. Further intensive studies are being conducted and aim at defining the relationship between constructional features of mill functional systems and useful energy-consumption characteristics using computer-aided design and research systems.

ACKNOWLEDGEMENTS

Financial support of this research and advanced laboratory facilities provided by the State Committee for Scientific Research in Poland are gratefully acknowledged (Grant No. 7 T08E 008 17).

REFERENCES

- [1] Flizikowski J., Bieliński M., 1988. Rozdrabniacz wielotarczowy zwłaszcza do materiałów ziarnistych. Patent PRL, P – 140486, UP Warszawa.
- [2] Flizikowski J., Bieliński M., 1989. Rozdrabniacz wielotarczowy zwłaszcza do materiałów ziarnistych i kawalkowych. Patent RP, P – 144566, UP Warszawa.
- [3] Flizikowski J., 1996–1998. Raport z grantu KBN PB-462/T08/96/11 pt.: Badania i rozwój wielotarczowych rozdrabniaczy reżykatów tworzyw termoplastycznych. ATR Bydgoszcz.
- [4] Flizikowski J., 1990. Badania i podstawy konstrukcyjne rozdrabniaczy wielotarczowych. Rozprawy 42, Wyd. Uczeln. ATR Bydgoszcz.
- [5] Flizikowski J., Macko M., Pahl M., 1999. CAD application in multiple disk shredder – design. Mat. konf.: Maszyny i urządzenia spożywcze – Żywnie człowieka – Hotelarstwo – Piekarstwo, ATR Bydgoszcz.
- [6] Shamoto E., Altintas Y., 1999. Prediction of shear angle in oblique cutting with maximum shear stress and minimum energy principles. J. Manufacturing Sci. and Eng. 8.
- [7] Macko M., 2000. Wpływ cech konstrukcyjnych zespołu wielotarczowego na charakterystyki użytkowe procesu rozdrabniania rurowych reżykatów tworzyw sztucznych. Praca doktorska WM ATR Bydgoszcz.
- [8] Flizikowski J., Macko M., 2001. Metodyka oceny sprawności quasi-ścianiania reżykatów rur optotelekomunikacyjnych. POLIMERY 1, XLVI, 53-59.
- [9] Flizikowski J., Macko M., 2000. Computer aided designing of multiple disc shredder. Zesz. Nauk. Inżynieria Maszyn. Recykulacja w budowie maszyn ICMR. ATR Bydgoszcz.
- [10] Kaldor S., Venuvinod P.K., 1997. Macro-level optimisation of cutting tool geometry. J. Manufacturing Sci. and Eng. 2.
- [11] Flizikowski J., 1998. Projektowanie środowiskowe maszyn. Wyd. Uczeln. ATR Bydgoszcz.
- [12] Polański Z., 1984. Planowanie doświadczeń w technice. PWN Warszawa.

Adam Mazurkiewicz

University of Technology and Agriculture

Faculty of Mechanical Engineering

Department of Mechanical Engineering Basics and Mechatronics

CALCULATIONS OF FATIGUE LIFE ACCORDING TO POLISH REGISTER OF SHIPS FOR SELECTED RESEARCH RESULTS

Summary. The aim of this article is to present non-standard calculation methods for fatigue life node construction welded and experimental verification. The method follows the requirements of the Polish Register of Ships introduced in the supplement Rules, Classification and Building Sea Ships, part II. Hull: 'Analysis of steel ship hull fatigue strength'. The experimental results verification concerned the ship welded nodes obtained from the Faculty of Oceanotechnics and Shipbuilding of the University of Gdańsk. Comparative analysis of the results of calculations of fatigue life and the results of experimental investigations showed the results of calculations on the safe side of the Wöhler's graph.

Key words: welded joint, fatigue life, calculation method

1. INTRODUCTION

Welding is a universally practical method to assembly large constructions, often of great significance, including bridges or hulls. However a complicated building of such constructions makes describing their fatigue life complex. The literature offers sample calculations for welded constructions with the permissible stress method [1], terminal states method [1,2] or cracking mechanics methods [3]. The calculations, which draw on these methods, are frequently very complicated and time-consuming and errors of coefficients can bring about substantial negative results. The present method of calculation for welded constructions follows the Polish Register of Ships for welded nodes hull calculations. The method allows for estimating fatigue life nodes construction welded in a simple way and shows the calculation sequence as well as comparative analysis of fatigue life calculations results with those obtained in the experiment for a given construction node.

2. ALGORITHM CALCULATIONS

The algorithm calculations have been developed following the Polish Register of Ships [4].

2.1. Selecting the node to be analyzed

Selecting the node to be analyzed or calculated is essential for accurate calculations of construction fatigue-life as the total construction life depends on its weakest point, most frequently one of the nodes. The construction examined should

separate the nodes which are more likely to be crucial for the construction strength by investigating either loads acting on the construction of the selected section or cracks in constructions already operating.

2.2. Calculating stress extension

2.2.1. Resultant global stress extension

Resultant global hull bending stress extension in vertical and horizontal planes is described by the formula:

$$\Delta \sigma_g = \max (C \cdot \Delta \sigma_v, C \cdot \Delta \sigma_h) + 0,3 \cdot \min (C \cdot \Delta \sigma_v, C \cdot \Delta \sigma_h) \quad [\text{MPa}] \quad (2.1)$$

where:

- $\Delta \sigma_v, \Delta \sigma_h$ – general-bending-hull stress extension in vertical and horizontal planes,
- C – stress concentration factor. Calculations of fatigue life based on nominal stress extensions from well chosen Wöhler's graph $C=1$ is accepted.

If the hull fatigue strength analysis considers also the hull torsion, then $\Delta \sigma_f$ stands for stresses extension from simultaneous horizontal-plane bending and from torsion transverse-section deformation. To calculate $\Delta \sigma_f$, torsion and bending algebraic stresses are to be added and the result is to be multiplied by $2 \cdot (0,5)^{\frac{1}{\xi}}$, where ξ stands for Weibull's stresses extension shape factor.

2.2.2. Local stresses

Local stresses are described with the following formula:

$$\Delta \sigma_l = \max (C \cdot \Delta \sigma_z, C \cdot \Delta \sigma_w) + 0,4 \cdot \min (C \cdot \Delta \sigma_z, C \cdot \Delta \sigma_w) \quad [\text{MPa}] \quad (2.2)$$

where:

- C – stress concentration factor,
- $\Delta \sigma_z$ – external pressures stress extension [MPa],
- $\Delta \sigma_w$ – internal pressures stress extension [MPa].

Under certain conditions one of the $\Delta \sigma_z, \Delta \sigma_w$ components can equal zero. $\Delta \sigma_z, \Delta \sigma_w$ values in the above formula are to be considered as non-negative (absolute) values.

2.2.3. Resultant stress extension

Resultant stress extension is described by the following formula:

$$\Delta \sigma_r = \max (\Delta \sigma_g, \Delta \sigma_l) + K_{gl} \cdot \min (\Delta \sigma_g, \Delta \sigma_l) \quad [\text{MPa}] \quad (2.3)$$

where:

K_{gl} – loads simultaneousness factor (undimensional). Its value:
 for construction elements on the level of basic hull plane $K_{gl}=0.7$;
 for construction elements above the present waterline: $K_{gl}=0.6$.

For construction elements between the basic plane level and present waterline level (immersion T_1 [m]), the following is assumed:

$$K_{gl} = 0,7 - 0,1 \cdot \frac{z}{T_1} \tag{2.4}$$

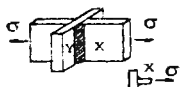
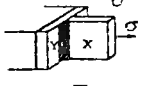
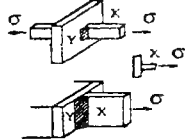
where:

z – stands for the distance of the element from the basic plane.

2.3. Wöhler’s graph selection

The Wöhler’s graph type is selected for the element examined having classified its constructional type. Table 1 offers a sample typical details construction fragment [4]. The details have been assigned to the adequate Wöhler’s curve type for the elements features described and additional explanations.

Table 1. Classification of constructional elements

Item	Drawing	Wöhler’s curve	Elements description and cracking details	Additional explanations
IV. Butt and fillet welds, loaded perpendicularly to weld axis				
6		-	Native material cracks around the weld (X element)	Element Y can be treated as element welded on, as in 3a and 3b
6a		F	Full-penetration weld; weld edges ground (without undercut)	-
6b		F 2	Incomplete-penetration or fillet welds; weld edges ground (without undercut)	Cracking can appear inside the weld if its thickness is not sufficient

2.3.1. Wöhler’s graphs

The selection of Wöhler’s curve type makes it possible to define its adequate equations as:

$$N = \frac{K}{(\Delta\sigma)^m} \tag{2.5}$$

where:

N – number of cycles leading to the element destruction (complete break or tear) for a constant $\Delta\sigma$ of stresses extension;

m, K – curve parameters shown in Table 2 assumed as independent from the material properties.

Table 2. Wöhler's curve parameters m, K

Curve type	$N \leq 10^7$		$N > 10^7$	
	m	K	m	K
B	3	$5.800 \cdot 10^{12}$	5	$4.034 \cdot 10^{16}$
C	3	$3.464 \cdot 10^{12}$	5	$1.708 \cdot 10^{16}$
D	3	$1.520 \cdot 10^{12}$	5	$4.329 \cdot 10^{15}$
E	3	$1.026 \cdot 10^{12}$	5	$2.249 \cdot 10^{15}$
F	3	$6.319 \cdot 10^{11}$	5	$1.002 \cdot 10^{15}$
F2	3	$4.330 \cdot 10^{11}$	5	$5.339 \cdot 10^{14}$
G	3	$2.481 \cdot 10^{11}$	5	$2.110 \cdot 10^{14}$
W	3	$9.279 \cdot 10^{10}$	5	$4.097 \cdot 10^{13}$

$\Delta\sigma$ value is based on the formula 2.3

2.3.2. Wöhler's curves corrections

Wöhler's curves need correcting due to compression stresses in load cycle, element thickness, corrosive effect of water and cargo and construction assembly inaccuracies, all of which requires the change in $\Delta\sigma$ value in Wöhler's curve parameters.

Effect of compression stresses

If in a single load cycle $\sigma_{\min} < 0$, then the stresses extension is calculated as:

$$\Delta\sigma = \Delta\sigma_1 = \sigma_t + 0.6 \cdot \sigma_c \quad (2.6)$$

where:

$$\sigma_t = \max(\sigma_{\max}, 0),$$

$$\sigma_c = \min(\sigma_{\max} - \sigma_{\min}, |\sigma_{\min}|).$$

Effect of element thickness

If the thickness of welded plate is greater than $t_B = 25$ mm and the crack develops from the weld edge deeper into the material, then stresses extension $\Delta\sigma_1$ is to be corrected as follows:

$$\Delta\sigma = \Delta\sigma_2 = \frac{\Delta\sigma_1}{\left(\frac{t}{t_B}\right)^{0.3}} \quad (2.7)$$

where:

t – stands for plate thickness, mm.

For $t \leq t_B$ no corrections apply.

Corrosive influence of sea water and cargo

When the cathodic protection or hermetic painter coats were used, the curves do not require any correcting; otherwise the value of K coefficient, see Table 2, should be divided by 2.

Assembly construction accuracy

Whenever butt-weld 'e' value translation occurs, then the value of the stresses concentration coefficient is obtained from the formula:

$$C_e = 1 + \frac{3 \cdot e}{t} \quad (2.8)$$

whose value should be introduced to equations (2.1) and (2.2).

3. SAMPLE WELDED-NODE CALCULATIONS

The calculations were verified for a single node type selected commonly applied in shipbuilding [5,6].

3.1. Node construction and support

Fig. 1 presents the construction and load type for a two-sided supported node with a continuous-load; the node is made of two welded I-sections.

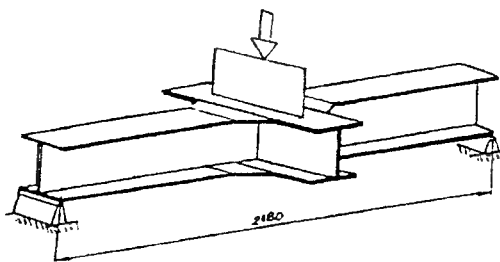


Fig. 1. Node construction, support and load type



3.2. Node load parameters

Table 3 presents node load parameters for two load levels.

Table 3. Node load parameters

Parameter	Level 1	Level 2
σ_{\max} [MPa]	114	159
σ_{\min} [MPa]	5.7	7.96
$R = \sigma_{\min} / \sigma_{\max}$	0.05	0.05

4. CALCULATIONS AND EXPERIMENTAL RESULTS COMPARED

The results of calculations and investigations, carried out in the laboratory of the Faculty of Oceanotechnics and Shipbuilding, the University of Gdańsk, described by Chayiboun [5] are shown in Table 4. A graphic comparison of calculation and experimental life for each node is given in Fig. 2.

Table 4. Results of calculations and investigations

Load level 1 - low				Load level 2 - high			
Node no.	Life			Node no.	Life		
	Investigated	Calculated	C/I		Investigated	Calculated	C/I
1	$910 \cdot 10^3 / 3^*$	$248 \cdot 10^3$	0.27	4	$518 \cdot 10^3 / 18^*$	$90 \cdot 10^3$	0.17
2	$970 \cdot 10^3 / 2^*$	$248 \cdot 10^3$	0.26	5	$840 \cdot 10^3 / 20^*$	$90 \cdot 10^3$	0.11
3	$1398 \cdot 10^3 / 30^*$	$1148 \cdot 10^3$	0.82	6	$950 \cdot 10^3$	$505 \cdot 10^3$	0.53

* Crack length observed for a given life, mm

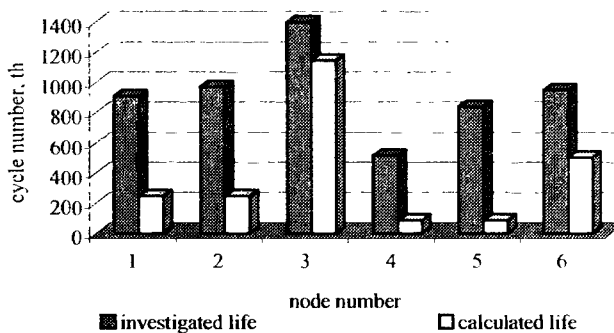


Fig. 2. Calculated and experimental life compared

4.1. Results analysis

The results presented show a certain regularity. In each case the calculated life is smaller than the experimental one. The quotient of the life calculated C to the experimental life I ranges from $0.11 \div 0.82$. An average calculated life accounts for 36 % of the experimental life, which is favourable as far as safety is concerned, as the results of the calculations make the safe fatigue life reserve available. However, a too excessive safety reserve (e.g. node 5) is not cost-effective. Ship constructions are very complex and each premature replacement of the element which could still work increases running costs. All that calls for optimal accuracy of the calculations, which is not always feasible due to the complex method of qualifying stresses or due to changing work conditions.

5. CONCLUSIONS

1. The method of calculation locates the results on the safe side of the experimental life.
2. The discrepancy between the calculated and the experimental results must be due to:
 - a partial failure of matching the construction of a given elementary joint in which a crack occurred to the joint type according to Table 1.
 - inaccurate definition of the moment of the crack: Table 2 gives the experimental results together with the length of the crack the moment it was identified; the number of cycles the crack needed to occur of the constant observable length was smaller than the number of cycles it was observed in; which would lead to a greater overlap between the results of calculations and of the experiment.
3. The method proposed is relatively simple and easy, which makes it justifiable to apply it to calculations for typical machine elements of common or standardised load spectrums.

REFERENCES

- [1] Porębska M., Skorupa A., 1997. Połączenia spójnościowe. PWN Warszawa.
- [2] PN - 90/B - 03200.
- [3] Kocańda S., Szala J., 1997. Podstawy obliczeń zmęczeniowych. PWN Warszawa.
- [4] Polski Rejestr Statków. 1997. Analiza wytrzymałości zmęczeniowej stalowego kadłuba statku. Gdańsk.
- [5] Chayiboun I., 1999 Ocena skuteczności metody naprawy uszkodzeń zmęczeniowych skrzyżowań wiązarów kadłuba statku. Praca doktorska, Politechnika Gdańska. Gdańsk.
- [6] Rosochowicz K., Behilil M., Chayiboun I., 2000. Problemy napraw zmęczeniowych uszkodzeń wiązań okrętowych. Wyd. Uczeln. ATR Bydgoszcz, 397-406.

Kazimierz Peszyński

*University of Technology and Agriculture
Faculty of Mechanical Engineering
Department of Control and Machinery Design*

Zdeněk Trávníček

*Czech Academy of Sciences
Institute of Thermomechanics*

JET FLOW VISUALISATION FOR AN AXI-SYMMETRIC NOZZLE

Summary: An axi-symmetric annular jet was studied experimentally using air as working fluid. The jet was actively controlled according to fluidic principles. The nozzle investigated was designed without any mechanical movable parts and equipped with a spoiler, which suppressed a hysteresis effect during a jet switching. Flow visualisation confirmed bistable behaviour of the jet as well as proper function of the spoiler. A potential use of the present nozzle at a periodic forcing is discussed.

Key words: jets, fluidics, flow visualisation, jet impingement, flow control, nozzle

1. INTRODUCTION

Impinging jets have been a subject of numerous investigations over the past four decades, the most important results were summarised in an outstanding monograph by Dyban and Mazur [1] and in the representative reviews [2,3]. Theoretical, experimental and numerical research continues perpetually, see, e.g. the recent review [4] and experimental study [5] or considerable literary coverage compiled in the publications cited. The main stimulation of this effort comes from industrial applications, oriented to heat transfer enhancement by impinging jets. The most important areas of applications and major advantages of impinging jets are summarised in Tables 1 and 2.

Fluid mechanics of impinging jets and resultant heat transfer to exposed surfaces were investigated in many variants of geometry, at miscellaneous Reynolds number ranges in laminar as well as turbulent flow regimes, and under different thermal boundary conditions. Basic configurations, when a jet issues from round or slot nozzle, have been frequently studied. However, no research can stagnate at the basic nozzle geometry when stimulation comes primarily from applications. Many investigations referred to in literature have been performed with a rather simple but more specifically defined nozzle geometry such as undeveloped pipe flow, orifice through thick wall with sharp, rounded or chamfered edges, truncated cone nozzle, diverging nozzle, etc.

Table 1. Applications of impinging jets

APPLICATIONS OF IMPINGING JETS
Drying technology and dryers of various materials
<ul style="list-style-type: none"> • Paper (paper industry, cardboard, Scotch tape; print lines) • Fabric – drying; thermo-fixing stenters • Veneer and plywood • Films • Ceramics and porcelain; plates • Coated sheet metal
Cooling
<ul style="list-style-type: none"> • Turbine blades – for temperature up to 1500°C • Sheet glass • Rolling mills of thin/thick sheet metal • Cooling of electronic components
Heating
<ul style="list-style-type: none"> • Precise control of a cylinder temperature in paper industry • Aircraft de-icing systems

Table 2. Advantages of impinging jets

ADVANTAGES OF IMPINGING JETS
<ul style="list-style-type: none"> • High intensity of heat/mass transfer • Adaptable according to a surface shape • Relatively easy and cheap for applications

2. MOTIVATIONS

The flow field of impinging jet is commonly classified as a *complex flow* even at one of the basic geometry cases such as round or slot nozzle since it consists of many tasks bound together (stagnation flow, laminar flow, transition to turbulence, shear layer flow, etc.). The present paper focuses on impinging jet which still seems relatively far from the main research field, namely *impinging multistable jet*: a combination of *impinging jet* with *jet control* by means of *fluidic* principles.

A multistable behaviour of impinging jet can be observed even without any active jet control when jet is split into separate branches and a possible multistability results from their interaction. Multistable flow switching can be considerably complicated when hysteresis occurs. Two-dimensional *bistable* impinging jet from *two-slot-nozzle* (slot nozzle with centrally inserted crossbar) has been investigated recently [6]. Bistable switching was confirmed by measurement of wall pressure, nozzle pressure drop and local mass transfer coefficient on the surface. Hysteresis was identified at a rather large range of nozzle-to-surface spacing. Annular impinging jet was studied numerically [7], and its bistable behaviour was predicted, including a hysteresis character. Experimental investigation of annular impinging jet was presented by Maki and Yabe [8] and four flow regimes were identified; three of them characterised as re-circulating unsteady flow. A recent experimental and numerical study [9] presents multistable annular jet, where five states of flow were identified; surprisingly, no hysteresis was referred to – the phenomenon is, apparently, not common but depends on a specific geometry.

The term *fluidics* means a technology of flow handling based on the fluid flow interaction without action of moving components which has been investigated during the past 40 years mainly in two, seemingly remote, fields: (1) control devices as an alternative of electronics, (2) "power fluidic" for control of very hot aggressive and dangerous fluids [10]. Nowadays fluidics seems to gain importance in MEMS – microfluidic valves [11] and in a gas turbine exhaust nozzle of high performance fighter/attack aircraft [12].

A combination of impinging jet with fluidics seems to be very efficient for heat transfer enhancement. An idea of oscillating jet, which is flipping by two control feedback loops as a fluidic oscillator, was used formerly [20]. Recently, two-dimensional oscillating impinging jet has been designed following the same principle mainly to improve a cooling of gas turbine blades. Heat transfer has been studied experimentally at a flipping frequency from 20 Hz to 100 Hz, the frequency was tuned by variation of the nozzle width and feedback tube length. A bistable axi-symmetric nozzle has been recently designed [13], a refinement of its geometry has been supported by experimental as well as numerical investigation [14,15].

Figures 1 and 2 show a schematic view of the present nozzle. The main nozzle is annular, the control nozzle is radial; the control nozzle is located close to the internal edge of main nozzle.

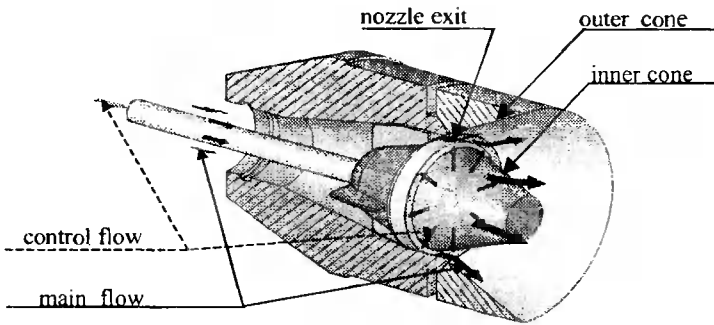


Fig. 1. Annular nozzle with active control

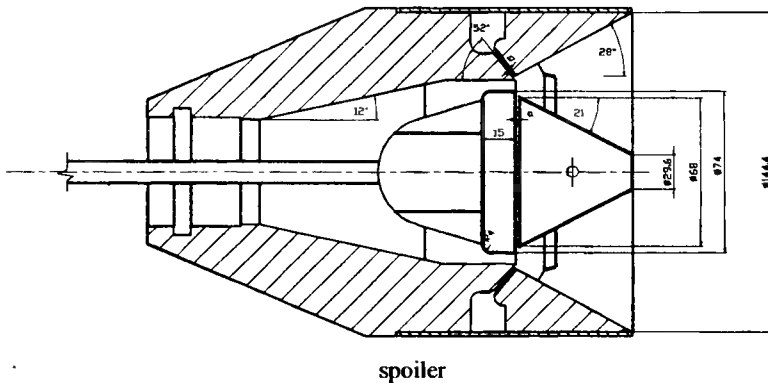


Fig. 2. Annular nozzle with active control equipped with a spoiler

The present nozzle features two states of jet, switching from state 1 to state 2 is forced by transversal control jet, see Figures 3 and 4:

- State 1 (Fig. 3) is without active flow control. The air from the main nozzle is inclined by Coanda Effect towards the inner nozzle cone, then it continues along cone surface, and, finally, the jet is focused into the nozzle axis.
- State 2 (Fig. 4), with control jet. The air issues from the main nozzle, and is immediately forced by control jet towards the outer nozzle cone. It attaches and flows along the surface, the final jet is spread in diagonal direction out of the outer cone edge. A cross-section area of the jet is larger and its velocity lower, as compared with state 1.

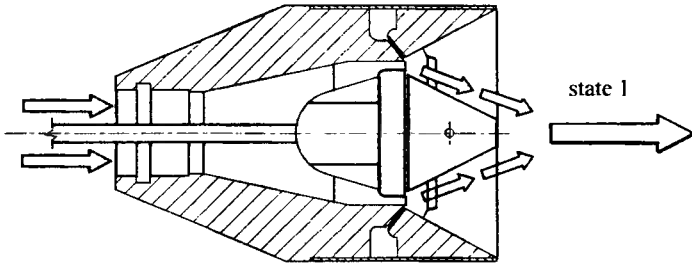


Fig. 3. State 1 annular jet

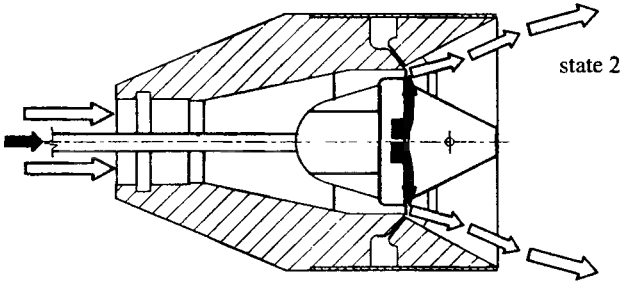


Fig. 4. State 2 annular jet

The nozzle was equipped with a spoiler (flow divider), plotted in Fig. 2. The spoiler causes a return of air flow from state 2 back to state 1, when the control jet is turned off. Otherwise, the spoiler practically suppresses the hysteresis effect. Spoiler geometry was designed earlier, different sizes and different positions were tested, and the final design is presented here. The spoiler was situated near the outer cone surface and was adjusted approximately parallel to the inner cone surface. Its chord length was 5.0 mm and the gap between the leading edge and the outer cone surface was adjusted approximately to 7 mm.

The present nozzle could be used with periodic forcing to create an oscillating impinging jet. It is evident in principle, at least by low-frequency modulated control jet. This possibility was one of the reasons for present design with an *artificial* elimination of hysteresis effect. It is well known that periodic oscillations could be the source of additional heat transfer enhancement. One shall bear in mind that flow oscillations do not imply this enhancement automatically. Herman [16] demonstrates that heat transfer

in oscillating flow can be sometimes enhanced and sometimes decreased, or the effect is inconsiderable. Although this paper deals with a steady flow solely, heat transfer enhancement using the present nozzle with periodic control jet could be promising for the future development. On the other hand, a stagnation region of each impinging jet, particularly of annular impinging jet, is characterised by unsteady behaviour with a large-scale fluctuation [8]. It should be helpful for potential heat transfer enhancement to correlate these natural unsteady large-scale fluctuations with periodic external forcing.

The present jet flow is rather complicated as it consists of several tasks bound together:

- pipe flow into the main nozzle, which is undeveloped, diverging and converging, with separation and reattachment areas,
- pipe flow into the control nozzle, through inner nozzle cone,
- an interaction of two perpendicular flows: annular main jet and radial control jet,
- Coanda Effect: air jet is inclined towards either inner or outer nozzle cone and reattaches on the surface,
- an entrainment of air from surroundings into the jet.

A mathematical model cannot be proposed without many simplifications, however, too many simplifications might essentially move a hypothetical result away from the correct solution. Adequate quantification of geometric parameters is rather difficult, which is evident from the nozzle geometry, see Figures 1 and 2. Numerical methods seem to be very attractive for design optimisation of nozzle geometry, however the results should be interpreted carefully [18].

A development of the nozzle design was based primarily on an experimental investigation [13,14]. Some partial modification was supported by a numerical simulation using solver FLUENT and ANSYS [15,17]. The present paper focuses on the experiment which provides data to confirm the previous numerical simulation. It is expected, following common trends as well as the present experience, that the role of numerical simulation will increase further in the investigation.

3. EXPERIMENTAL TECHNIQUE AND RESULTS

Figures 1 and 2 show schematic view on the present nozzle. It is situated horizontally and supplied by two independent air flow sources; main flow is supplied by centrifugal blower and controlled by the frequency regulator, control flow is supplied by the building compressor and controlled by the pressure regulator. Upstream of the nozzle, the main airflow passes through a horizontal pipe 47.2 mm in diameter, and control flow through a flexible tubing approximately 8 mm in diameter. Both the main and control airflow rates are measured upstream the nozzle by the plate orifice and rotameter, respectively. The average velocity at the jet exit (i.e. the minimum cross-section of nozzle, see Fig. 1) was calculated based on the airflow rate. The main nozzle was annular, its outside and inside exit were 84.0 mm and 74.0 mm in diameters. The nozzle contraction was 1.41 against the main airflow supply. Control nozzle was radial 68.0 mm in diameter and the slot width – 0.5 mm.

A combination of qualitative global imaging of flow, the field and the point measurement localised on several representative cross-sections seems quite an effective approach to experimental study of complex flows and to a geometry optimisation.

A typical example is available as a combination of smoke wire visualisation technique with a hot-wire anemometer which has been recently used for an investigation of round jet impinging on a cylindrical surface [5]. The same combination was used in the present study. Our choice results from specific circumstances of engineering optimisation when the geometry investigated is intended to refine basically in many steps.

A well-known smoke-wire technique was used for the visualisation of air jet downstream the nozzle. The smoke-wire was uniformly twisted from three resistance wires 0.1 mm in diameter and was located horizontally across the investigated jet axis. It was coated with paraffin oil before each test, and heated by Joule effect of direct current. The oil is evaporated from heated wire and condensed by air stream speedily. White filaments, which trace the airflow, are traditionally called a “*smoke*”. In fact, filaments consist of tiny droplets of oil (oil aerosol).

The contrast white streaklines on black background was observed and photographed. Digital camera Olympus C-2500L Camedia was fixed above the nozzle, and oriented downwards. This configuration partly eliminates buoyancy effect. Pictures were taken at a flashlight. A photo-flash was located beside the nozzle, approximately in the smoke wire extension. It was equipped with optic system converging the light smoke wire downstream. The camera shutter released the flashlight, while the power supplied to the wire was synchronised manually.

Hot-wire flow velocity measurement was made by using StreamLine System CTA90 (DANTEC) – an integrated measuring system based on the CTA in combination with a PC. The results of CTA measurement were referred to recently [14].

Figures 5 and 6 show flow visualisation in states 1 and 2, respectively. The nozzle is at the bottom of figures, flow direction is from below to upward, the average velocity at the jet exit was $4.4 \text{ m}\cdot\text{s}^{-1}$. Reynolds number was calculated from the average diameter of annular nozzle and from the slot width, it was 22000 and 1400, respectively. Fig. 5 shows state 1, when air jet is formed along nozzle axis. Visualised flow is turbulent. laminar-turbulent transition occurs in the nozzle, which was not tested.

Fig. 6 shows state 2 when air jet is forced by control jet out of the nozzle axis. The control flow rate fell within 9 % to 10 % against the main flow rate. Air is entrained into the nozzle, and is mixed with main jet. Final jet is turbulent and is formed downstream the outer cone end as annular jet. When the control jet was turned off, flow regime was returned immediately to state 1. No hysteresis effect was observed, which confirms previous estimation that the present spoiler geometry can suppress the hysteresis effect fully.

Figures 7 and 8 show flow visualisation of impinging jet in states 1 and 2, respectively. Nozzle-to-wall spacing was 80 mm.

- Fig. 7 shows annular impinging jet in state 1. Flow field near the central stagnation point qualitatively resembles a basic case of round impinging jet. This case of annular impinging jet is referred to as “closed type pattern” [7] (re-circulation flow does not touch wall). The stagnation point on the wall is located in the point of intersection of nozzle axis with a wall, no other stagnation points are on the wall. This regime has recently been referred to as more aptly as “centrifugal case” [9] as streamlines on the wall exposed run away from the central stagnation point. Fig. 8 shows annular impinging jet in state 2, the control flow rate falls within 9 % to 10 % against the main flow rate. Nozzle-to-surface space is filled up with a bubble of separated flow, all the re-circulation area is bordered by annular jet issued from nozzle. This case of annular impinging jet is referred as “open type pattern” [7]

or flow with “reverse stagnation point” [8]. Recently, this flow pattern has been called more aptly as “centripetal case” [9]; wall streamlines run from an outer stagnation circle towards the central (reverse) stagnation point.

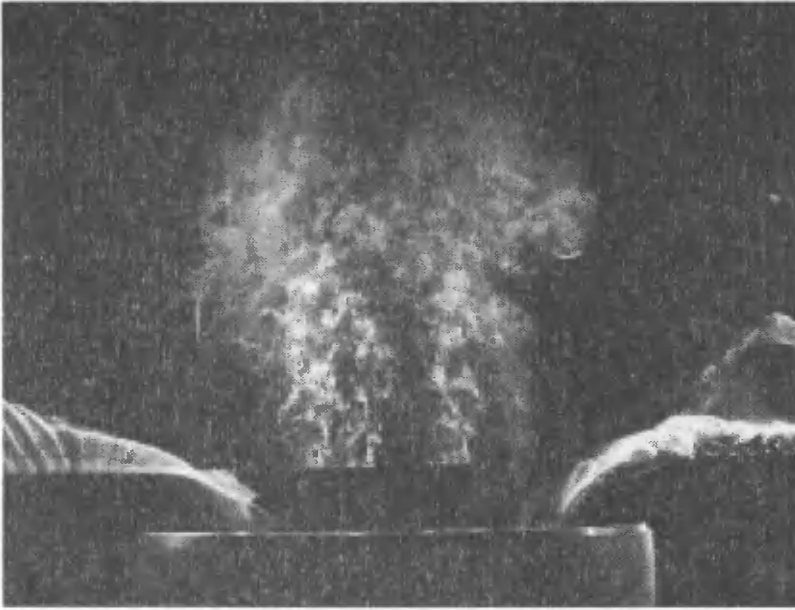


Fig. 5. State 1 annular jet

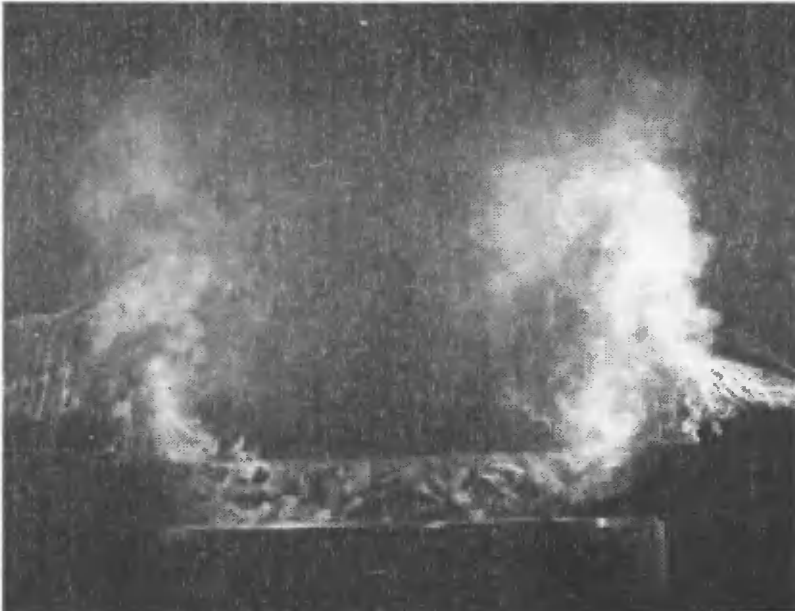


Fig. 6. State 2 annular jet

Like in the non-impinging jet, no hysteresis was identified during jet switching at the jet impingement case. When the control jet was turned off, flow field followed immediately and changed to state 1, which confirms a proper function of the present spoiler.

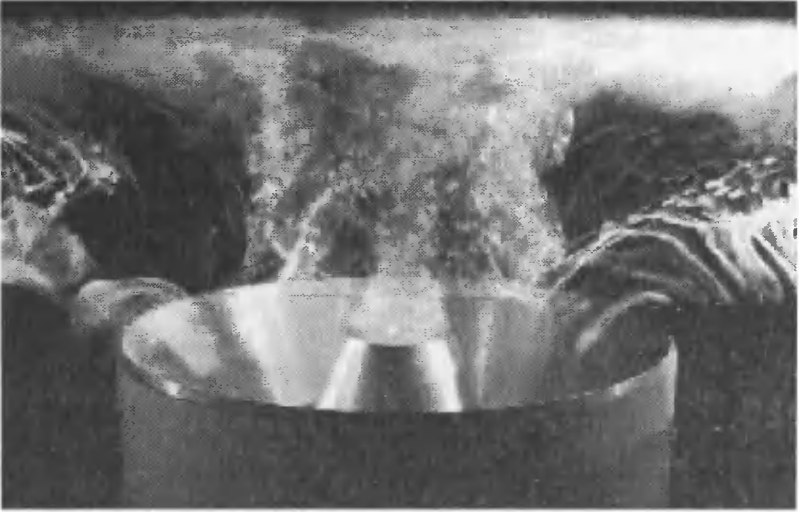


Fig. 7. State 1 annular jet impinging

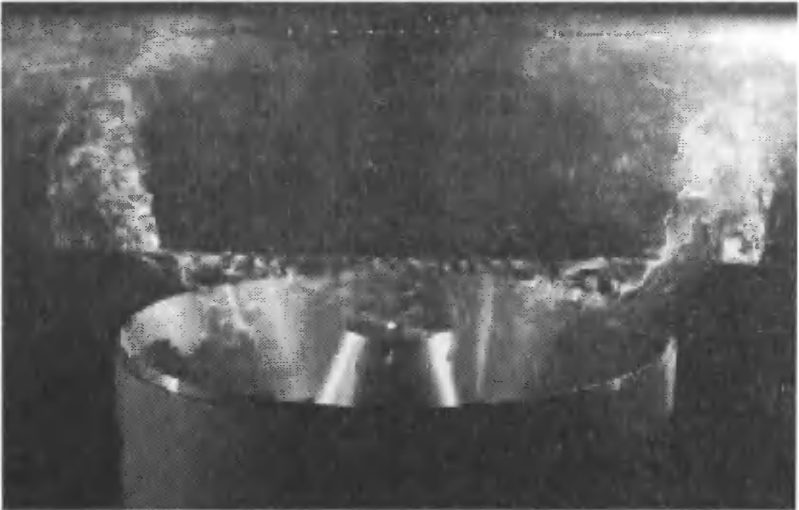


Fig. 8. State 2 annular jet impinging

4. CONCLUSION

The flow visualisation of actively controlled air jet was performed in the Institute of Thermomechanics, Czech Academy of Sciences in a co-operation with the Bydgoszcz-based University of Technology and Agriculture (ATR). Flow visualisation confirmed bistable behaviour of annular, actively controlled, non-impinging and impinging jets.

The nozzle has been equipped with a flow spoiler (flow divider), present visualisation confirms its proper function, namely a suppression of the hysteresis effect at jet switching. This result is considered to be significant for potential periodic forcing of nozzle, thus for creating an oscillating impinging jet.

A further development of the nozzle and geometry optimisation is planned in the near future by using a combined experimental and numerical approach.

ACKNOWLEDGEMENT

We gratefully acknowledge the support of the Grant Agency of the Czech Republic (projects no. 101/99/0059 and 101/99/0060), and the State Committee for Scientific Research grant (Poland), project no. Z/19/3/98 (ATR BW-8/98).

REFERENCES

- [1] Dyban E.P., Mazur A.I., 1982. Konvektivnyj teploobmen pri strujnom obtekanii tel. Naukova Dumka, Kiev.
- [2] Martin H., 1977. Heat and Mass Transfer Between Impinging Gas Jets and Solid Surfaces. *Advances in Heat Transfer* 13 (160), 1-60.
- [3] Jambunathan K., Lai E., Moss M.A., Button B.L., 1992. A Review of Heat Transfer Data for Single Circular Jet Impingement. *Int. Jour. Heat and Fluid Flow* 2, 106-115.
- [4] Garimella S.V., 1999. Heat Transfer and Flow Fields in Confined Jet Impingement. *Annual Review of Heat Transfer* XI, 413-494.
- [5] Comaro C., Fleischer A.S., Goldstein R.J., 1999. Flow visualization of a round jet impinging on cylindrical surfaces. *Experimental Thermal and Fluid Science* 20 (2), 66-78.
- [6] Trávníček Z., Křížek F., 1999. Impinging jet and combined slot nozzle (Impaktströmung und die Zusammengesetzte Schlitzdüse). *Heat and Mass Transfer* 35 (5), 351-356.
- [7] Kokoshima Y., Shimizu A., Murao T., 1991. Numerical analysis of annular turbulent jet impinging on a flat plate. [In:] 3rd triennial Int. Symp. Fluid control, Measurement and Visualization, FLUCOME'91, ASME, San Francisco, 205-210.
- [8] Maki H., Yabe A., 1989. Unsteady characteristics of the annular impinging jet flow field and reverse stagnation point heat transfer. [In:] HTD-Vol. 107, Heat Transfer in Convective Flows, National Heat Transfer Conference, Philadelphia, Pennsylvania, 163-168.
- [9] Tesáľ V., Jilek M., Randa Z., 2001: Topology changes in an annular impinging jet flow. [In:] Topical Problems in Fluid Mechanics 2001, Institute of Thermomechanics CAS, Prague, 121-124.
- [10] Tesáľ V.. 1985. Power fluidics. [In:] Fluid control and measurement, Ed. M. Harada, Pergamon Press, Tokyo, 1, 393-402.
- [11] Tesáľ V.. 2001. Microfluidics for MEMS- Microfluidic valve. [In:] 4th Pacific International Conference on Aerospace Science and Technology. Kaohsiung, Taiwan, (accepted).

- [12] Federspiel J.F, Bangert L.S, Wing D.J., Hawkes T., 1995. Fluidic control of nozzle flow - some performance measurements. [In:] 31st AIAA/ASME/SAE/ASEE Joint Propulsion Conference, San Diego, California, AIAA, 95-2605.
- [13] Peszyński K., 1998. Flow control by axisymmetric fluidic device with radial switching. [In:] Engineering Mechanics '98, National conference with international participation, Czech Academy of Sciences, Svratka, Czech Republic.
- [14] Peszyński K., Hošek J., Kuszyński Z., Trávníček Z., Wawrzyniak S., 2000. Active control of annular bistable jet. [In:] Proceedings of Engineering Mechanics 2000, International conference, Svratka, Czech Republic, Czech Academy of Sciences IV, 149-154.
- [15] Peszyński K., Kamiński A., 1999. Modelowanie numeryczne strumieniowej dyszy pierścieniowej. IX Międzynarodowa Konferencja Naukowo-Techniczna – ICMR '99, Bydgoszcz.
- [16] Herman C. The impact of flow oscillations on convective heat transfer. *Annual Review of Heat Transfer* (in press).
- [17] Tesař V., 1997. Axisymmetric fluidic valves for use in automobile exhaust gas after treatment. Proc. of FLUCOME'97 – Fifth Triennial International Symposium on Fluid Control, Measurement and Visualisation, Hayama, Japan, 2, 529.
- [18] Dvořák R., Kozel K., 1996. *Matematické modelování v aerodynamice*. Publishing House ČVUT (Czech Technical University in Prague).
- [19] Eckert E.R.G. et al., 2000. Heat transfer – a review of 1997 literature. *Int. Journal Heat and Mass Transfer* 43, 2431-2528.
- [20] Viets H., 1975. Flip-Flop Jet Nozzle. *AIAA Journal* 13 (10), 1375-1379.

Tomasz Piątkowski

*University of Technology and Agriculture
Faculty of Telecommunications and Electrical Engineering
Division of Postal Technology*

Janusz Sempruch

*University of Technology and Agriculture
Faculty of Mechanical Engineering
Department of Control and Machinery Design*

PHYSICAL MODELS OF THE UNIT LOADS STREAM SORTING PROCESS

Summary. The paper investigates the automatic separating process of the unit loads stream (parcels). The article reviews the effects of sorting machine technical solutions and analyses dynamic phenomena which coincide with loads sorting methods.

Key words: modelling, sorting process, separating machine

1. INTRODUCTION

Automatic sorting systems are applied in logistic centres: big post offices, airports and assembly lines. Universal solutions are offered for unit loads sorting and distribution: collecting unit loads, directing their flow and sorting identified loads to the particular destination lines. The notion of a unit load is very broad and incorporates a high-dimensional container, pallet, box and smaller-dimensional loads with a parcel, luggage, agriproduct, chemical goods. High-dimensional loads are operated with various kinds of carts, gantries and cranes. The other machines and devices are used for the selection of such loads as parcels. Parcel dimensions, shapes and mechanical properties vary considerably and remain very changeable. Parcel packaging can be made of carton and reinforced with a self-adhesive tape, glue, staple or string; it can be in a form of towel or paper bag. Mechanical property of the parcel depends not only on the type of packaging but also on their contents. The capacity of the load very often refers to different contents at the same time: loose materials, liquids, foodstuffs, clothes and empty spaces. All that makes the objects differ not only from one another but also within a single load. They are referred to as unisomorphic sticky-springy loads. Unit loads stream into particular directions, depending on the destination, is automatically distributed with the separating machine combined with the conveyors system. In order to assure a proper work of a transport system, the sorting machine must account for a corresponding specific capacity, weight, dimensions and mechanical properties of the loads. Sorting machines can be broken down into two major groups (Fig 1.) depending on the dividers construction (i.e. sorting machine operating devices): stationary and streaming [3].



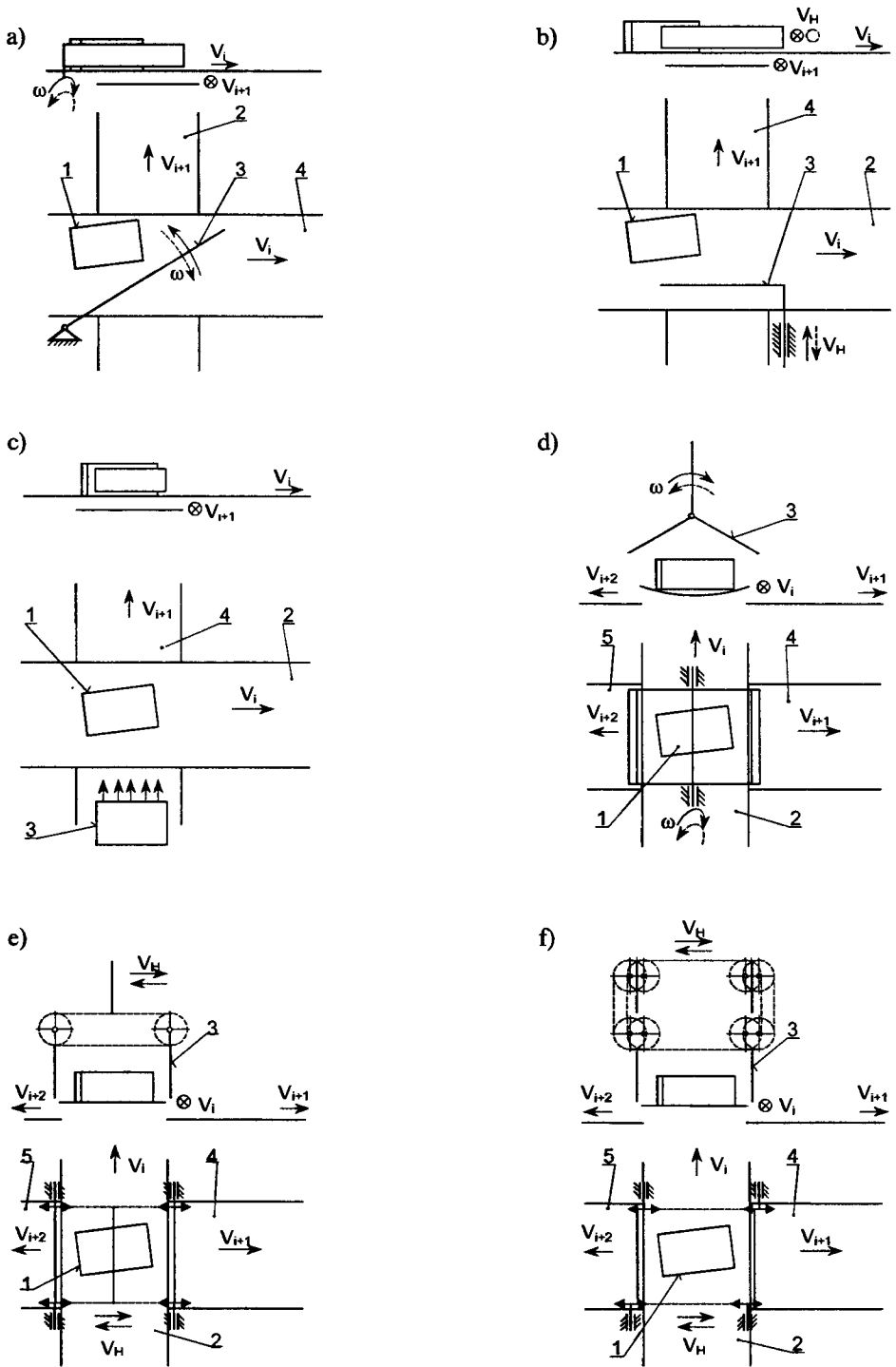
Fig. 1. Physical models of sorting machine of: a) stationary, b) streaming; 1 – load, 2 – conveyor, 3 – divider, 4 – skid, V – linear speed, V_H – speed of divider working element, Δc – minimal permissible distance between loads

The first group is equipped with dividers which are placed down the conveyor (main part of the sorting machine) and combined with the machine frame. The operating principle of the dividers of this type is to scrape loads from the conveyor flight with the use of active arms which can make various working motions (translatory, rotary, deflection). Streaming sorting machine dividers, as an integral part of the machine conveyor, carry the elements and move with the convection velocity of the loads moved on the conveyor. Dividers can be in a form of deflection trays or trays with surfaces in the form of separate belt conveyors. The trays are led in the rails – closed separating loop. Other kinds of dividers are sorting systems with interleaving slat conveyors fitted with sliding shoes.

To justify the selection of a given sorting machine solutions to meet individual logistic centre transporting system needs and requirements, one must take up modelling and analysis of the unit loads sorting process for a given machine. The theoretical sorting model allows for an application of well-known and potential new designs of sorting machines.

2. REVIEW OF PHYSICAL SORTING MODELS

One of the stationary divider solutions is a device whose operating principle is to scrape loads from the belt conveyor flight with the use of deflection scraper (Fig. 2a). This solution is readily applied to sorting machines, also in Poland, due to its reliable and low running costs as a result of the construction simplicity. In order to recognise the effect of scraping parameters on the sorting effect (achieved sorting capacity, fulfilling sorting reliability and allowable overloading), a theoretical model was built. Numerical and experimental examinations showed a high potential of deflection scraper in terms of capacity level formation once scraping conditions are considered [1]. The results refer to the following conditions:



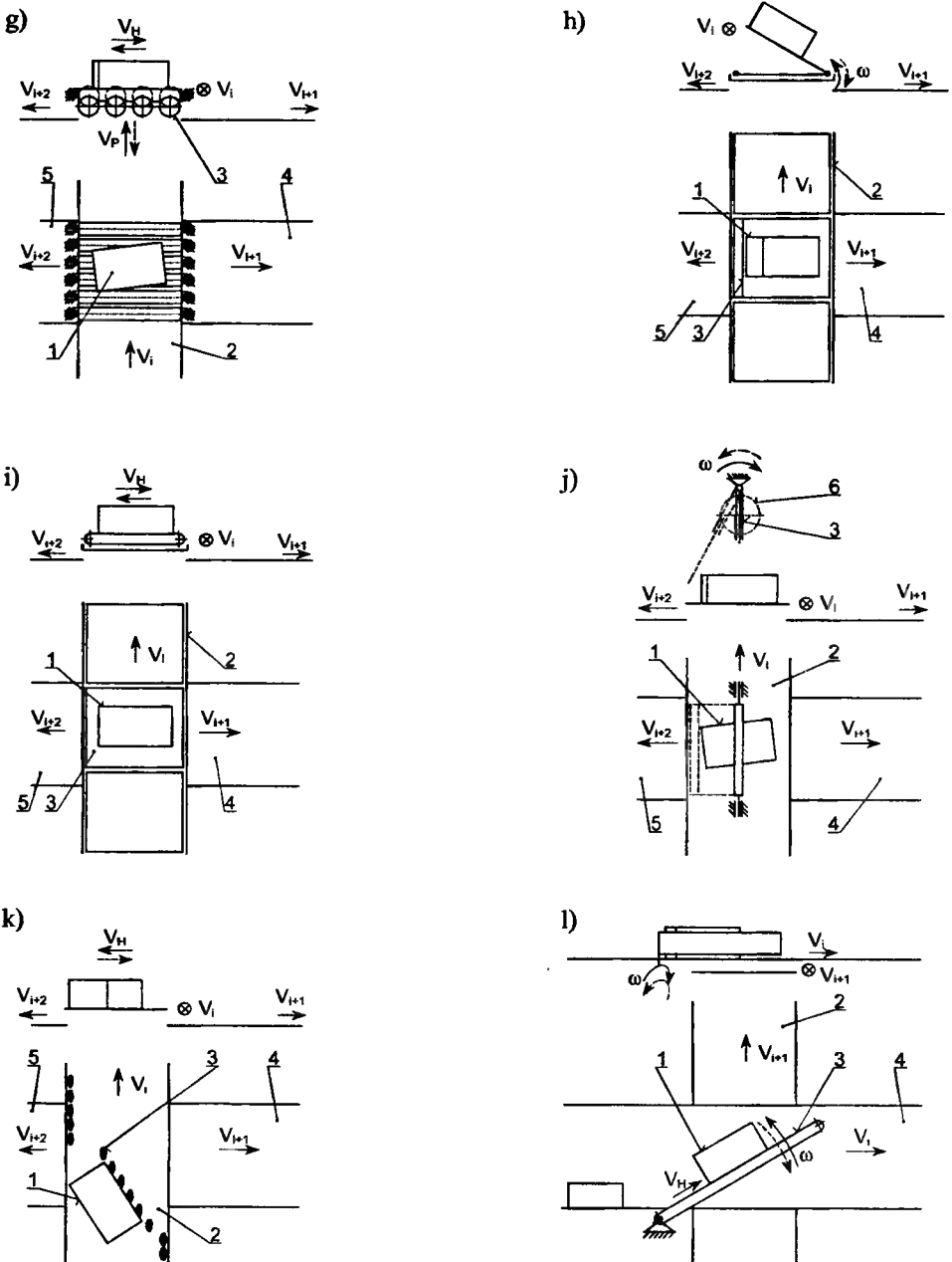


Fig. 2. Physical models of dividers: a) deflection, b) transverse, c) pneumatic, d) rotary three-armed, e) translatory three-armed, f) translatory four-armed, g) roll-disc, h) tilt tray, i) cross-belt tray, j) telescopic, k) divert shoes, l) deflection with belt; 1 – load, 2 – main conveyor, 3 – working element (arm, tray, shoe, nozzle, disc), 4 & 5 – discharge conveyors, 6 – circular cam, V_i – conveyor linear speed, V_H – linear speed of divider working element

- load overloading can reach dynamic overloading obtained by load during its free fall from 0.3 m onto a non-deformed base [2],
- maximal weight of the sorting loads amounts to 15 kg for the length of 200-700 mm, width of 100-500 mm and for the height of 40-600 mm.

A load drop from an allowable height, especially hitting a corner or an edge, inflicts serious permanent deformations. Greater sorting process requirements, especially the allowable overloading obtained by the loads, restrict possibilities of sorting process control considerably. The solution has a serious defect – occurrence of sorting process strike which is hard to illustrate with a mathematical model and which is a source of intensive dynamic effects. The strike shows a disadvantageous effect on the load and scraper mechanism. A further research is needed which would source out enhanced sorting systems. The present review of loads sorting systems evaluates the sorting process models available.

The dividers based on scraping loads from the belt conveyor include a device with a crosswise-moving arm (Fig. 2b) whose motion of the arm can be performed by linear pneumatic (hydraulic) engine or by lever mechanism transforming the rotary motion of electric engine into translatory motion. Another solution is a three-armed scraping device that can turn round to the left and to the right (Fig. 2d). Scraper working cycle equals the arms turn at an angle of 120° . The scraper is situated above the belt conveyor surface that is let in cradle in form of circle segment. The scraper presented in Fig. 2j is also situated above the belt conveyor and consists of telescopic arm 3 fastened in one point, driven by circular cam 5. The arm in its starting position is situated in the extreme top position that the loads can get to under the arm. At the moment when the load comes to its destination (on the left or the right of the conveyor), the drive of the circular cam starts and the arm sticks out in the opposite side to the planned load drop place. After load scraping the arm returns to its initial position. The working cycle equals the turn of the circular cam at an angle of 360° . Fig. 2e presents a scraping device with three scraping arms fastened to chains. The working cycle equals $1/3$ of the chain length. During the scraping process the arm which scrapes the load moves to translatory motion and the other two arms – rotary motion. Another variant of chain scraping device is a divider with four scraping arms (Fig. 2f) whose arms move only in a translatory motion. The scraping device presented in Fig. 2g consists of drive discs 3, situated under drive rolls. The discs can move vertically – up and down. The moment when the load is situated on the rolls and the scraping device is to be directed to the left or right of the conveyor, the discs pull out above the rolls surface and move load to the proper skid. In sorting the loads compressed air steam (Fig. 2c) can also be used [5]. This kind of scraping can be effective only for small and light loads. An example of streaming divider is a tilt tray sorter shown in Fig. 2h. Tilt trays are carrying surfaces which are top part of trolleys driven in rails in the form of a closed loop. The tray deflexion makes the gravity scrape load and move it to the proper skid. Another variant of streaming divider is a cross-belt tray (Fig. 2i) which consists of a system of interconnected carts. Each cart is equipped with a cross-belt unit and runs in a closed machine frame. The divider from Fig. 2k is an example of a streaming device whose operating principle is to scrape loads by means of diverts shoes 3. The heart of the sorting system is an interleaving slat conveyor fitted with sliding diverts shoes for transverse sorting. The sorting is possible with the shoes which are positively diverted to the right or left of the slats by a mechanism arranged beneath the conveyor surface to act on the

longitudinal side of the loads. Each diverting operation is carried out by the predetermined number of shoes.

3. CONCLUSIONS

Not percussive character of the sorting systems work is found only in tray-streaming machine, independently of the load position on the sorting conveyor. The main producers of automatic tray sorting systems include Mannesmann (Germany), Sandvik (Italy) and Crisplant (Denmark) [4] and the technical solutions of the sorting machines are complicated mechanical systems, which consist of a big number of precise elements. A new sorting system is extremely expensive due to high running costs. The strike in stationary dividers Figs. 2a, b, e, f, j can be avoided by a proper stream formation before loads sorting (application devices positioned the loads, e.g. letting unit loads along conveyor border opposite their destination). A substantial reduction in dynamic overloading obtained by the loads being scraped is feasible due to drive system elements with plastic-and-elastic properties (with e.g. pneumatic, hydraulic elements in the divider) and to their adequate control. Deflection scraper work conditions (Fig. 2a) can be enhanced by introducing an additional drive belt conveyor covering scraper arm (Fig. 2l). Loads scraping can be enhanced by additional conveyor helping loads dislocation and avoiding sticking to the scraper arm.

REFERENCES

- [1] Piątkowski T., Sempruch J., 1999. Model and Analysis of Selected Features of Scraping Process. Tenth World Congress on the Theory of Machines and Mechanisms. Oulu, 159-168.
- [2] Informacja o dopuszczeniu do obrotu pocztowego paczek pocztowych w typowych opakowaniach i kartonach, 1993. Technika i Eksploatacja Poczty 4.
- [3] Postal Technology International, 1999. UK & International Press, Dorking.
- [4] Materiały informacyjne firmy Crisplant, 1999. Individual handling with care. Aarhus.
- [5] Siniakiewicz A., 1987. Urządzenia pocztowe i ich sterowanie. Wyd. Uczeln. ATR Bydgoszcz.

Eugeniusz Ranatowski

*University of Technology and Agriculture
Faculty of Mechanical Engineering
Department of Material Engineering*

SOME ASPECTS OF CONSTRUCTIONS DIMENSIONING WITH FRACTURE MECHANICS

Summary. The first part of the work covers the classical strength effort hypothesis and the applicability to dimensioning of materials and constructions - low when the defects, such as cracks, occur which calls for materials and constructions dimensioning involved in fracture mechanics with its parameters and criterions. The second part characterises basic fracture mechanics parameters and criterions, including stress intensity factor K_{II} , strain energy release rate G , crack tip opening displacement δ (CTOD) and integral Rice – Čerepanov J and their criterions. The third part is devoted to practical application of those parameters and criterions to construction dimensioning.

Key word: rules of dimensioning, fracture mechanics, parameters and criterions, analytical examples

1. INTRODUCTION

The problem of optimal design of structures is very complex and various attempts have been made to obtain effective methods which might be used in engineering, which requires appropriate dimensioning of materials and constructions. The application of the classical strength effort hypothesis is inconsiderable when defects, such as cracks, occur. The classical effort hypothesis, such as Huber–Mises equivalent of stress and their modifications, does not assess the effort of the construction as no real conditions of material effort are considered. For example [1]:

- the “scale effect” and the geometric feature of the constructions are not considered,
- the state of the microstructure of the materials, their heterogeneity, internal discontinuity and other defects inflicted on in the manufacturing process and exploitation are not considered,
- the course of material damage is not considered,
- constitutive physical rules are created with the continuum model of material.

The discontinuities, such as cracks, show that the Huber–Mises equivalent of stress exceeds critical value at low load. Elasticity solutions of problems involving stress concentrations show that the stress becomes singular as the notch root radius tends to zero; the theoretical stress at the notch is singular. Additionally, the uniform strength in the elastic state or the prescribed load carrying capacity are required, in some cases also limitation of admissible elastic deformation. Taking such a general approach, the optimum design remains very difficult and does not lead to effective solutions. The uniform strength design in the elastic state is very difficult even when simple structural elements and infeasible when cracks occur. Various approximate methods of calculation are often

used in designing, e.g. reducing internal forces, yet the best approach is based on fracture mechanics and its parameters and criterions. The application of fracture mechanics parameters to materials and constructions dimensioning is a great step towards effort process modelling compliant with the modelling rules, which justifies the aim of the present research - physical characteristics of the main parameters and criterions of fracture mechanics and its applicability to structure designing and dimensioning.

2. BASIC MODELLING RULES REQUIREMENTS

The theoretical structure of research object is defined with the use of:

- physical (calculation) model, describing the real object,
- mathematical model, an equation or system of equations, describing some correctness of processes together with boundary conditions, characteristic for a given phenomenon.

The basic physical laws are described mathematically, receiving first generation of mathematical models which are later modified (some of those modifications have empirical relations).

In compliance with Riemann consolidations, real basic rules occur for infinitely small magnitudes and must be formulated as partial differential equations. An integration of such equations leads to settlements and rules for larger portions of space and time. High conformity and ability of anticipating are obtained if definite phenomenon modelling rules are fulfilled.

Adequate research requires adequate models and conditions depending on their likeness. With the equation describing a given process, criterions and constants of similarity can be found.

If a given variable is marked x_i in real object and \bar{x}_i in model object, then the relation can be created [2]:

$$\frac{x_1}{x_1} = c_1, \dots, \frac{x_i}{x_i} = c_i, \dots, \frac{x_n}{x_n} = c_n \quad (1)$$

where:

c_i – a modelling scale.

Modelling scale is a transforming factor. Therefore, the following relation can be given:

$$\Phi(x_1, x_2, \dots, x_n) = \Phi(c_1 \cdot \bar{x}_1, c_2 \cdot \bar{x}_2, \dots, c_n \cdot \bar{x}_n) \quad (2)$$

A similar physical phenomenon is described by:

$$\Phi(x_1, x_2, \dots, x_n) = \Phi(\bar{x}_1, \bar{x}_2, \dots, \bar{x}_n) \quad (3)$$

Equation (3) is fulfilled if c_n is in conformity with:

$$\Psi(c_1, c_2, \dots, c_n) = 1 \quad (4)$$

$$\Psi(c_1, c_2, \dots, c_n) = \frac{\Phi(c_1 \cdot \bar{x}_1, c_2 \cdot \bar{x}_2, \dots, c_n \cdot \bar{x}_n)}{\Phi(x_1, x_2, \dots, x_n)} \quad (5)$$

Following Federman, it is known that if a number of variables used in experiment is equal to n and a few of them are independent $k < n$, then there are $(n - k)$ equations expressed by modelling scale c_i [2]. Therefore, a few dimensionless numbers may be proposed by an experimenter and may be the constants of similarity. The remaining ones are described by dimensionless numbers and Federman's settlements and are called similarity criterions. The indispensable conditions for existing phasic processes are given by:

- differential equations,
- verification of similarity criterions.

3. CHARACTERISTICS OF FRACTURE MECHANICS PARAMETERS AND CRITERIONS

The origin of fracture mechanics goes back to Griffith's publication on the glass fracture. In an elastic solid, such as the one considered by Griffith, if U and V , respectively, refer to the work of the external forces and the elastic energy and if γ refers to the specific surface tension energy of the solid, then Griffith's energy balance may be expressed as follows:

$$\frac{d}{dA}(U - V) = \gamma \quad (6)$$

where:

A – the surface area of the crack.

From the physical terms described in (6), it is clear that the stability of (quasi-static) fracture propagation may be determined from:

$$\left[\frac{d}{dA}(U - V) - \gamma \right] \begin{cases} > 0 - \text{unstable fracture,} \\ < 0 - \text{stable fracture,} \\ = 0 - \text{neutral equilibrium.} \end{cases} \quad (7)$$

For an infinite plane under uniform tension σ in y direction and which constrains a through crack of length $2a$ along the x axis, it may be shown that for the fixed grip, the total strain energy (per unit thickness) is:

$$V = \frac{1}{2} \frac{\sigma^2}{E} v_0 - \frac{1+\kappa}{8\mu} \pi \sigma^2 a^2 \quad (8)$$

where:

- v_0 – total volume (per unit thickness),
- μ – shear modulus,
- E – Young's modulus,
- $\kappa = 4-3\nu$ – for plane strain,
- or $\kappa = (3 - \nu) / (1+\nu)$ – for plane stress,
- ν – Poisson's ratio.

For the fixed grip $dU = 0$ and $dA = 4da$ (where da is the extension of the crack at each end) from equations (6) and (8),

$$\frac{1+\kappa}{8\mu}\pi\sigma^2a = 2\gamma \quad (9)$$

where:

$$\frac{1+\kappa}{8\mu} = \frac{1}{E} \quad \text{for plane stress,}$$

$$\frac{1+\kappa}{8\mu} = \frac{(1-\nu^2)}{E} \quad \text{for plane strain case.}$$

Furthermore, it should be pointed out that the energy balance relation (6) is the only condition for crack growth.

The revival of the Griffith theory came about after the X-ray work indicated that even in materials fracturing in a purely brittle manner there were extensive plastic deformations on the fracture surfaces, which led Irwin and Orowan, independently, to suggest that in the energy balance theory the rate of plastic work at the crack front should also be considered as a dissipative energy component. It was established that in a fracturing elastic solid if the characteristic size of the zone of large plastic deformation or energy dissipation around the crack front is very small, compared to the length parameter of the crack, then it is reasonable to assume that the energy (U-V) "pumped" into the fracture zone will come from the elastic bulk of the solid. In this situation then it will not be dependent on the details of the stress state very near the crack front. The stress state in elastic bulk of the solid will not differ from a purely elastic crack solution to any significant extent. The significance of this observation lies in the fact that one may now be justified in calculating the energy (U-V) available for fracture from a purely elastic solution [3].

Another contribution of Irwin was his recognition of the universality of the asymptotic stress and displacement fields around the crack tip of the interpretation of the fixed-grip strain energy release rate, which involves the strain energy distribution in the entire solid. He also introduced a new parameter G, which for a small crack extension da may be calculated as follows:

$$G = \frac{d}{da}(U - V) \quad (10)$$

The parameter G describes the strain energy release through the crack - closure energy. Then the term d(U-V) can be given as:

$$d(U - V) = 2 \int_0^{da} \frac{1}{2} \sigma_{yy}(r) v(da - r) dr \quad (11)$$

where:

$$\sigma_{yy} = \left(\frac{8\mu}{1+\kappa} \frac{G}{\pi} \right)^{\frac{1}{2}} \frac{1}{\sqrt{2r}} \quad (12)$$

$$v = 2 \left(\frac{1+\kappa}{8\mu} \frac{G}{\pi} \right)^{\frac{1}{2}} \sqrt{2r} \quad (13)$$

The above equations (10) + (13) show that the energy available for fracture per unit crack extension may be related to the coefficient of the singular form in the expression of the stress state at the crack tip described by G.R. Irwin as stress intensity factor:

$$k_1 = \left(\frac{8\mu}{1+\kappa} \frac{G}{\pi} \right)^{\frac{1}{2}} \quad (14)$$

which determines the stress and displacement states in the close neighbourhood of the smooth internal boundary of a plane crack in linearly elastic solid.

Furthermore the relation between k_1 and G , equation (14), gives a new form of stress intensity factor as:

$$\pi k_1 = K_I^2 \quad (15)$$

where:

K_I – being the new stress intensity factor.

Very useful tools in fracture mechanics include also such parameters as: crack tip opening displacement CTOD and the integral Rice – Čerepanov J . Below a short characteristics of the main fracture parameters is presented.

Stress intensity factor K_n

As seen above, the stress intensity factor is a parameter which determines the level of the stress or of the strain, energy density, elastic singularities near the tip of an ideal crack in a stressed linear elastic solid. The asymptotic stress and displacement components may be expressed as follows [4]:

$$\sigma_{ij}(r, \theta) = \frac{1}{\sqrt{2\pi r}} \left[K_I f_{ij}^I(\theta) + K_{II} f_{ij}^{II}(\theta) + K_{III} f_{ij}^{III}(\theta) \right] \quad (16)$$

$$u_i(r, \theta) = \frac{1}{2\mu} \sqrt{\frac{r}{2\pi}} \left[K_I g_{ij}^I(\theta) + K_{II} g_{ij}^{II}(\theta) + K_{III} g_{ij}^{III}(\theta) \right] \quad (17)$$

where:

- r – distance from the crack tip,
- θ – angle, second polar co-ordinate,
- $f_i^n(\theta), g_i^n(\theta)$ – dimensionless functions of the angle θ ,
- K_n – stress intensity factor ($n = I, II, III$ distinguish the models: I – opening mode, II – sliding mode, III – tearing or antiplane mode),
- i, j – index refers to either the Cartesian co-ordinates (x, y, z) or the cylindrical co-ordinates (r, θ, z).

Compliant with above, the stress intensity factor K_n is a fundamental quantity that governs the level of stress field in the vicinity of the crack tip or of the strain. Furthermore, it affects the strain energy density, elastic singularities near the tip of an ideal crack in a stressed linear elastic solid at $r = 0$ ($r \rightarrow 0, \sigma_{ij} \rightarrow \infty$), Fig. 1a. In reality some inelasticity in the neighbourhood of the crack tip is always present in the form of

plasticity. G. R. Irwin presents a simplified model for determination of the plastic zone attending the crack tip under small-scale yielding. The observation led Irwin to suggest that the effect of plasticity makes the plate behave as if it had a crack longer than the actual crack size, Fig. 1b: $a_{\text{eff}} = a + r_p$.

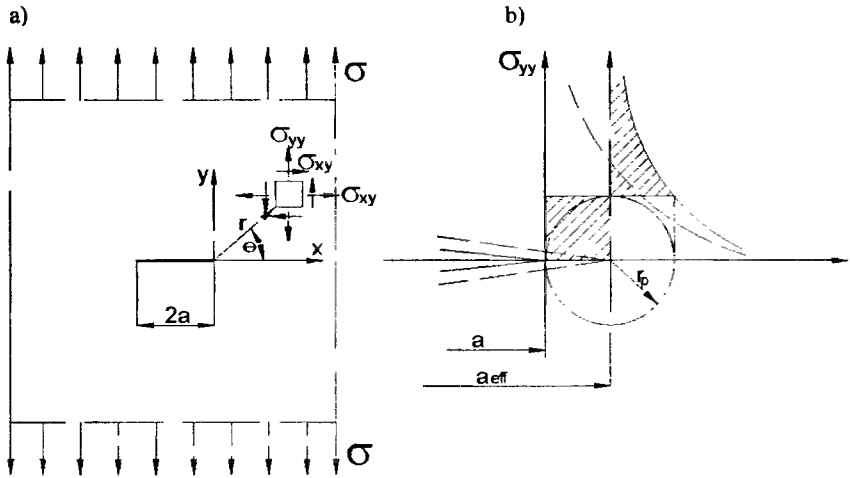


Fig. 1. Model of the plate with the crack $2a$ and the state of stress at the crack tip:

a) in elastic state of material with ideal crack under tension,

b) with extended crack length by plastic deformation a_{eff} – fictitious crack length

A study of the local stress fields for the three models (I, II, III) of loading showed their general applicability and can be generally given by the values of three stress intensity factors [4]:

$$K_I = \lim_{x \rightarrow a} \sqrt{2\pi(x-a)} \sigma_{yy}(x,0,0) = \lim_{x \rightarrow a} \sqrt{2\pi r} \sigma_{yy}(x,0,0) \quad (18)$$

$$K_{II} = \lim_{x \rightarrow a} \sqrt{2\pi(x-a)} \sigma_{xy}(x,0,0) = \lim_{x \rightarrow a} \sqrt{2\pi r} \sigma_{xy}(x,0,0) \quad (19)$$

$$K_{III} = \lim_{x \rightarrow a} \sqrt{2\pi(x-a)} \sigma_{yz}(x,0,0) = \lim_{x \rightarrow a} \sqrt{2\pi r} \sigma_{yz}(x,0,0) \quad (20)$$

For structural elements different than the infinity plate and unit thickness with crack $2a$, the stress intensity factor is a function of the loading of the body, including applied loads and displacements, of the crack size, of the geometry of the body and of the crack. For example, if the plate with finite dimension $2H \times W$ and thickness B with the crack $2a$ is affected by the action from tension stress σ , then the stress intensity factor is equal [5]:

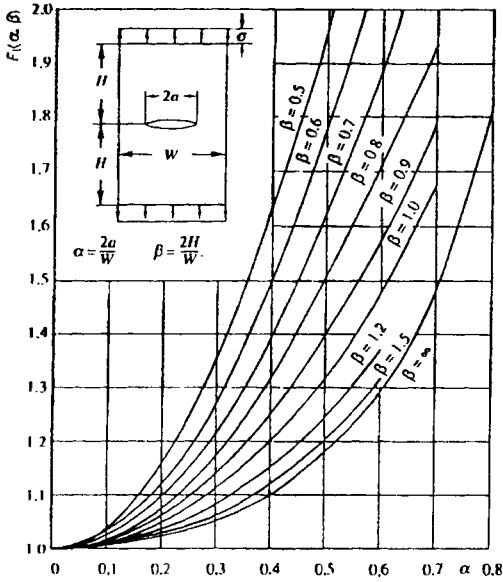
$$K_I = \sigma \sqrt{\pi a} F_1(\alpha, B) \quad (21)$$

where:

$$\alpha = 2a / W,$$

$$B = 2H / W.$$

The diagram of the function $F_1(\alpha, B)$ is presented in Fig. 2.

Fig. 2. Diagram of the function $F_1(\alpha, B)$ [5]

The solution of the linear fracture mechanics may be used in practice when the plastic deformation at the crack tip fulfils the condition: $r_p < 0.01 a$. The value of r_p depends on the relation $(K_I / R_e)^2$ and for mode I is:

– plane strain

$$r_p = \frac{1}{2\pi} \left(\frac{K_I}{R_e} \right)^2 \quad [\text{m}] \quad (22)$$

– plane stress

$$r_p = \frac{1}{6\pi} \left(\frac{K_I}{R_e} \right)^2 \quad [\text{m}] \quad (23)$$

where:

R_e – yield point of material,

then compliant with the equation (21) we can establish:

– size of the admissible defect (crack):

$$a \leq \frac{K_I^2}{\pi [\sigma \cdot F_1(\alpha, B)]^2} \quad [\text{m}] \quad (24)$$

– value of the allowable stress:

$$\sigma \leq \frac{K_I}{\sqrt{\pi a F_1(\alpha, B)}} \quad [\text{MPa}] \quad (25)$$

The above solutions are obtained by making the assumption that the radius of curvature at the crack tip $\rho_e \rightarrow 0$. When $\rho_e \neq 0$, K_I can be expressed as:

– plane strain

$$K_I = \sqrt{2\pi}(1-\nu)\mu\sqrt{\rho_e} \quad (26)$$

– plane stress

$$K_I = \sqrt{4\pi}\mu\sqrt{\rho_e} \quad (27)$$

where:

- ν – Poisson's ratio,
- μ – Shear modulus.

In dynamic problems the stress intensity factor is the function of time $K_n(t)$ for models $n = I, II, III$.

Strain energy release rate G

G was described previously by equation (10); G is related to the stress intensity factors as follows:

– in plane stress

$$G_I = \frac{K_I^2}{E} \quad (28)$$

$$G_{II} = \frac{K_{II}^2}{E} \quad (29)$$

$$G_{III} = (1+\nu)\frac{K_{III}^2}{E} = \frac{K_{III}^2}{2\mu} \quad (30)$$

– in plane strain

$$G_I = (1+\nu^2)\frac{K_I^2}{E} \quad (31)$$

$$G_{II} = (1+\nu^2)\frac{K_{II}^2}{E} \quad (32)$$

$$G_{III} = (1+\nu^2)\frac{K_{III}^2}{E} = \frac{K_{III}^2}{2\mu} \quad (33)$$

At the composed state of loading ($n = I, II, III$), the total value of G as:

$$G = G_I + G_{II} + G_{III} \quad (34)$$

After inserting the equations (28) ÷ (30) and (31) ÷ (33) into (34), we receive:

– in plane stress

$$G = \frac{(K_I^2 + K_{II}^2)}{E} + \frac{K_{III}^2}{2\mu} \quad (35)$$

– in plane strain

$$G = \frac{(K_I^2 + K_{II}^2)(1 - \nu^2)}{E} + \frac{K_{III}^2}{2\mu} \quad (36)$$

G is also related to the variation of the compliance C of the element with as follows:

$$G = \frac{1}{2} F^2 \frac{\partial C}{\partial A} \quad (37)$$

where:

C – compliance ($u = CF \rightarrow C = uF^{-1}$) $N^{-1}m$

F – force, N.

Crack tip opening displacement CTOD - δ

Very often in linear elastic fracture mechanics the parameter δ - CTOD is used to characterise the effort of the plastic zone at the crack tip situated in elastic-plastic materials. The concept of a crack tip opening displacement as a fracture parameter δ was used for the study of crack initiation in situations where significant plastic deformation precedes fracture. A measure of the amount of crack – tip plastic strain is the separation of the crack faces or crack opening displacement (COD), especially very close to the crack tip. A simplified model for plane stress yielding which avoids the complexities of a true elastic – plastic solution has been introduced by Dougdale. The model refers to thin plates in which plane stress conditions dominate for materials with elastic – perfectly plastic behaviour which meet the Tresca yield condition, (Fig. 3). By Dougdale, the following hypotheses are made:

- all plastic deformation concentrates in a line in front of the crack,
- an effective crack that is longer than the physical crack by the length of the plastic zone is considered.

According to Neimitz [5], the opening of the effective crack at the tip of the crack is given by:

$$\delta = \frac{8\sigma_y a}{\pi E} \ln \left(\sec \frac{\pi \sigma}{2\sigma_y} \right) \quad (38)$$

By expanding equation (38) in Maclaurin series and retaining only the first term for a small value of σ / σ_y , we get:

$$\delta = \frac{K_I^2}{E\sigma_y} \quad (39)$$

If we base on the Irwing's solution, the distance δ of the faces of the fictitious crack at the tip of the initial crack of length $2a$ is given by:

$$\delta = \frac{4}{\pi E} \frac{K_I^2}{\sigma_y} \quad (40)$$

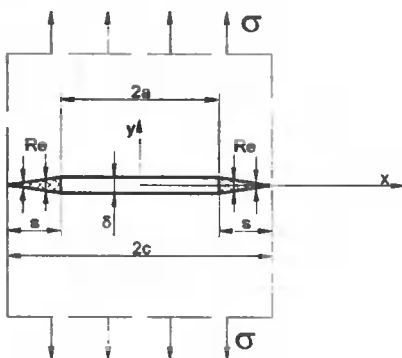


Fig. 3. Dougdale model for mode I crack of length $2a$ situated in very thin and an infinite plate subjected to uniaxial uniform stress σ at infinity perpendicular to the crack plane

By comparing equations (39) and (40), we can deduce that the Irwin model overestimates δ , as compared to the Dougdale model, by 27 per cent.

The equations (39) and (40) combined with equation (28) yield, respectively:

$$G = \sigma_y \delta \quad (41)$$

$$G = \frac{\pi}{4} \sigma_y \delta \quad (42)$$

The experimental investigations indicate that the above relations are appropriate when $\sigma \leq \sigma_y$.

Rice – Čerepanov J integral

The mathematical formulation of the conservation laws applicable to elastostatics in the form of path independent integrals of some functionals of the elastic field over the bounding surface of a closed region was proposed recently by Rice and independently by Čerepanow [4]. They introduced the J -integral for notch problems.

The increment of the difference between the stored elastic energy W_e and work of the external loads U per unit increment of an ideal crack surface area A in non-linear elasticity makes it possible to establish J as [4]:

$$J = -\frac{\Delta P}{\Delta A} \quad (43)$$

or

$$J = -\frac{\partial P}{\partial a} \quad (44)$$

where:

P – potential energy.

In elasticity the strain energy release rate J is equal to the Rice – Čerepanov J integral defined as:

$$J = \int_F \left(W dy - \sigma_{ij} n_j \frac{\partial u_i}{\partial x} ds \right) \quad (45)$$

where:

- W – strain energy density,
- Γ – contour around the tip joining one point on a face of the crack to another point on the opposite face, Fig. 4,
- ds – differential element of the contour,
- u_i – displacement vector,
- n – unit outward normal to Γ ,
- $\sigma_{ij}n_j$ – normal component of the stress tensor to the contour Γ at ds , known as a traction vector,
- σ_{ij} – stress tensor,
- $\sigma_{ij} n_j \frac{\partial u_i}{\partial x} ds$ – unit energy density release from stress field σ_{ij} ,
- x, y – Cartesian co-ordinate system.

In linear elasticity $J = G$. Furthermore, the J integral is independent of the contour in elasticity. This property is also extended in plasticity in monotonic radial loading. Under the same conditions the strain energy release rate can be assumed to be equal to the J integral, as in elasticity.

The J integral characterises the crack tip singularities of stress, strain and strain energy density in non-linear elasticity and in plasticity.

As for the deformation plasticity, it can be shown that J controls the stress and strain near-tip fields as K does in linear elasticity. The proof was given independently by Hutchinson, Rice and Rosengreen [6,7] and is designated as (HRR) fields. Let (r, φ) be polar co-ordinates with the origin in the crack tip. Then for $r \rightarrow 0$ the stress and deformation as a function of J integral the following is obtained:

$$\sigma_{ij} = \sigma \left[\frac{J}{I_n \sigma_0 \varepsilon_0 A r} \right]^{\frac{1}{n+1}} \cdot \tilde{\sigma}_{ij}(\varphi, n) \quad (46)$$

$$\varepsilon_{ij} = \sigma \left[\frac{J}{I_n \sigma_0 \varepsilon_0 A r} \right]^{\frac{1}{n+1}} \cdot \tilde{\varepsilon}_{ij}(\varphi, n) \quad (47)$$

where:

- $A, n, \varepsilon_0, \sigma_0$ – constants of the Ramberg – Osgood law,
- I_n – dimensionless factor depending on the hardening exponent n and on the crack mode (I, II, III) and is tabulated, e.g. in [6],
- $\tilde{\sigma}_{ij}(\varphi, n)$ – dimensionless function determined in [8, 9].
- $\tilde{\varepsilon}_{ij}(\varphi, n)$ – dimensionless function determined in [8, 9].

Near the crack tip the strain energy density, which varies as r^{-1} , is proportional to J .

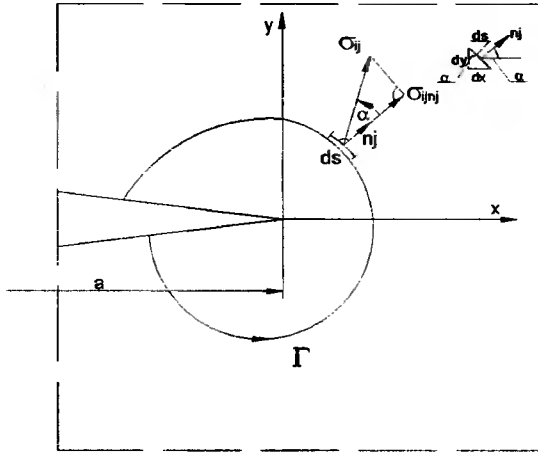


Fig. 4. A two-dimensional cracked body with a path Γ starting from lower and ending to the upper face of a notch with traction vector

Fracture criterions

To make it an effective tool for studying the mechanical failure of the defect geometry, the intensity of applied loads is based entirely on the motions of continuum solid mechanics. The materials resistance to fracture also needs to be developed. To establish a simple fracture criterion, one may thus assume that [11]:

- the characteristic size of the energy dissipation or fracture process zone around the growing crack front is small compared to the length of the crack,
- the size and shape of the dissipation zone remain relatively constant as the crack extends.

According to [10,11], basic fracture criterions can be established as follows:

$$K_n = K_{nC} \quad (48)$$

$$G_n = G_{nC} \quad (49)$$

$$\delta = \delta_C \quad (50)$$

$$J_n = J_{nC} \quad (51)$$

where:

$n = I, II, III$ modes.

The left hand-side of criterions (48) ÷ (51) has been characterised as above. The right-hand side of this equation characterises by the fracture toughness which described a material resistance to crack extension. The criterions (48) and (49) are mainly used for brittle fracture in linear elastic fracture mechanics. The residual criterions (50), (51) are used in elasto-plasticity.

For example, the criterions for mode I condition can be expressed as follows:

$$K_I = K_{IC} \quad (52)$$

$$G_I = G_{IC} \quad (53)$$

$$\delta = \delta_C \quad (54)$$

$$J_I = J_{IC} \quad (55)$$

Plane strain fracture toughness under mode I is K_{IC} or G_{IC} . For the pure mode II or III crack extension it is difficult to reach the value of K_I or G_{IC} when plane mode I. Since K_I is constant, for unstable fracture one must have $\partial K_I / \partial a > 0$, “ a ” being a length parameter of the crack. An additional change in terminology seems to be referring to K_{IC} as the fracture toughness of the material. As well, since G_{IC} is constant, $\partial G_I / \partial a$ determines the fracture stability mainly as according to the hypothesis of the fracture toughness G_{IC} is practically constant.

The critical value of the crack tip opening displacement CTOD can be used to characterise the fracture toughness in elasto-plasticity. The CTOD at unstable propagation up to 0.2 mm crack growth or at pop-in and is designated by δ_C , equation (54) [4].

The critical value of the strain energy release rate J can be used to characterise the fracture toughness and they are designated as the fracture resistance J_{IC} equation (55). The fracture resistance is observed at unstable crack propagation up to 0.2 mm of crack growth or to a pop-in [4].

Under the plane strain condition, the critical value of J , J_{IC} is related to the plane strain fracture toughness K_{IC} by the following equation:

$$J_I = \frac{1 - \nu^2}{E} K_{IC}^2 \quad (56)$$

Efforts have been made to extend the realm of applicability of the J -integral fracture criterion to ductile fracture where extensive plastic deformation and possibly stable crack growth precede fracture instability.

Integral J is also equal to G , and this property holds only for linear elastic material response under “dead-load” loading during crack growth and then:

$$J_{IC} = G_{IC} \quad (57)$$

Finally, integral J can be related to the crack tip opening displacement by a simple relation:

$$J = M \cdot \sigma_y \delta \quad (58)$$

where:

$M = 1$ for the Dougdale model.

The parameters K_{IC} , G_{IC} , δ_C and J_{IC} are determined experimentally by the use of certain procedures established by appropriate standardised tests such as ASTM, BS, PN etc., [12–16].

In impact loading, K_{IC} is simply replaced by K_{ID} which is obtained from standardised impact tests [17,18] and

$$K_I(t) = K_{ID} \quad (59)$$

4. SOME REMARKS ON THE ACTUAL APPLICATION OF THE FRACTURE MECHANICS TO MECHANICAL ENGINEERING

Fracture mechanics design methodology is based on the realistic assumption that all materials contain initial defects that affect the load-carrying capacity of engineering structures. Defects are initiated in the material by manufacturing procedures or can be created during the service life, like fatigue, environment-assisted or creep cracks. Usually, one dominant crack is assumed. Two pieces of information are needed to make a prediction of the failure behaviour in structural components containing defects such as cracks. They are the deformation behaviour of the structure and the fracture behaviour. The deformation behaviour gives the relationship between load and displacement of the component or an analogous relationship such as stress and strain. It is usually done independently of the fracture behaviour but with the inclusion of the effect of the defect. Deformation behaviour usually combines a linear-elastic and an elastic-plastic contribution. The fracture parameters are also determined from the deformation behaviour of the structure and would include a combination of a linear elastic term, usually K_n based and an δ . The deformation behaviour usually requires some knowledge of the tensile properties of the material in the structure.

A fracture safe design can be also influenced by constraint effect, especially in weld structures. The current work has concentrated more on constraint effects on the fracture behaviour. The effect of constraint on deformation behaviour must also be considered, especially in the non-linear region of behaviour. The non-linear local deformation takes place in mismatched weld joints of the structures. The Engineering Treatment Model (ETM) applied to an analysis of mismatched weld joint uses calibration functions in which load is normalised by limit load and toughness in input at a point [19]. The ductile fracture methodology uses a similar normalised approach and treats the ductile fracture characterisation as a procedure to keep account of the current crack length which, in turn, modifies the deformation behaviour [20].

Recently the Engineering Treatment Model (ETM) was modified by introducing the constraint factor for under- and overmatched weld joints [21]. In all of these methods the deformation behaviour plays an important role in determining the maximum load attained to the failure load. The deformation process and fracture parameters calibrations are influenced by constraint; hence the importance of determining the deformation behaviour and fracture parameters as a function of constraint.

5. CONCLUSION

Fracture mechanics design methodology is based on more realistic parameters and criterions than the classic continuous mechanics. With the above procedures there were determined the maximum allowable loads applied for a specified crack size, or the maximum permissible crack size for specified load applied. Some further effort is needed on the effects of constraint on deformation behaviour during the fracture process, especially in weldments.

REFERENCES

- [1] Olesiak Z., 1988. Stress concentration and contact stress. In strength of structural components. PWN Warszawa.
- [2] Gabryszewski Z., Gronostajski J., 1991. Mechanics of the plastic forming process. PWN Warsaw.
- [3] Orowan E., 1955. Energy criteria of fracture. *Welding Journal*.
- [4] François D., 1996. ESIST C7D-1-96D. Guidelines for terminology and nomenclature in the field of structural integrity. *Fatigue & fracture of engineering materials & structures*.
- [5] Neimitz A., 1998. Fracture mechanics. PWN Warsaw.
- [6] Hutchinson J.W., 1968. Plastic stress and strain fields at a crack tip. *Journal of the Mechanics and Physics of Solids* 16.
- [7] Rice J.R., Rosengren G.F., 1968. Plane strain deformation near a crack tip in a power-law hardening material. *Journal of the Mechanics and Physics of Solids* 16.
- [8] Shih C.F., 1974. Small-scale yielding analysis of mixed mode plane-strain crack problems. [In:] *Fracture Analysis*. ASTM STP 560.
- [9] Rice J.R., 1967. Stresses due to sharp notch in work-hardening elastic-plastic material loaded by longitudinal shear. *Journal of Applied Mechanics* 34.
- [10] Gołaski L., 1992. Elements of the experimental fracture mechanics. Technological University of Kielce.
- [11] Rice J.R., 1968. Mathematical analysis in the mechanics of fracture. *Fracture, an Advanced Treatise* 2. Ed. H. Liebowitz Academic Press.
- [12] PN-87/H-04335. Test method for plane strain fracture toughness.
- [13] PN-88/H-04336. Test method for a measure critical value of fracture toughness J , J_{IC} .
- [14] ASTM-E 399-83. Standard test method for plane strain fracture toughness of metallic materials.
- [15] ASTM-E 813-89. Standard test method for J_{IC} a measure of fracture toughness.
- [16] BS 5447/1977. Method of test for plane strain fracture toughness K_{IC} of metallic materials.
- [17] ASTM-E 24.03.03. Proposed standard method of test for instrumental impact testing of precracked Charpy specimens of metallic materials. Draft 2c. 1980.
- [18] a. ISO 14556-Charpy-V pendulum impact test – Instrumented test method.
b. ISO Charpy fracture test method. Draft – preconditioning.
- [19] Schwalbe K.H., 1992. Effect of weld metal mis-match on toughness requirements: some simple analytical considerations using the Engineering Treatment Model (ETM). *International Journal of Fracture* 56.
- [20] Landes J.D. et al., 1991. An application methodology for ductile fracture mechanics. *Fracture Mechanics*. ASTM STP 1189.
- [21] Ranatowski E., 2000. Analysis of the heterogeneous weld joints in aspect of fracture mechanics. *Advances in mechanical behaviour plasticity and damage* 1. Eds D. Miannay et al., Elsevier.

Andrzej Skibicki

University of Technology and Agriculture

Faculty of Mechanical Engineering

Department of Material Engineering

FEM IN CALCULATION OF THE STRESS AND DEFORMATION OF WELDING CONSTRUCTIONS

Summary: The article describes the analysis of temperature and residual stresses on welded elements. The experiments were carried out on St3S steel to measure the temperature during welding and residual stresses. The FEM numerical analysis was used to calculate temperature, transient and residual stresses. Two models for St3S and aluminum alloy are shown. There was observed a satisfactory overlap between the numerical and experimental results.

Key words: welding, residual stress, temperature, FEM

1. INTRODUCTION

Welding is one of the basic techniques of connecting metals. Melting metal, which makes the weld, needs introducing a great amount of heat. Both the weld and the construction are heated. The results reveal structural changes, which makes the mechanical properties of metal lower. The results in the deformation and residual stresses category are also important. They can pose a threat for the construction. If the material thickness is small while the plasticity high – there are also additional loads needed to destroy the construction. The risk is higher for fragile materials. Thick metal sheets are during and after welding in 3 dimensional (3D) stress state. A crack can occur in both. The residual deformation changes the form of the construction and can make their operation impossible. The shrinkage and deformation make it difficult to keep the tolerances. The practical methods of reducing deformation and stress are the results of long-term experience. The technical development and economy introduces new technologies and materials. The quality is growing up. The job of technologists and scientists can be considerably facilitated by new computer methods. The FEM (Finite Element Method) simulation may give ready-to-use methods or decrease expensive experimental researches.

The FEM-enhanced calculation is shown. ANSYS5, which was used, is a program popular with engineers and researchers as it makes easier the co-operation with the calculations of strength, fatigue, optimisation etc. Welding, as a physically complex process, requires complicated modelling and solving procedures which are being developed [8–11].

2. RESEARCHES

2.1. Experimental researches

The experimental research aimed at examining the quality of numerical research. The conditions applied are reproduced in the form of the FEM model. The specimen size: 150 x 100 mm, thickness 3.8 mm and the outline are shown in Figure 1.

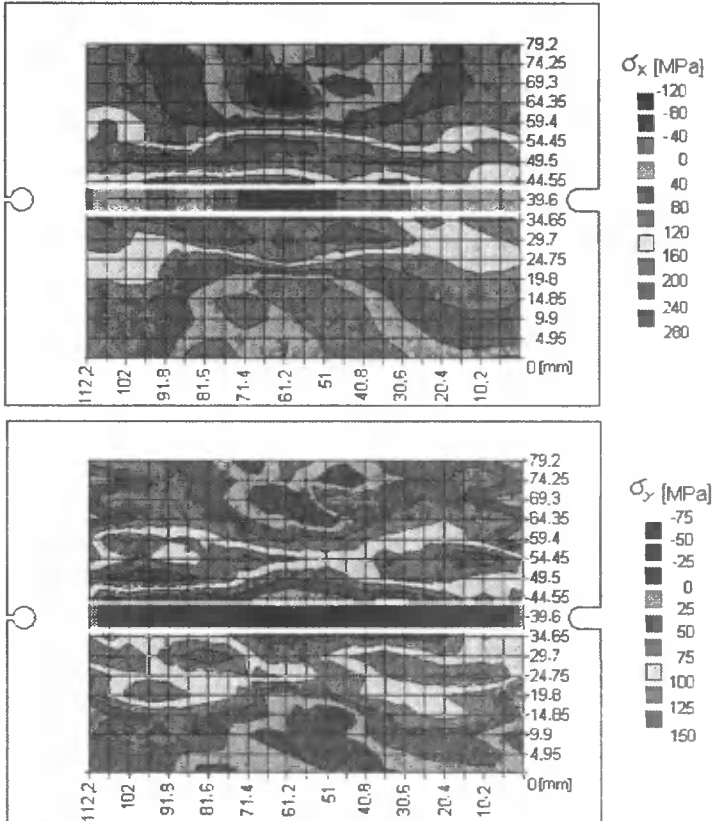


Fig. 1. Longitudinal and transverse residual stress measured, St3S

The specimen was made from St3S (chemical composition PN-88/H-84020) steel sheet. The 100 mm long groove was cut by 1.6 mm mill. Yield stress R_e was measured as 252 MPa after normalisation and 302 MPa after quick cooling (water, to simulate rapid weld cooling with cold metal close by) from the temperature of 830 °C. Welding was carried out by the Polytechnic of Gdansk (Department of Welding Technology). MIG methods were used. The protective gas was 98 % Ar + 2 % O₂, the wire SpG2, ϕ 1.2 mm, given with the speed of 9.5 m·min⁻¹. The welder BDH 320, with electronic registration of welding parameters (voltage and current) was used. On the average $U = 27.2$ V and $I = 265$ A were registered. The transient temperature was registered in 5 points, with Ni-NiCr thermocouple (ϕ 0.6 mm, mantle type). The residual deformation was measured. The residual stresses were measured in one specimen, with a relatively cheap magnetic

method, which is based on the Barkhausen effect [1]. Longitudinal and transverse residual stresses are measured in 391 points. The results are shown in Fig. 1. The measurement on the weld line and at the boundary of the sample were not possible. Microstructure and HV were also examined with other methods.

2.2. Numerical research

2.2.1. Assumptions

The bases of the FEM calculations are shown by Zienkiewicz [2]. The calculations covered two phases, as uncoupled thermal and mechanical calculations. The scheme is shown in Fig. 2. Accurate calculations are possible, especially for deformations and stresses, only with the use of non-linear dependence of physical material properties on temperature. The material properties depend also on deformation. The properties here included elasto-plasticity with isotropic hardening. A search for the FEM solution is iterative (Fig. 2). The modelling of the welding process lasted for 10.3 s, with cooling time (until 800 s). The position of the heat source was changing, while heating (loading) and cooling of models occurred. This way the "step by step" technique was used. The results of step 1 were necessary for the calculation of step 2, the results of step 2 will be necessary for the calculation of step 3, etc until the final step. Both the processes prolonged the problem solving considerably (factor 10E5).

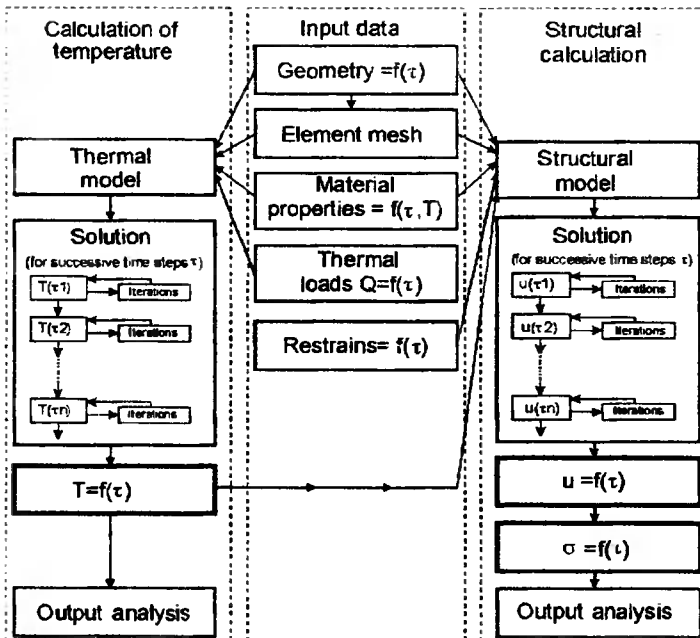


Fig. 2. Schematic diagram of uncoupled thermal-structural calculations

Full 3D calculations require very efficient computers. The 2D model was then used, lying on the surface of welded sheets aiming at the optimal formulation of welding physics. In the 2D geometry, the higher perpendicular thickness of grain and root of weld was declared. Because of the models symmetry only $\frac{1}{2}$ of the surface was

calculated. The adequate boundary conditions were used. All this made the time of the calculations shorter. Finite elements were used from the library of the program ANSYS5: SHELL57 in thermal calculations and PLANE42 in the structural calculations. 892 elements were used. The mesh of the elements was shown in Fig. 3. The restrains relate to those appropriate in the experiment. The size of elements is smaller near the welding lines due to high gradients here (of degrees of freedom e.g. temperature or deformation). Distributed volume heat source, suggested by Goldak, [3] for MIG/MAG, was moving along the line of the weld. There were welds in the place of grooves due to completing the model by previous removal of finite elements from the model ("killed"). On both surfaces, upper and bottom, the loss of heat through convection was taken into account. The convection near the weld was intensified to account for the heat radiation.

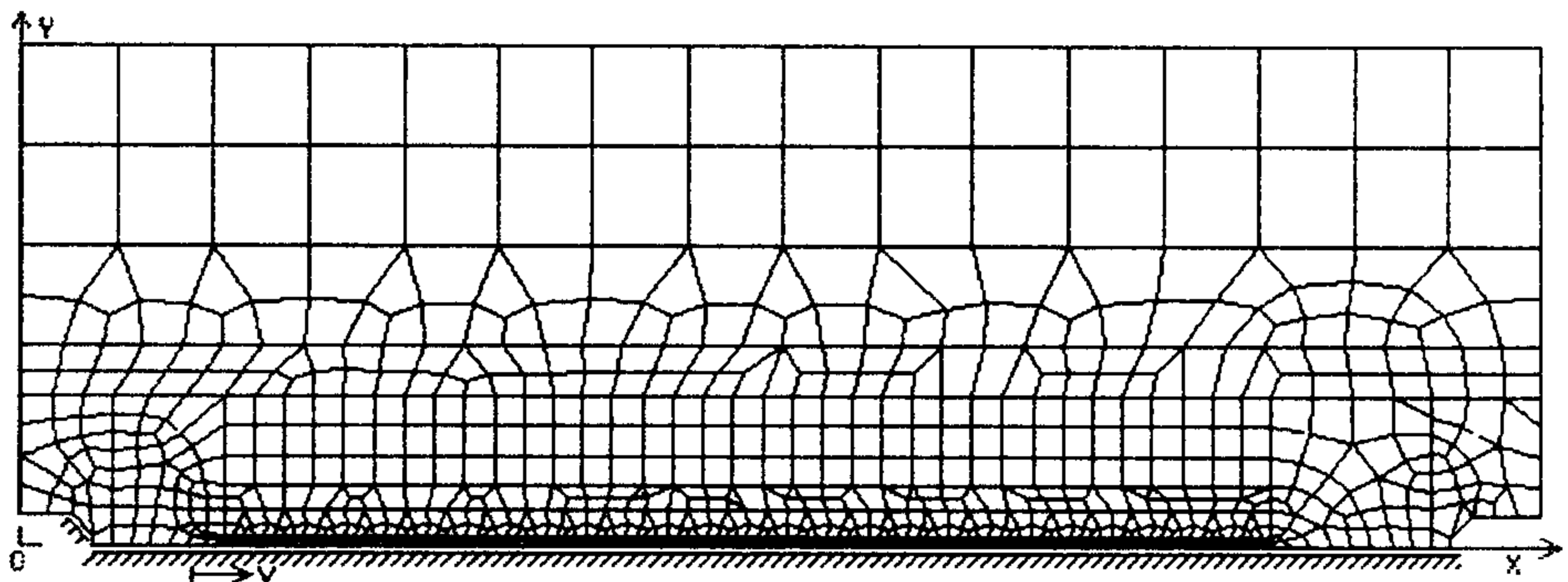


Fig. 3. Finite element mesh used in both analyses

2.2.2. Calculation for the steel plate

The calculations made for the experimental model are described in 2.1. The heat source was 4.88 kW, which corresponds to $U \cdot I = 7.2$ kW, taken into consideration the efficiency $\eta = 68\%$ [7]. The speed of welding reflected the time registered in the experiment ($10 \text{ mm} \cdot \text{s}^{-1}$). Fig. 4 shows thermal material properties dependent on temperature. The value of λ (for $t > 1490$ °C) was raised from 40 till 230 W/m·K to factor in the intensive mixing of liquids in the weld pool [3]. Fig. 6 shows the temperature field at the end of welding.

Mechanical properties of St3S materials are very important. They depend on the present temperature, the speed of cooling and phase changes connected. The material is elasto-plastics with isotropic hardening. Part of the data comes from the literature [4,5]. Numerous experimental research were carried out for higher accuracy of the results. The properties of base material, called MAT1, the base material cooled rapidly in water from 830 °C (MAT2) and the weld material (MAT3) were examined. A special attention was given to R_e , E_T and α_T . The properties referred to as MAT2 and MAT3 were connected with the parts of the model area which were quickly cooled by cold metal close by or were welded over the cooling phase. The properties R_e , E , E_T , ν and α_T were in Fig. 5.

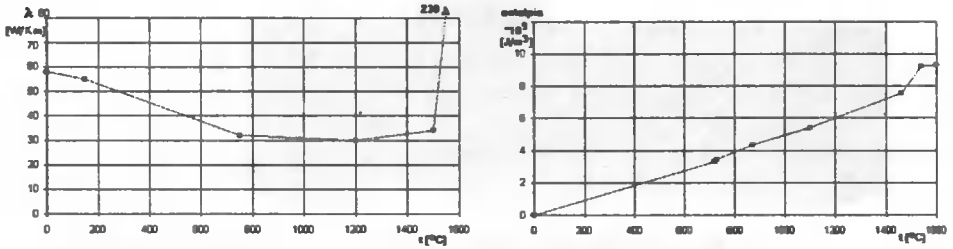


Fig. 4. Specific enthalpy and thermal conductivity λ , St3S

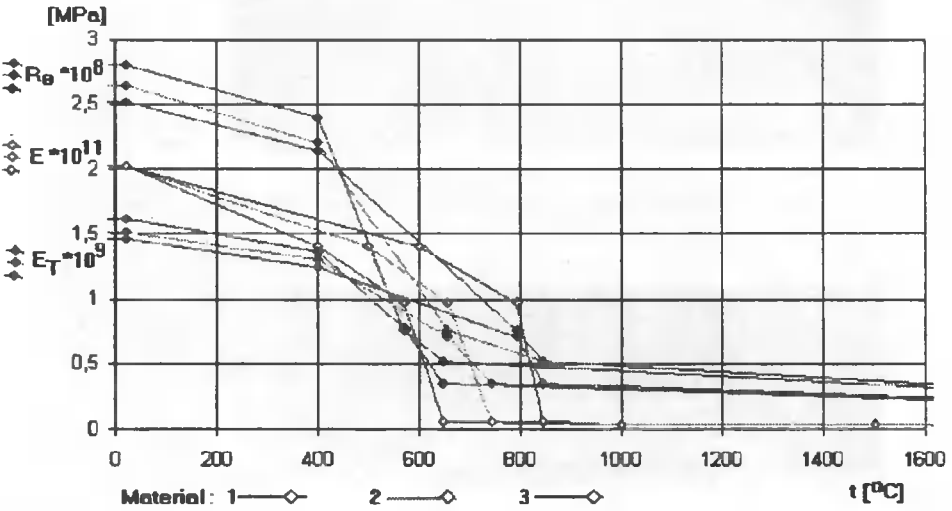
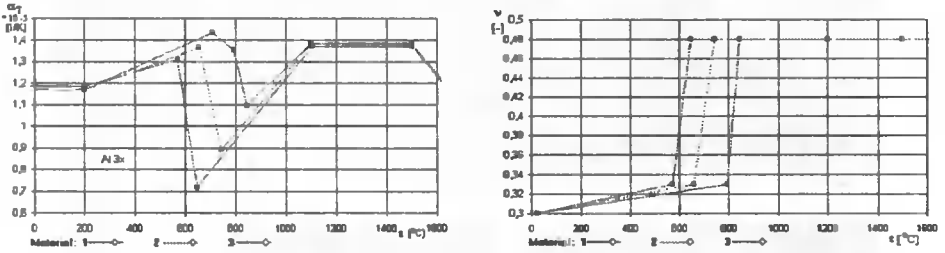


Fig. 5. Mechanical properties for the St3S steel as a function of temperature and material history. a) Poisson's ratio ν , b) thermal dilatation α_T , c) elastic module E , yield stress R_e , hardening modules E_T for the base material (1), filler material (2) and rapidly cooled material (3)

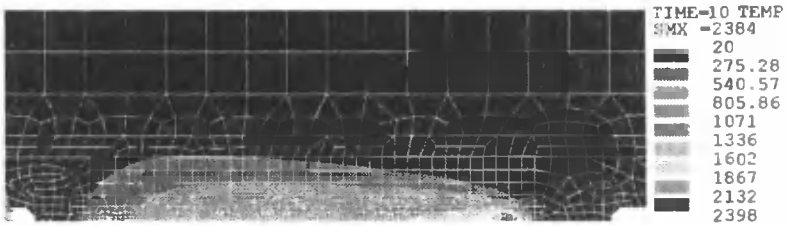


Fig. 6. Calculated temperature field, °C, at time $t = 10$ s, St3S

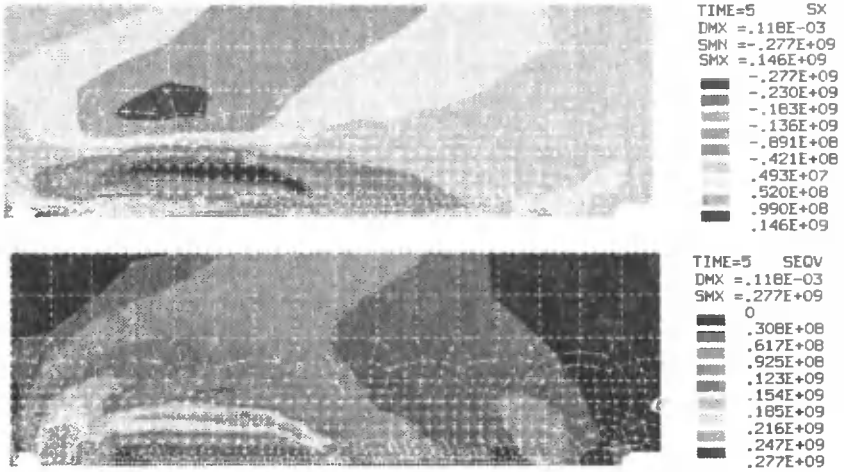


Fig 7. Calculated transient longitudinal and reduced (von Mises) stress, Pa, for $t = 5$ s, St3S

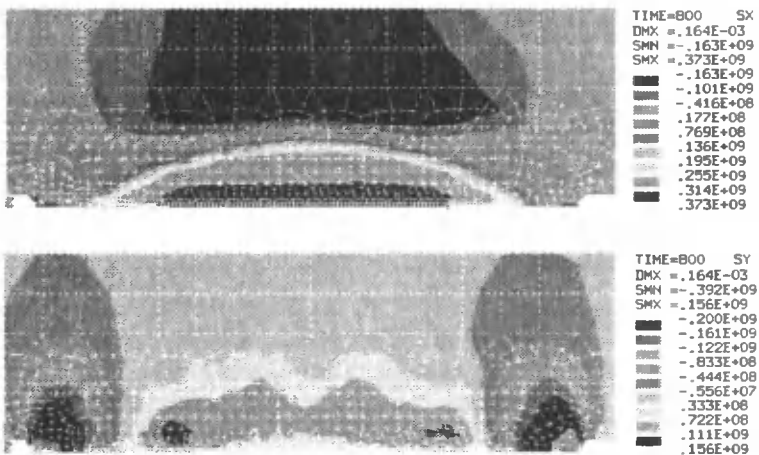


Fig. 8. Calculated longitudinal and transverse residual stress, Pa, St3S

2.2.3. Calculation for the welded plate of aluminum alloy

As the second one, the model of the plate from aluminum alloy welding was calculated, without measurements, as an important constructional material and its properties are very different from steel. As for the model described in 2.2.2, the power of the heat source (3.4 kW) and material properties [6], non-linear temperature dependent, were changed. Fig. 9 and 10 give sample results.

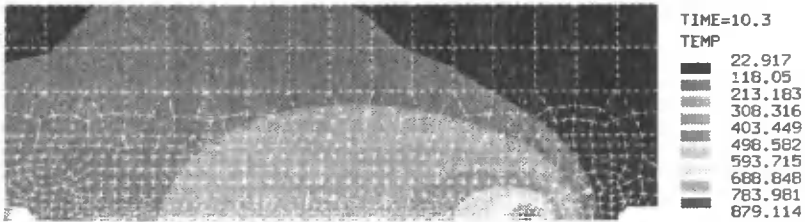


Fig. 9. Calculated temperature field, °C, at time $t = 5$ s, aluminum alloy

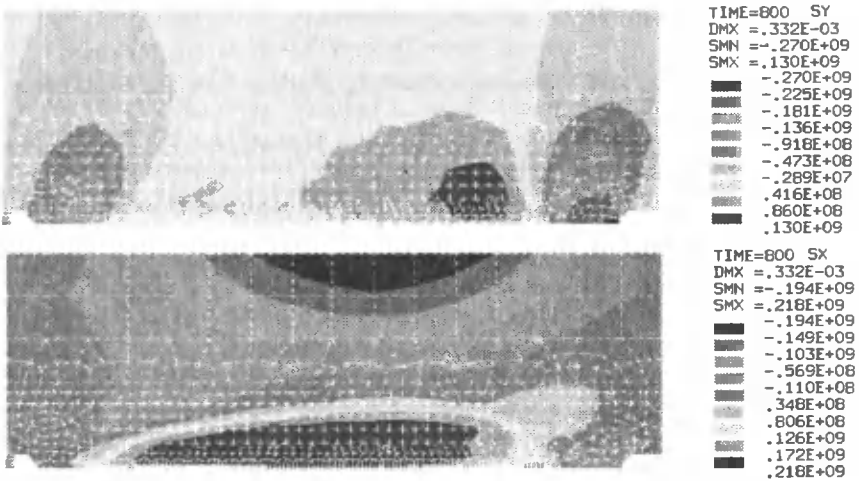


Fig. 10. Calculated longitudinal and transverse residual stress, Pa, aluminum alloy

3. RESULT ANALYSIS

- Analysing results of measurements and calculations, the following are observed:
 - temperature fields coincide considerably for range, maximums and changes in time,
 - stresses coincide considerably for range, signs, values and maximums,
 - deformations show a similar form, sign, and approximate value.
- The manner of stresses location is different for aluminum alloy and for steel, which is not revealed by analytic methods.
- The values of transient stresses obtained for location, sign of value and maximums are completely different from the residual values.

4. OBSERVATIONS AND CONCLUSIONS

1. There was observed a considerable agreement between the results of the experiment and the calculations compared, which was visible both in thermal and structural parts.
2. FEM is adequate for the calculation of the residual and transient welding stress.
3. The agreement of the results may be the basis for a possible justification for the calculation method used (modelling, numerical solution procedure) and determination of physical properties.
4. The application of the commonly applied ANSYS makes it possible to implement the calculations method suggested.
5. Values of transient residual stresses are very difficult to obtain in the experiment yet they can be very useful; applying FEM can be well-justified and effective.

REFERENCES

- [1] Augustyniak B., Degauque J., 1996. Microstructure Inspection by Means of Mechanical Barkhausen Effects Analysis. *Journal De Physique IV*, 6 (8), 527-530.
- [2] Zienkiewicz O.C., 1972. *Metoda Elementów Skończonych*. Arkady Warszawa.
- [3] Goldak J. i in., 1986. Computer Modelling of Heat Flow in Welds. *Metallurgical Transactions B.*, 9, 587-600.
- [4] Richter F., 1973. Die wichtigsten physikalischen Eigenschaften von 52 Eisenwerkstoffen. Duesseldorf, Staleisen.
- [5] Richter F., Born L., 1984. Die spezifische Wärmekapazitaet von metallichen Werkstoffen. - I. Teil: Ferritische, umwandlungsfahige Staehle. *Arch. Eisenhuettenwes* 55, 3.
- [6] Skibicki A., 1998. Identyfikacja stanu termicznych i mechanicznych skutków procesu spawania wybranych elementów z uwzględnieniem metod numerycznych. Praca doktorska. Wydział Mechaniczny ATR Bydgoszcz.
- [7] Masubuchi K., 1991. *Analysis of welded structures*. Pergamon P.
- [8] Mochizuki M., 1997. A simplified analysis of residual stresses at welding joints between plate and penetrating pipe. *JSME International Journal* 1, 8-14.
- [9] Yeung K.S., Thornton P.H., 1999. Transient thermal analysis of spot welding electrodes. *Welding Research Supplement*, 1-6.
- [10] Frewin M.R., Scott D.A., 1999. Finite element model of pulsed laser welding. *Welding Research Supplement*, 15-21.
- [11] Fu L., Duan L., 1998. The coupled deformation and heat flow analysis by FEM during friction welding. *Welding Research Supplement*, 202-207.

Sylwester Wawrzyniak

University of Technology and Agriculture

Faculty of Mechanical Engineering

Department of Control and Machinery Design

CT ANEMOMETRIC VELOCITY PROFILE INVESTIGATION BEHIND THE AXI-SYMMETRIC NOZZLE

Summary. The article presents rules of thermo-anemometric measurements with a single HOT-WIRE probe and shows the point of measurements as well as selected results obtained for variable working device parameters. Both the sampling frequency and the number of measurements in each point of range measurement were changed. The investigations aimed at finding such measurement parameters for which the measurement time would be minimal ensuring the assumed accuracy of results.

Key words: axi-symmetric nozzle, thermo-anemometric method

1. METHODS OF MEASUREMENTS

The report includes a thermo-anemometric measurement method for fields of speed of air flowing out from axi-symmetric nozzle whose constructional and geometric features were presented in earlier reports [3,5]. The investigations aimed at qualifying parameters of measurements, such as sampling frequency and the number of measurements in every measuring-point for optimization of the measurement duration time and, foremost, at accuracy of measurements.

The variable parameters investigated included: the sampling frequency and the number of measurements in a single measurement-point. For results, see graphs.

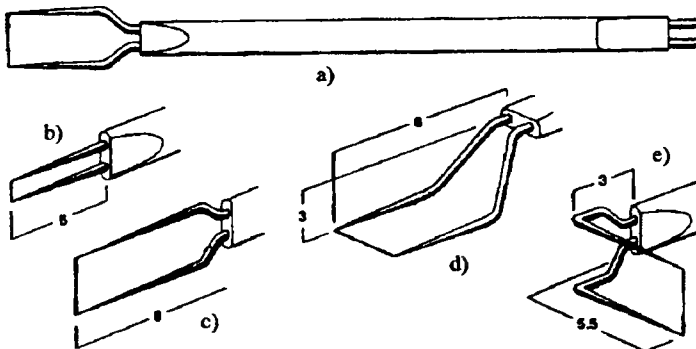


Fig. 1. Hot-wire probes: a) general view probe, b) non-plated, c) plated, d) boundary-layer probe, e) probe with bent prongs; dimensions in millimeters [1]

The probe shown in Fig. 1b was investigated.

Modes of HWA (Hot Wire Anemometry) operation.

The two main modes of operating a hot-wire probe include:

- the Constant-Current (CC) mode in which the probe temperature varies,
- the Constant-Temperature (CT) mode in which the probe resistance, and hence its temperature, is kept virtually constant by changing the current.

The aerodynamic laboratory experiments were performed with CT methods supplied by air blower.

Time means and fluctuating components of velocity magnitudes in meridional planes were measured by StreamLine® CTA 90C10 hot wire constant-temperature anemometer supplied by Dantec; a single-channel instrument, unable to determine the velocity direction, which is crucial to interpreting the results which cannot discriminate between positive and negative values of the velocities.

Maintaining the hot-wire at a constant operational temperature and thereby at a constant hot resistance has major advantages since the thermal inertia of the sensor element is automatically adjusted when the flow conditions vary. This mode of operation is achieved by incorporating a feedback differential amplifier into the HWA circuit to obtain rapid variation in the heating current to compensate for instantaneous changes in the flow velocity.

The principle of a CT circuit is illustrated in Fig. 2. A hot-wire probe is placed in a Wheatstone bridge. As the flow conditions vary, the error voltage $e_1 - e_2$ will be a measure of the corresponding change in the wire resistance. These two voltages move from the input to the operation amplifier. The selected amplifier has an output current i , which is inversely proportional to the resistance change of the hot-wire sensor. Feedback to the top of bridge will restore the sensor resistance to its original value. Modern amplifiers have a very fast response, and in the CT mode the sensor can be maintained at a constant temperature, except for very-high-frequency fluctuations.

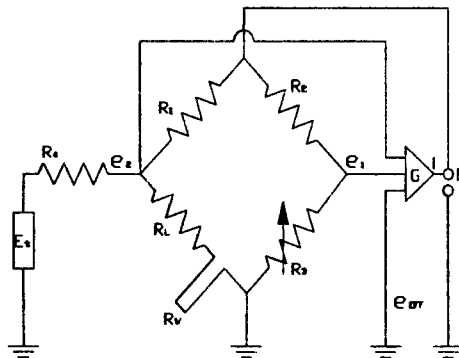


Fig. 2. A CT anemometer containing a Wheatstone bridge, a feedback amplifier and an electronic-testing subcircuit: R_w – probe resistance; R_1 – cable resistance; R_3 – adjusting resistance; R_1, R_2, R_4 – constant resistance; G – amplifier; e_1, e_2 – voltage; E – output voltage; i – output current

Anemometer is equipped with a probe to measure temperature. The probe is placed in a stream of air. The temperature read from this sensor is used to correct the results.

Adjustable parameters are directly connected with the measurement method:

- a) frequency measurements f ,
- b) number of measurements n .

All changes and arrangements of the parameters take place in STREAM WARE program provided with the device. The parameters were changed in a setup window of entrance – signals (Fig. 3). The frequency measurement can be changed in the range from 0.015 kHz up to 200 kHz and the number of measurements – in the range from 0 to 8355840.

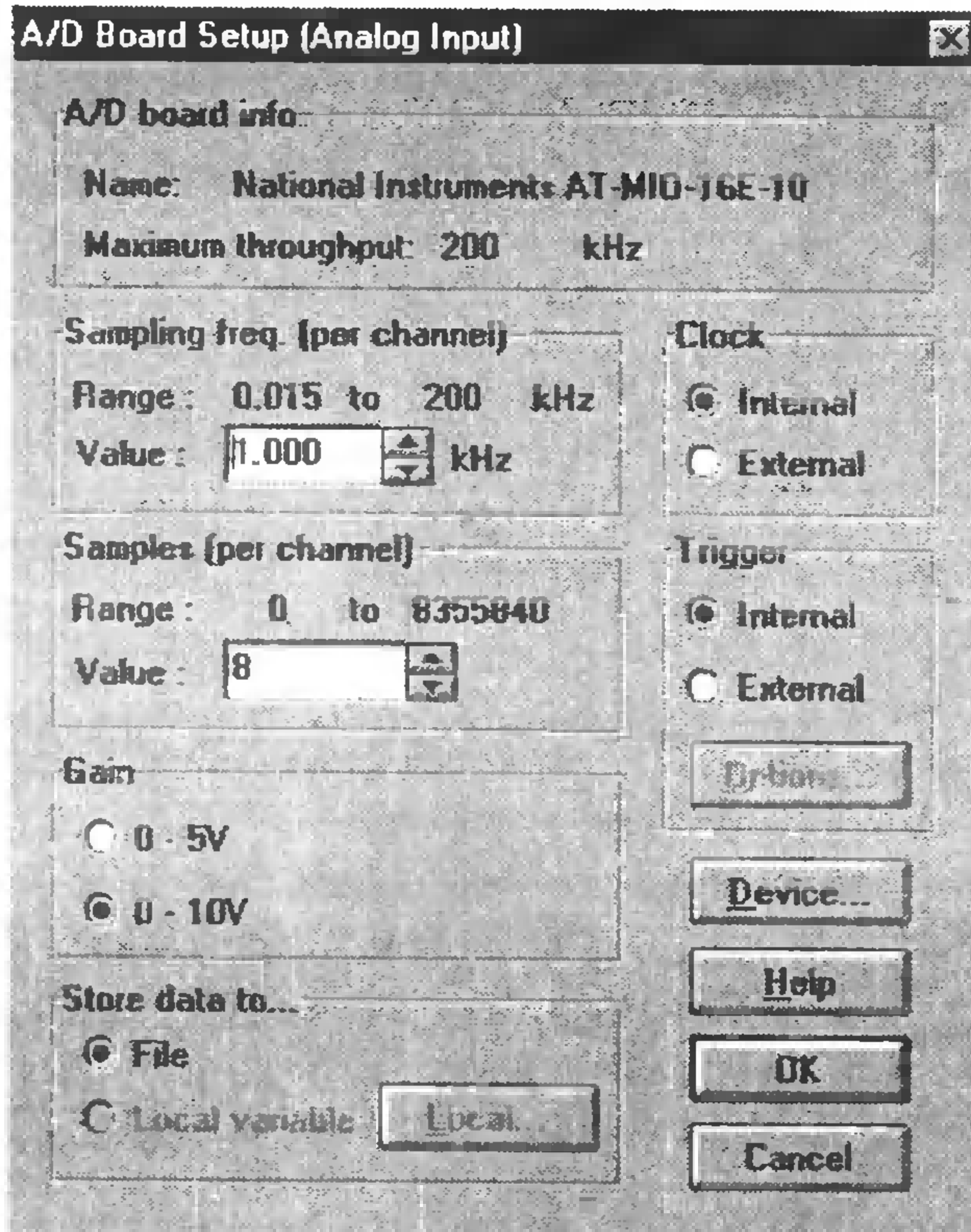


Fig. 3. Window of programmatic arrangements of sampling frequency and numbers of measurements

Changes of these parameters affect an individual measurement when they occur. Definition time of single measurements uses the following equation:

$$t = n \cdot 1/f,$$

where:

- t – single measurement time [s],
- f – sampling frequency [Hz],
- n – number of samples.

The aim of the investigations was to qualify the effect of sampling frequency and the number of samples on the accuracy of the final results. Due to a stormy flow of

liquid, an inconsiderable number of measurements would cause a random reading of values of speed of air stream flowing out from the nozzle, while an excessive number of measurements would prolong the total time of measurement considerably.

2. RESULTS

The investigations were carried out for speeds on entrance $-7.5 \text{ m}\cdot\text{s}^{-1}$, the probe was placed in the distance of 40 mm from the end of nozzle. The measurement concerned the range from -70 to $+70$ mm from the axis of symmetry nozzle with 2-mm step.

Fig. 4 shows six sampled results of outer velocity field measurements for different time measurements.

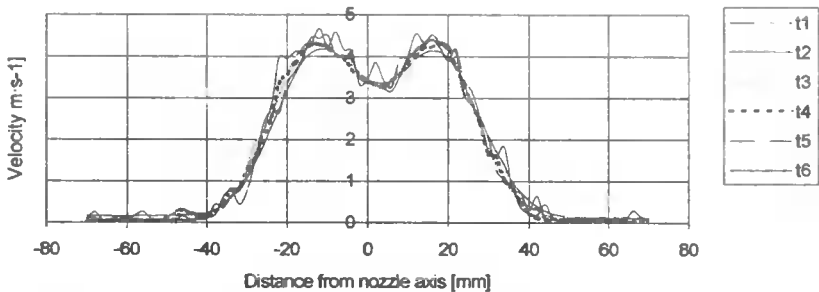


Fig. 4. Velocity of air stream from axi-symmetric nozzle for different sampling parameters

t1 – $f = 10.00 \text{ kHz}$; $n = 262144$;	t2 – $f = 1.00 \text{ kHz}$; $n = 4096$;
t3 – $f = 0.015 \text{ kHz}$; $n = 128$;	t4 – $f = 1.00 \text{ kHz}$; $n = 128$;
t5 – $f = 1.000 \text{ kHz}$; $n = 8$;	t6 – $f = 0.03 \text{ kHz}$; $n = 8$.

As seen on the graph presented all measuring-series are similar. We can clearly see two series “t5” and “t6” being different from the remaining ones. These curves were obtained for parameters $f = 1.00 \text{ kHz}$ and 0.03 kHz for $n = 8$ measurements in every measuring-point. Fig. 5 presents the velocity of air measured in one point of the measuring-range. A single measuring-point was put 10 mm away from the axis of the symmetry nozzle and the velocity was represented for changed “f” and “n”.

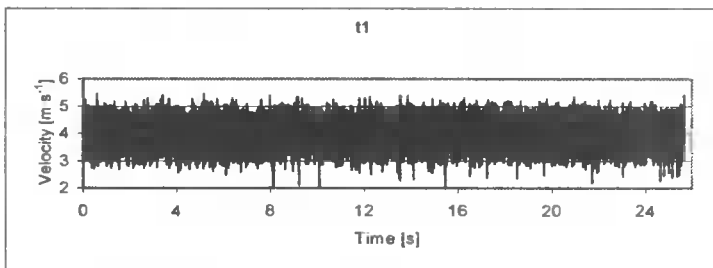


Fig. 5. Velocity for $f = 0.03 \text{ kHz}$ and $n = 128$ “t1”

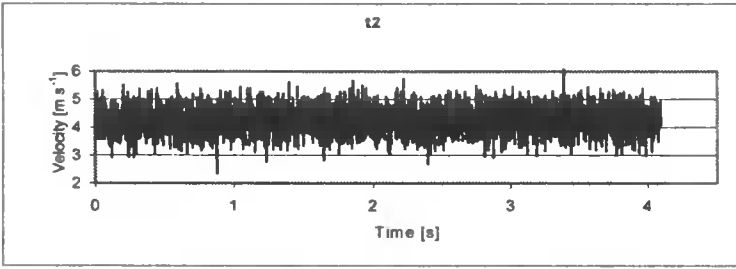


Fig. 6. Velocity for $f = 1.00$ kHz and $n = 4096$ "t2"

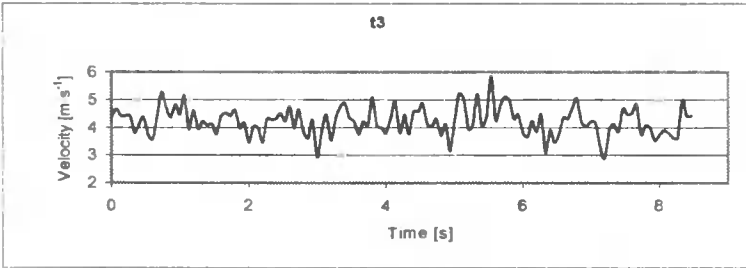


Fig. 7. Velocity for $f = 0.015$ kHz and $n = 128$ "t3"

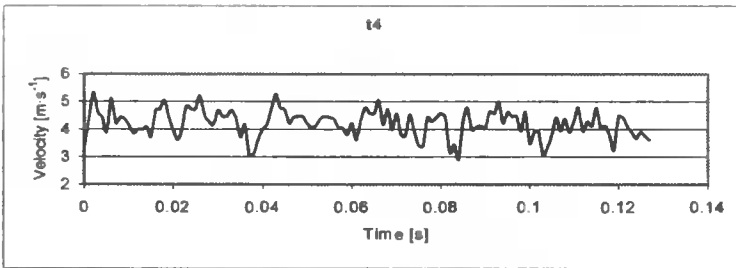


Fig. 8. Velocity for $f = 1.00$ kHz and $n = 128$ "t4"

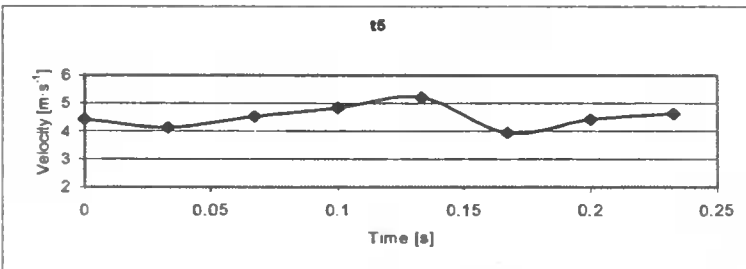


Fig. 9. Velocity for $f = 0.03$ kHz and $n = 8$ "t5"

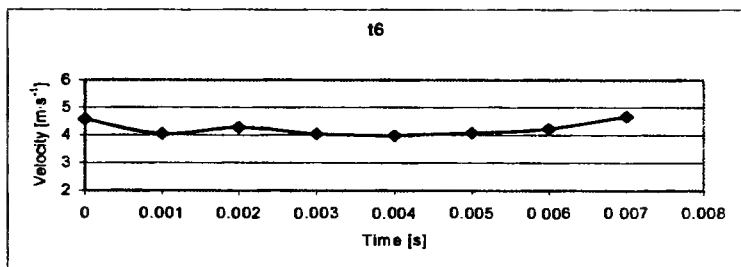


Fig. 10. Velocity for $f = 1.00$ kHz and $n = 8$ "t6"

Table 1. Mean velocity values

Series	t1	t2	t3	t4	t5	t6
Time of measurement	26.21	4.095	8.467	0.127	0.233	0.007
Mean velocity	4.159075	4.25627	4.21851	4.20224	4.50751	4.22825
Relative error	-2.4143	-0.1338	-1.0198	-1.4015	5.7608	-0.7912

3. CONCLUSIONS

As shown in Fig. 6–10, the last two series t5 and t6 differ significantly from the remaining ones due to the inconsiderable number of measurements in each measurement-point. Mean velocities in the measurement-point presented in Table 1 show that for the series t6 the value does not vary from the remaining, as in the series t5. One can conclude that the accuracy of the results is guaranteed after a considerable number of measurements. However, then a sampling frequency should not be low not to prolong the time of measurement in a single measurement-point. The figures show that the parameters $f = 1$ kHz and $n = 4096$ assure a sufficient accuracy of results and do not prolong the time of measurement. The time of a single measurement for $t = 1/f \cdot n$ equals 4s and, as such, it is not time-consuming.

REFERENCES

- [1] Brunn H.H., 1995. Hot-wire anemometry. Principles and signal analysis. Oxford University Press. Oxford. ISBN 0 19 856342 6.
- [2] Dantec Stream Line Documentation, 1996. Dantec Measurement Technology A/S
- [3] Peszyński K., Hosek J., Kuszynski Z., Travnicek Z., Wawrzyniak S., 2000. Active control of annular bistable jet. International conference: Engineering Mechanics 2000. Svratka. 149-154.
- [4] Wawrzyniak S., Peszyński K., 2000. Problematyka pomiaru prędkości miejscowych przy pomocy termoanemometru w urządzenia technologicznych. Jubileuszowa Międzynarodowa Konf. Nauk.: Recyrkulacja w budowie maszyn. Bydgoszcz, 41-46.
- [5] Wawrzyniak S., 2000. Numeryczne modelowanie elementów strumieniowych. Forum młodych. Bydgoszcz-Borówno 19-20 czerwca 2000, 237-242.
- [6] Wawrzyniak S., Peszyński K., 1999. Analiza wpływu parametrów konstrukcyjnych na własności dyszy osiowo symetrycznej. Seminarium Naukowe: Postępy w sterowaniu i konstrukcji. Bydgoszcz, 39, pełny tekst na płycie CD-ROM.

Ryszard Wocianiec

University of Technology and Agriculture

Faculty of Mechanical Engineering

Department of General Mechanical Engineering and Mechatronics

Jaroslaw Zdrojewski

University of Technology and Agriculture

Faculty of Telecommunications and Electrical Engineering

Division of Digital Technology

Dariusz Skibicki

University of Technology and Agriculture

Faculty of Mechanical Engineering

Department of Control and Machinery Design

COMPLEX MILLING OF PLATE-LIKE ELEMENTS

Summary. This article presents milling technology created for the part sets based on fixing of the two. In the construction process, a choice of geometrical and material features depends on the technology described. The milling method described is eliminating, usually necessary, several workpiece positioning and fixing steps and it finally results in a significantly improved quality of the machined parts. Additionally manufacturing process becomes more effective, when concentrated, eliminating transport and reducing the number of tools and fixing.

Key words: complex milling, milling, CAM, machining

1. INTRODUCTION

There are many new ideas of improving machining technology [1,2]. The article presents a technology allowing simultaneous milling of many elements with two fixing places. The design process, e.g. the choice of geometrical and material features of the machined elements, supplemented the technology described. Due to the elimination of multiple re-fixing and re-location of the element, the machining time-effectiveness, technical value and appearance are enhanced.

2. DESIGN RESTRICTIONS

The technology of element accomplishing having been decided, the design process started, which must have restricted the shaping possibilities, kind of material and surface machining. As the design incorporates optical device, all the parts have to be blackened. The slide bearing elements were made as a mixture of Turcite-A plastic and a cold-hardened aluminum alloy. Locally hard surfaces were obtained through sticking onto the aluminum elements hardened and polished 0.5-mm steel strip with reversible adhesive tape.

The machining technology imposed caused some shaping limitations. The essential elements of the design are two frames with a window, where all parts were to be placed; 43 % of them were 2-12 mm thick (Fig. 1).

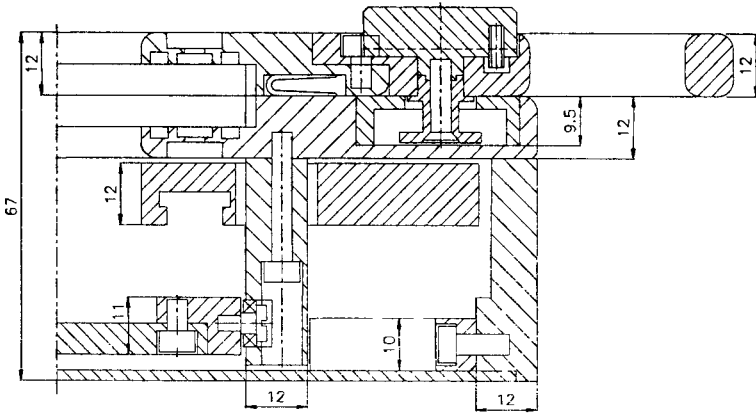


Fig. 1. Optimal design solution with the technology applied

Long elements, which do not correspond to the window size, were divided and both were fixed while assembling with spring-type straight pins and then screwed. Another restriction is the variety of tools that can be used and the ability to shape geometrical features of the design elements. The list of tools restricting the designer, and being a compromise of technological abilities and tool holder prices, is presented in Fig. 2.

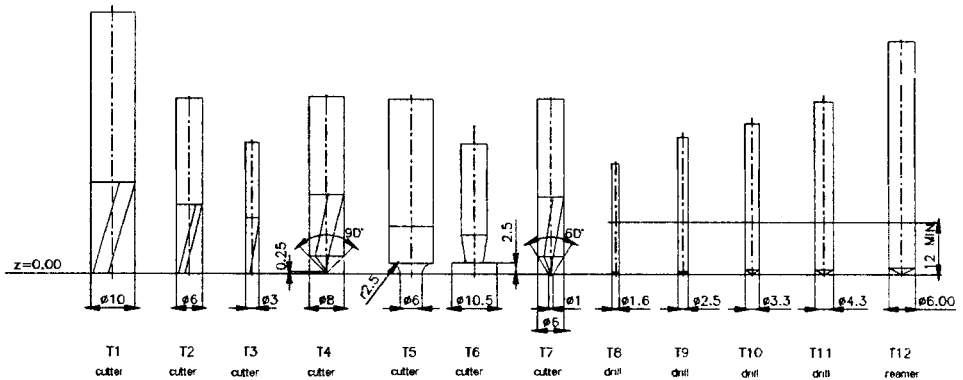


Fig. 2. Tools

For example, a 3-millimetre-diameter drill is used to make holes for M4 thread and M3 screws.

3. TECHNOLOGY

Fig. 3 illustrates a sample element arrangement in a 930 x 720 mm plate. The minimum assumed distance between the elements was 10.5 mm obtained with a mill 10 millimeter in diameter.

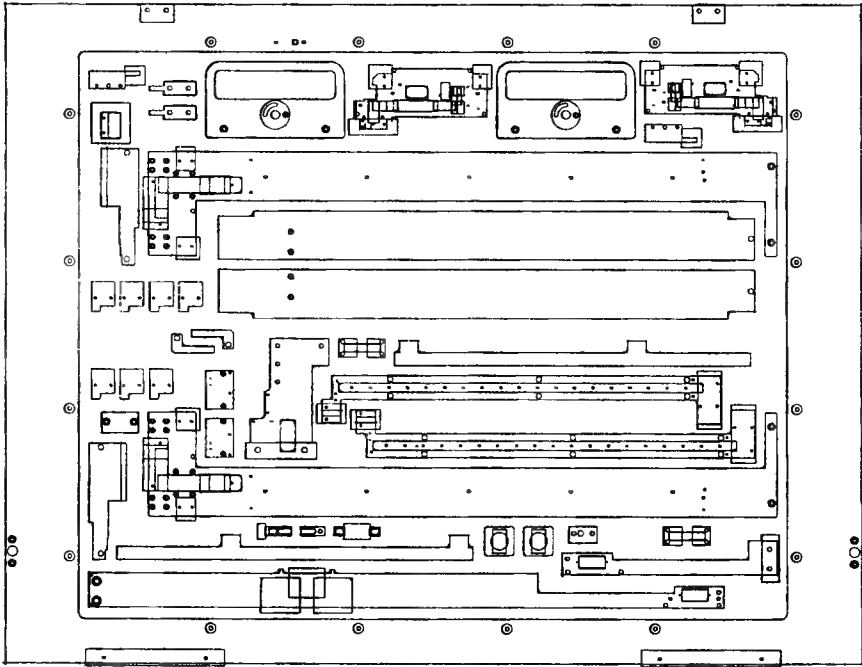


Fig. 3. Sample element arrangement

The plate is assumed to be machined in two fixings; drilling and milling is to continue until the total thickness is obtained, which requires indirect fixing to the machining tool table. Another assumption is to carry out the technological process in a way that will allow shortening the preparation and finishing time and that will eliminate the mistakes of the staff.

Machining with the technology presented includes the following stages:

1. Establishing and fixing the base plate, which is essential for the element quality. The plate is made of aluminum alloy with steel inserts in the place of threads and datum-holes. Two lines of datum-pins need to be allocated in the direction x , with the accuracy of ± 0.01 . One of the pins, the left one, is the datum-pin for all programs. To make the disassembly of the datum-pins for the plate easier, they are driven into a T-slot situated in the table. If the plate surface is not flat, it can be cut on the whole plane.
2. Once the base plate has been established and fixed, the machined plate is established and fixed. To ensure short preparation and finishing time, the base plate has a special structure (Fig. 4). The machined plate is assumed to have the external dimensions by 2 mm larger than the nominal ones, which makes it easier to fix it along

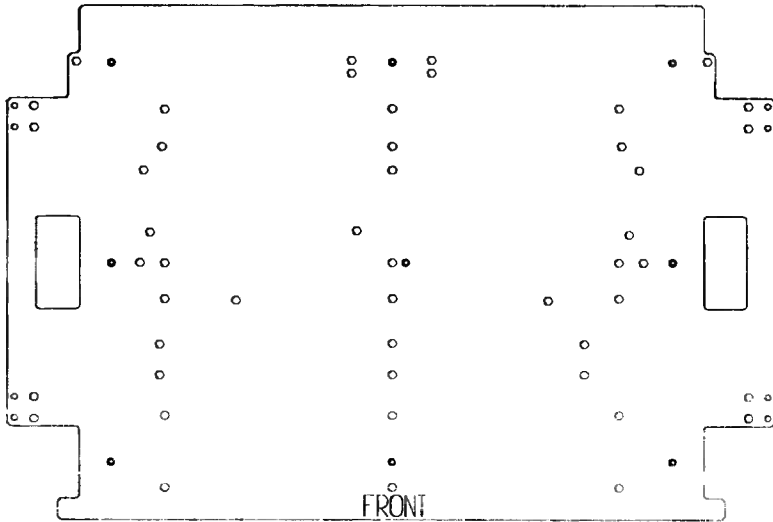


Fig. 4. Base plate

the sides of the base plate with little accuracy. The machined plate surface is the base for establishing the tools.

3. The next stage is to make fixing holes for the machined plate. To do this, it is fixed with four assembly jigs to the base plate, which has specially prepared holes. The first program performs the necessary holes, and after the plate is cleaned, it may be screwed to the base plate and the assembly jigs may be disassembled.
4. The main milling takes place when several separate stages performed as a sequence can be seen. The principle is to use a chosen tool within one program. The first one to work is a 10-mm-diameter mill of the following parameters:
 - cutting depth – g up to 6.5 mm
 - travelling rate – $p = 1000 \text{ mm} \cdot \text{min}^{-1}$.
 - rotation rate – $v = 10000 \text{ l} \cdot \text{min}^{-1}$.

It is a triple-bit cutter with a helical chip clearing groove enabling indenting milling. The technology allows producing elements of different thickness. While programming an element is given a thickness, which makes it possible to generate automatically the information about the allowance-to-be-removed from the workpiece (Fig. 5).

5. As a result, it is possible to mill parts of arbitrary thickness off the plate cost-effectively. Slotting mills different in diameter are used sequentially. The next to work is a countersinking mill, which chamfers the edges, performs the phases for non-standard holes larger in diameter than the one of drills used and does the countersinking in the places of drill holes. To ensure close plate contact for machining its reverse side, all edges for $z = 0$ have chamfered edges. Then profile cutters and drills are used.

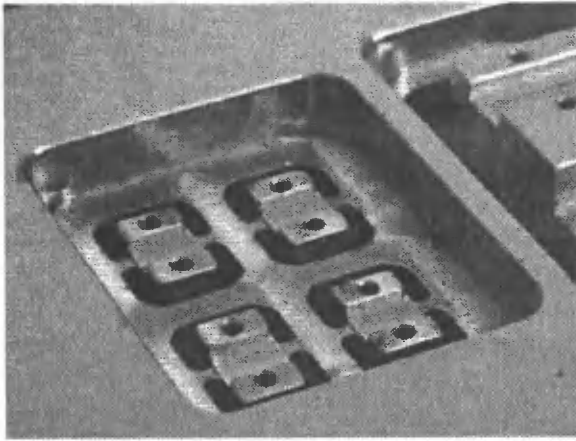


Fig. 5. Pocket on the plate surface for the non-standard thickness workpieces

- Once the plate is cleaned, it is turned over, established in relation to the base plate with two pins, fixed with the assembly jigs. Finally, countersinks for the screw heads are made and the plate is fixed and machined. 1-millimeter-thick material is left between the elements to join them. The last program cuts the elements off with a 3-millimetre mill with 5-millimetre bridges left joining all the parts. The subsequent stages of the technological process are shown in Fig. 6, while the final plate view is presented in Fig. 7.

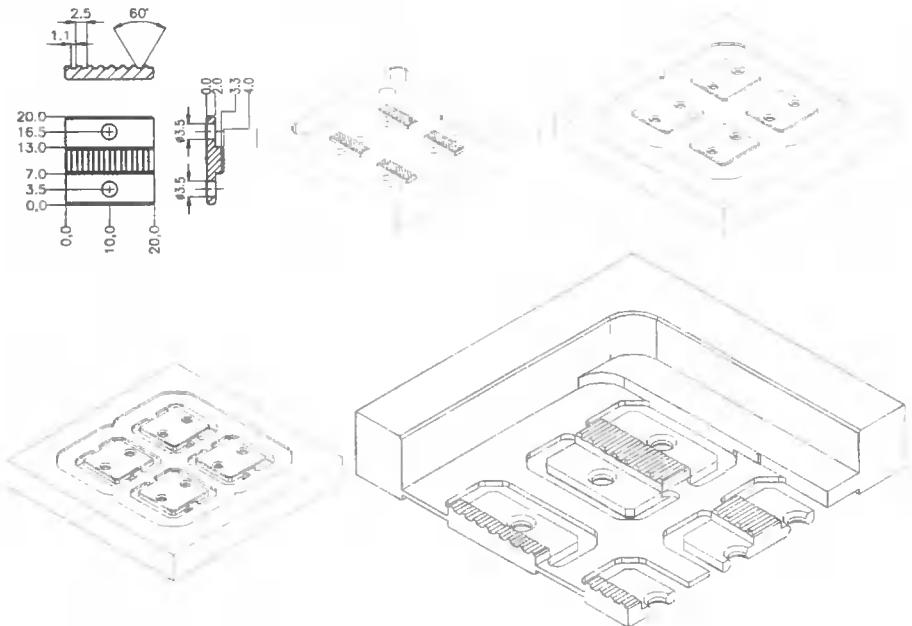


Fig. 6. Stages of the technological process: part drawing; the state after the first machining with a pocket compensating for the workpiece thickness; after machining the reverse side; cutting the elements off

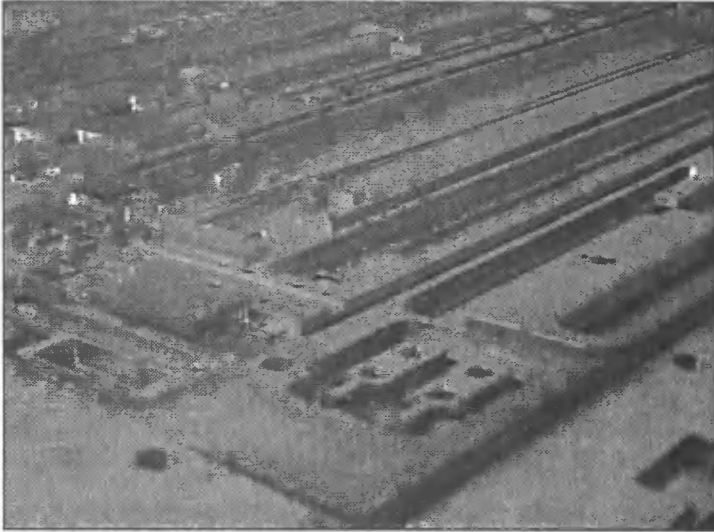


Fig. 7. Result of complex milling procedure

4. CONCLUSIONS

The milling presented, through eliminating multiple replacing and re-establishing the workpiece, enhances the technical value and appearance. The method rationalizes the manufacturing process by focusing, transport eliminating, simplifying the data circuit and by limiting the number of tools and grips. After machining, the workpiece requires only the element-joining bridges to be removed and some non-technological, from the point of view of the method presented, procedures, e.g. horizontal holes. It was not possible to machine M2-M5 threads with the machining tool. The machining the two 930 x 720 and 930 x 820 mm plates with 148 parts took 18 hours. Applying the traditional technology to individual part machining would consume more time and money. To implement the technology a milling center is essential provided that:

- travelling takes place in the x and y co-ordinates,
- the distance between the table and the spindle end is less than 200 mm,
- spindle rotation rate is not smaller than $20000 \text{ l}\cdot\text{min}^{-1}$,
- travelling rate up to $3000 \text{ mm}\cdot\text{min}^{-1}$ is ensured.

Almost all these are fulfilled by a FADAL milling center where the milling method was tested.

REFERENCES

- [1] Kosmol J., 1995. Automatyizacja obrabiarek i obróbki skrawaniem. WNT Warszawa.
- [2] Weiss Z., 1997. Projektowanie współbieżne wyrobów. Mechanika 7.

Ryszard Wocianiec

*University of Technology and Agriculture
Faculty of Mechanical Engineering
Department of General Mechanical Engineering and Mechatronics*

Jaroslaw Zdrojewski

*University of Technology and Agriculture
Faculty of Telecommunications and Electrical Engineering
Division of Digital Technology*

Dariusz Skibicki

*University of Technology and Agriculture
Faculty of Mechanical Engineering
Department of Control and Machinery Design*

PLATE-LIKE ELEMENTS MACHINING PROGRAMMING IN CAD ENVIRONMENT

Summary. The article presents the environment of computer aided design of numerically controlled machine tools. The environment includes programs to facilitate the creation of NC program graphical notation, programs for conversion of the notation into an NC code and for visualising machine tool work effects.

Key words: NC, CAD, CAM

1. INTRODUCTION*

There are many environments of computer aided design [1,2], however their major drawback is that programs are very complex or/and very expensive. The article presents an integrated environment for creating programs for numerical machine tools.

Designing the environment, it was assumed that the NC machine tool programming should take place in the CAD designer environment and the programming process should include drawing.

The environment includes the following three groups of computer programs:

- a) programs which facilitate the creation of tool path graphical notation,
- b) programs which translate graphical tool movement notation into the NC code,
- c) programs for two- and three-dimensional visualisation of the machine tool work effects.

2. TOOL PATH GRAPHICAL NOTATION

The first group of programs allows to generate tool paths in the form of drawing objects, such as lines, arcs and circles.

The program interprets these elements as the edges of the workpiece lateral surfaces. The tools were assumed to mill concurrently, only. If the milling cutter movement direction is consistent with the 'y' axis of the Cartesian co-ordinate system, the tool chooses the material to the left of the path drawn. It is essential for the objects

drawn to include not only the information about the vertex co-ordinates, but also about their sequence; hence the necessity to 'remember' the tool movement direction.

Fig. 1b presents the tool path for the external contour machining of the workpiece shown in Fig. 1a.

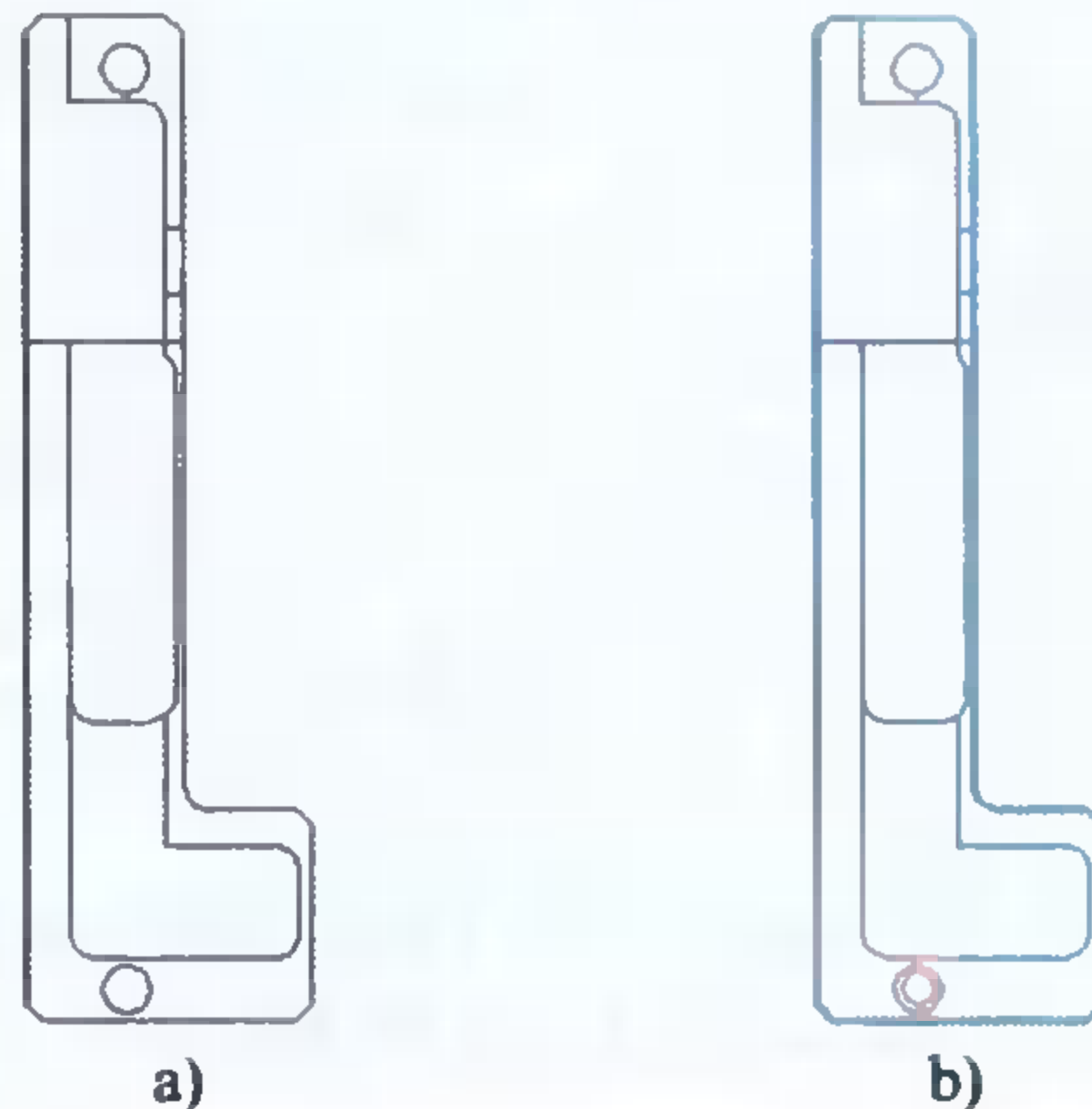


Fig. 1. Part view (a) and the external contour machining path (b)

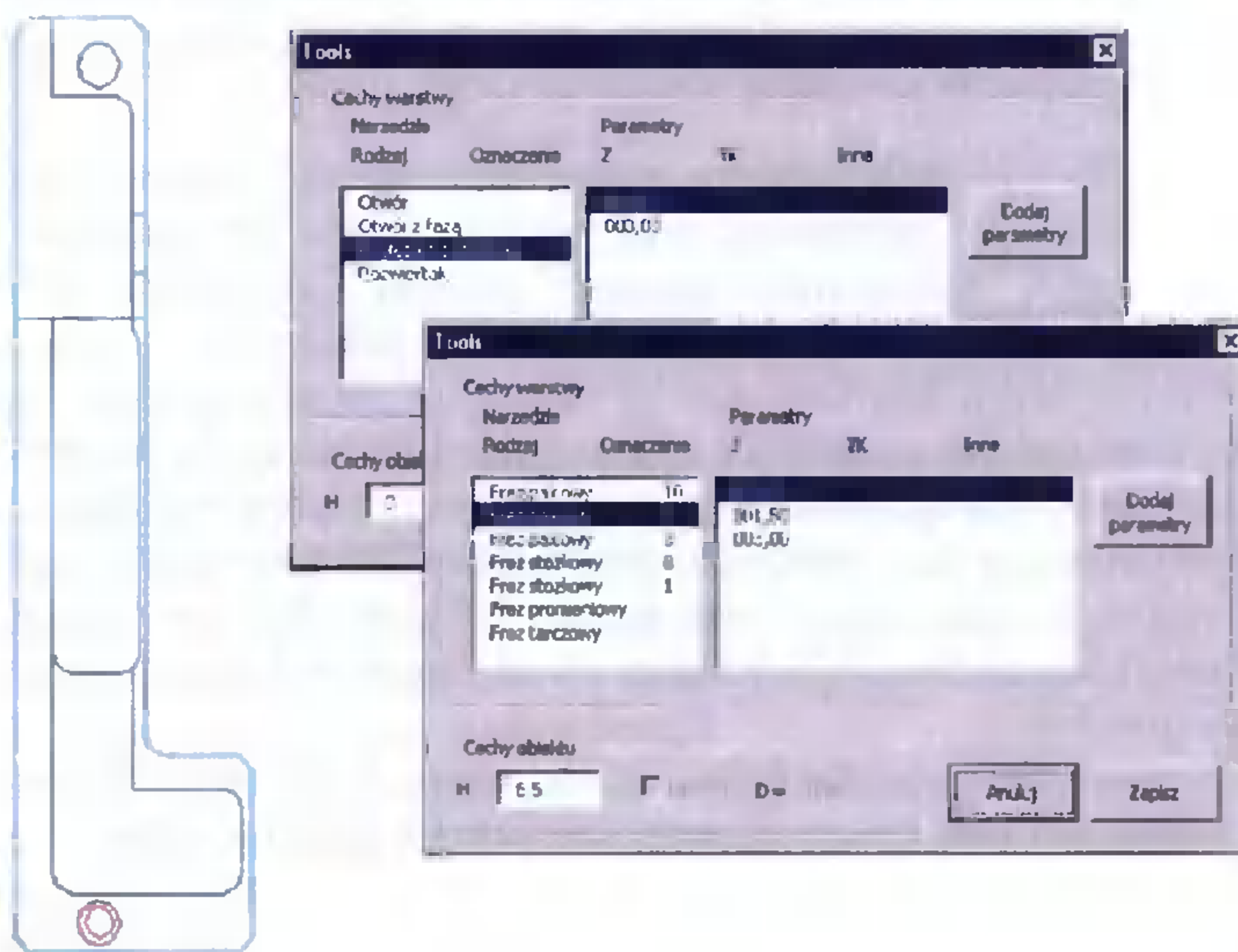


Fig. 2. Dialogue windows for working tool parameter defining

The milling cutter direction as well as other parameters of the tool work, including type, lost motion depth 'Z', machining depth 'H' and other quantities are assigned to the drawing objects by dialogue windows (Fig. 2).

When drawing simple objects, e.g. lines (Fig. 3a) or chains of line segments and arcs (Fig. 3b), the information allows programming the arbitrary path.

As for holes, the graphical object in the form of a circle additionally 'remembers' the way of accomplishing, for example, whether a hole is with or without a chamfer, or if it is only a countersunk hole.

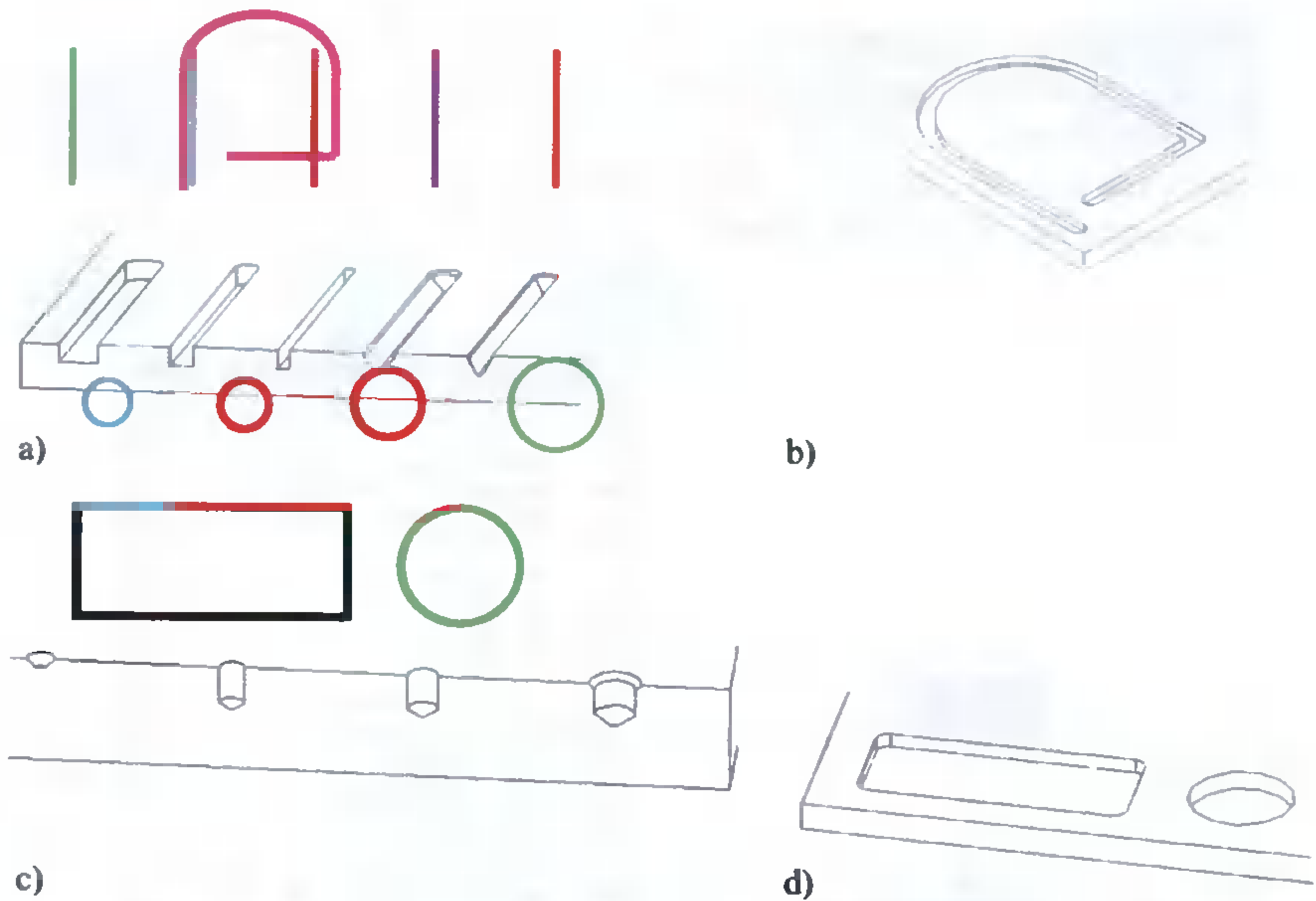


Fig. 3. Objects drawn

The most effective programming elements include pockets (Fig. 3d); the programmer defines the pocket overall dimensions only, without considering the recess algorithm of its contents.

Fig. 4 presents a sample program, ready to be used, incorporating the elements mentioned.

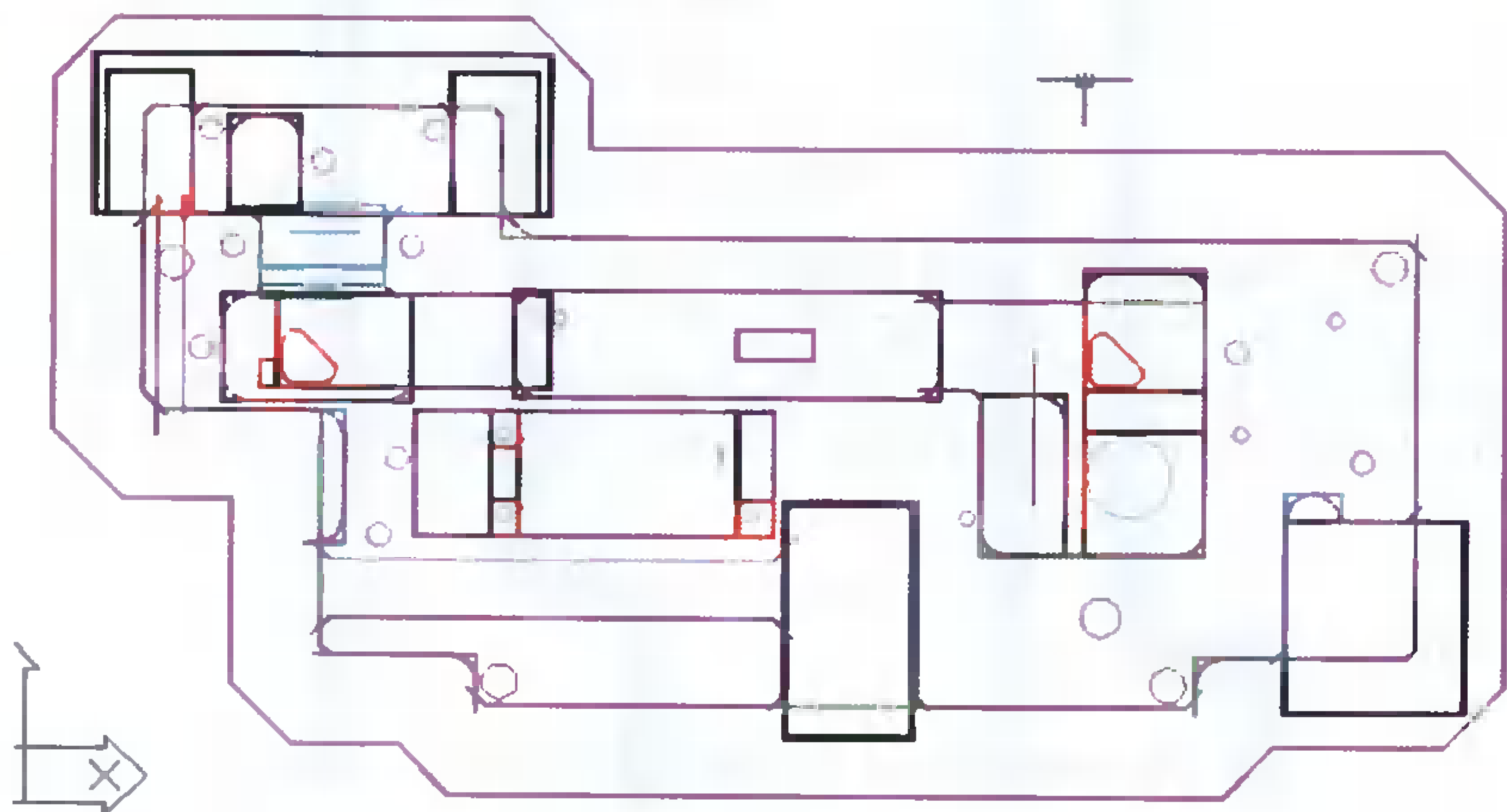
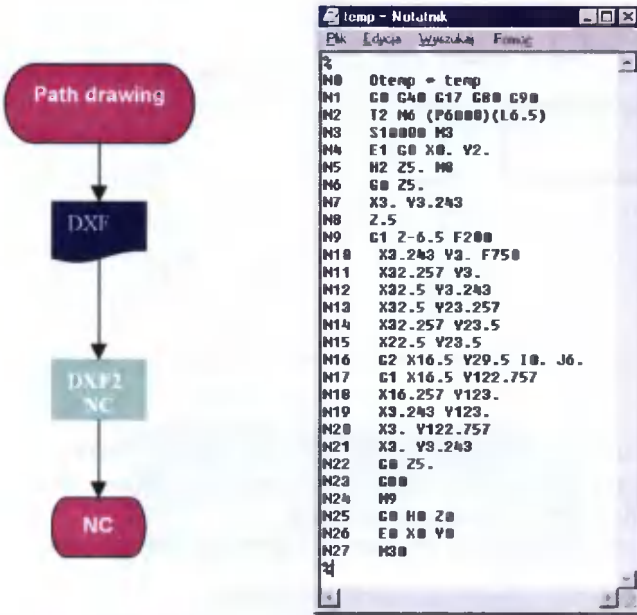


Fig. 4. Program ready to be used

3. TRANSLATION PROGRAMS

The second group of programs, based on technology graphical notation, creates a code understandable for a numerical machine tool (Fig. 5). The program not only

converts the graphical object co-ordinates into a text file of a numerical program, but also automatically decides about the sequence of the tool use, chooses parameters and optimises their movement. As for holes, the tool to be selected is decided about. If it is possible, for example, to use a drill for standard diameter holes, the drill is selected; otherwise, an end mill of the right diameter is chosen. For pockets, the optimal way of recessing the contents is appointed.



a) translation program performance DXF2NC

b) NC program listing

Fig. 5. Translation programs

This is how programs for single design elements are created. Milling is performed by compiling with any of the other part sub-programs into a whole-set milling program where a single plate is used. To unite the NC sub-programs, a program called Linker is used. Having joint the programs, Linker optimises the tool movement for the whole plate.

4. VISUALISATION

Tools for graphical presentation of a numerical machine tool program make it possible to obtain two-dimensional or three-dimensional (solid) visualisations (Fig. 6).

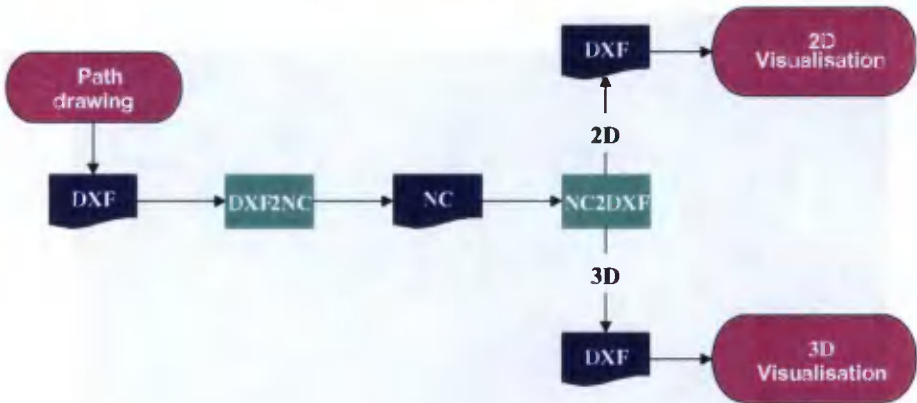


Fig. 6. Visualisation algorithm

To do this the NC code is translated into tool movement graphical representations. In two-dimensional visualisation, these are objects of the width which equals the tool diameter.

Fig. 7 presents the results of a 2D visualisation which enhances the identification of mistakes due to, e.g. a wrongly appointed tool path direction. The tool in Fig. 7a mills the contour of the workpiece correctly, while Fig. 7b mills the inside.

Such visualisation allows quick performance, however not all the mistakes can be found.

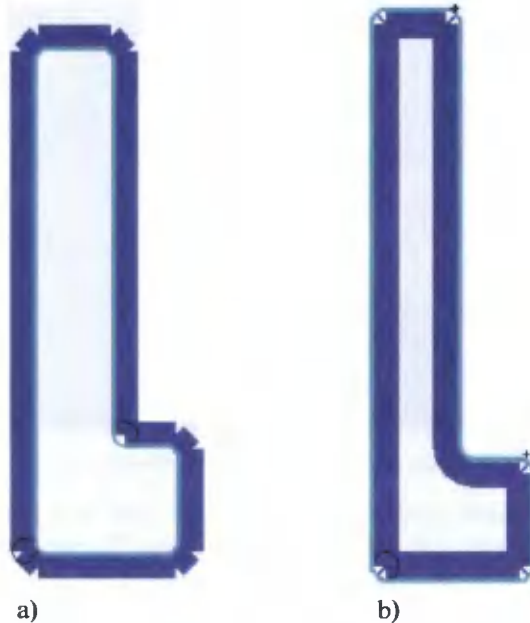


Fig. 7. 2D visualisation

To control the programming correctness completely, 3D visualisation should be used (Fig. 8). Usually a full visualisation of a part machining is to check the complete part program.



Fig. 8. 3D visualisation

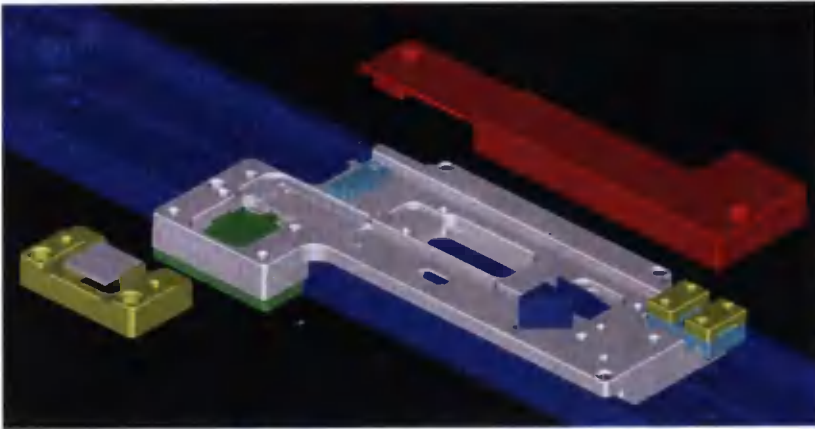


Fig. 9. Solids for a final machining technology check

3D visualisation gives solids. The objects can be used for a final check of the design and machining process. Fig. 9 shows a tool set from 3D visualisation - solids.

REFERENCES

- [1] Miecielica M., Kaszkiel G., 1999. Komputerowe wspomaganie wytwarzania CAM. Mikom.
- [2] Weiss Z., 1996. Projektowanie technologii maszyn w systemach CAD/CAM. Wyd. Politechniki Poznańskiej.

